



<https://theses.gla.ac.uk/>

Theses Digitisation:

<https://www.gla.ac.uk/myglasgow/research/enlighten/theses/digitisation/>

This is a digitised version of the original print thesis.

Copyright and moral rights for this work are retained by the author

A copy can be downloaded for personal non-commercial research or study, without prior permission or charge

This work cannot be reproduced or quoted extensively from without first obtaining permission in writing from the author

The content must not be changed in any way or sold commercially in any format or medium without the formal permission of the author

When referring to this work, full bibliographic details including the author, title, awarding institution and date of the thesis must be given

Enlighten: Theses

<https://theses.gla.ac.uk/>
research-enlighten@glasgow.ac.uk

STRUCTURAL STUDIES
WITH THE
ELECTRON MICROSCOPE.

Thesis submitted to the University of Glasgow
for the Degree of Ph.D.

by

Edward A.C. Follett.

Chemistry Department.

May, 1960.

ProQuest Number: 13850709

All rights reserved

INFORMATION TO ALL USERS

The quality of this reproduction is dependent upon the quality of the copy submitted.

In the unlikely event that the author did not send a complete manuscript and there are missing pages, these will be noted. Also, if material had to be removed, a note will indicate the deletion.



ProQuest 13850709

Published by ProQuest LLC (2019). Copyright of the Dissertation is held by the Author.

All rights reserved.

This work is protected against unauthorized copying under Title 17, United States Code
Microform Edition © ProQuest LLC.

ProQuest LLC.
789 East Eisenhower Parkway
P.O. Box 1346
Ann Arbor, MI 48106 – 1346

ACKNOWLEDGMENTS.

This work was carried out in the Physical Chemistry Department of Glasgow University, which is under the direction of Professor J.M. Robertson.

I am deeply indebted to Dr. Ian M. Dawson for his invaluable guidance and inspiration during the course of this work.

I should like to express my thanks to Dr. D.H. Watson for many helpful discussions.

My thanks are also due to the Department of Scientific and Industrial Research for a Studentship for two years and to the United Kingdom Atomic Energy Authority for a grant for one year.

E.A.C.F.

I n d e x.

Page

PART ONE.

STEARIC ACID

PREFACE	1
INTRODUCTION					
Crystal Structure	6
Crystal Growth	9
Polytypism	9
Related Monocarboxylic Acids	11
Replica Methods					
General Considerations	13
Types of Replica	14
Replicating Media	15
EXPERIMENTAL					
Crystal Preparation	17
Replica Preparation	17
Extraction	18
Electron Microscopy	21
RESULTS					
Growth Patterns	22
Multimolecular Steps	31
Step Height Measurements	35
Outgrowths					
Geometry and Lattice Orientation	35
Influence on Growth Pattern	42
DISCUSSION					
Growth Centres	46

	<u>Page</u>
Outgrowths 	51
Growth of Outgrowths 	57
Production of Dislocations by Impurities ...	63
Application to Other Compounds 	64

PART TWO.

SYNTHETIC GRAPHITE

INTRODUCTION

Crystal Structure 	65
Pore Structure 	71
Defect Structure 	73
Reactivity 	74
Object of Work	76
The Observation of Molecular Detail	
The Need for Electron Microscopy 	77
Molecular Resolution 	79
Direct Lattice Resolution 	80
Limitations on Lattice Resolution 	83
Indirect Lattice Resolution 	83
The Moiré Pattern 	83
Historical Development 	84
Formation of Moiré Pattern 	87
Interpretation of the Moiré Pattern ...	95
Application to Graphite 	98
Thin-Sectioning 	99

	<u>Page</u>
EXPERIMENTAL	
Scraping 	103
Rubbing 	106
Thin-Sectioning 	109
Microscopy 	117
RESULTS	
Embedding 	120
Thin-Sections 	120
Observation of Moiré Patterns 	121
Electron Diffraction	
1. Diffraction Patterns from General Areas ...	127
2. Diffraction Patterns from Moiré Patterns	131
Grain Structure of Synthetic Graphite ...	141
Grain Boundaries 	151
Observation of Dislocations 	155
Slip Lines 	162
DISCUSSION	
Nature of Sections 	163
Moiré Patterns 	163
a) Formation 	165
b) Interpretation 	169
Crystallite Size 	178
Pore Size and Distribution 	182
Dislocations 	183
Limitations of Technique 	188

				<u>Page</u>
Reactivity	189
GENERAL CONCLUSIONS		191
BIBLIOGRAPHY	193.

PART ONE.

(1) reduced to the rank of ∞ by Γ
 is condition (1) (2) by Γ . (3) (4)
 example of Γ may be given. With the
 assumption of Γ , the condition
 (1) (2) (3) (4) (5) (6) (7) (8) (9) (10)
 (11) (12) (13) (14) (15) (16) (17) (18) (19) (20)
 (21) (22) (23) (24) (25) (26) (27) (28) (29) (30)
 (31) (32) (33) (34) (35) (36) (37) (38) (39) (40)
 (41) (42) (43) (44) (45) (46) (47) (48) (49) (50)

P R E F A C E.

The present book is a sequel to the
 first book of the series, "The
 Theory of the Γ -Function", which
 was published in 1914. It contains
 a complete and systematic treatment
 of the Γ -function, and its
 properties, and its applications
 to the theory of the ζ -function,
 and to the theory of the η -function.
 The book is written in a style
 which is both clear and concise,
 and it is intended to be a
 valuable addition to the library
 of every mathematician.

The basic lattice structure of crystals, although originally deduced as far back as 1665 by Robert Hooke, was first confirmed in 1913 by W.L. Bragg using the powerful technique of X-ray analysis. With the ready elucidation, in favourable cases, of the positions of molecules in a crystal lattice, attention was then focussed on how such a structure could be produced from vapour, solution or melt and it is only in the past forty years that significant advances have been made in this field of crystal growth.

The classical theory of crystal growth or the theory of the growth of ideally perfect crystals was first introduced by J.W. Gibbs in 1878 and was developed by various workers, Volmer, Kossel, Stranski, Becker, and Doring, Frenkel, and Burton and Cabrera, between 1920 and 1948. This theory asserts that low index faces on a crystal in equilibrium with its vapour or solution are fundamentally flat and that growth on such a surface takes place by the formation of a two dimensional island monolayer which subsequently expands to cover the whole face. Such an island monolayer has a higher vapour pressure than the crystal as a whole and hence, there must be a critical supersaturation below which the island monolayer will be expected to evaporate and above which it will grow. In a study of the growth

rate of iodine crystals, however, Volmer and Schultze (1931) found that crystals continued to grow at a supersaturation at which it was later shown by Burton, Cabrera and Frank (1949), the formation of two dimensional island monolayers was theoretically impossible. In order to explain this result the dislocation theory of crystal growth was developed by Burton and Cabrera and mainly by F.C. Frank (1949).

When measurements of the mechanical properties of crystals are compared with the theoretically predicted values, the former are always low, usually by a factor of more than one hundred. This discrepancy is attributed to the presence of imperfections or dislocations in the crystal. Frank, in his theory of crystal growth, postulated that growth could take place round one particular type of dislocation, namely, a screw dislocation and, in this way, there was no need for the renucleation of fresh layers since during growth a crystal automatically reproduced a spiral ramp from one layer to the next.

Confirmation of this theory has been obtained from two sources, the optical microscope and the electron microscope. Although the earliest evidence of the polygonal, spiral steps on crystal faces characterising dislocation growth was obtained by Griffin (1950) in an examination of

natural beryl crystals under an ordinary optical microscope, the first clear photographs of spiral growth pyramids were obtained by Dawson and Vand (1951) studying the long chain paraffin n-hexatriacontane ($C_{36}H_{74}$) in the electron microscope. Since that time many crystals, both organic and inorganic, have been shown to exhibit the spiral growth pyramids predicted by Frank's theory. The electron microscope has been used by Dawson (1952), Anderson and Dawson (1953) and Dawson and Watson (1956) to study the crystal growth of a series of long-chain aliphatic compounds including paraffins, alcohols, acids and esters. The phase contrast microscope has produced evidence of dislocation growth in an even more diversified range of compounds. Notable contributions in this field have been made by Verma with Silicon carbide (1951) and (1952), Stearic acid (1953) and Palmitic acid (1955), Forty with Cadmium Iodide (1952) and Amelinckx studying long-chain aliphatic alcohols and acids, (1955) and (1956).

The results obtained by the above workers have amply confirmed Frank's original hypothesis. Yet, although the results from the two methods are fundamentally in agreement, there are several interesting discrepancies in detail.

A screw dislocation is characterised by its Burgers vector which may be a unit, multiple or, in some cases,

sub-unit of the molecule in the crystal. According to Frank (1951), this Burgers vector determines the height of the growth steps on the crystal face. This generalisation was apparently confirmed by the results of the workers using optical techniques who invariably reported multimolecular steps and, only in a few cases, monomolecular steps. The electron microscope results, however, pointed to a different conclusion. Dawson and Vand (1951) and Dawson (1952) found that in paraffins with an even number of carbon atoms, $C_{36}H_{74}$ and $C_{100}H_{202}$, which have unimolecular units in solution and a unimolecular c-axial translation, the step height was also unimolecular. Moreover, paraffins with an odd number of carbon atoms which have a unimolecular unit in solution but a bimolecular c-axial translation, gave only unimolecular growth steps. In the fatty acid, stearic acid, which has a bimolecular unit in solution and also a bimolecular c-axial translation, Dawson and Anderson (1953) reported only bimolecular growth steps. From these results it would appear, as was concluded by Anderson and Dawson, that the step height is determined not by the Burgers vector but by the size of the unit in solution. In contrast to this Verma and Reynolds (1953) using the light microscope, reported multimolecular steps on stearic acid crystals and later Verma (1955) reported multimolecular steps on the

related palmitic acid crystals.

A possible explanation of this failure to observe multimolecular steps in the electron microscope lies in the size of the crystals examined. The best electron micrographs are obtained from crystals which are very small and very thin, while for good optical micrographs almost the reverse holds. For example, Anderson and Dawson's crystals of stearic acid were 9 μ in diameter while Verma's were 300 μ in diameter. Such an explanation, however, does not provide an answer to the problem of the relation of the step height to the Burgers vector and the unit in solution. Comparison of the resolution given by optical and electron microscopes shows that the electron microscope has vastly superior lateral resolution while the optical microscope, used in conjunction with interferometric techniques, has superior vertical resolution. It would, therefore, be possible for the multimolecular steps observed in the optical microscope to be a closely bunched series of mono- or bimolecular steps, the step height then being dependent on the size of the unit in solution. Accordingly, it was decided to try and examine large crystals indirectly in the electron microscope in the hope of observing large steps.

195. H. H. H. H. H.

The compound chosen for this investigation is $C_{10}H_{12}O$, a long-chain, fat-soluble, primary alcohol. It is a colorless, odorless liquid, boiling at $170^{\circ}C$. and melting at $-10^{\circ}C$. It is soluble in all common organic solvents.

The compound was prepared by the reduction of decanoic acid with lithium aluminum hydride in ether solution.

INTRODUCTION.

Decanoic acid is a long-chain, fat-soluble, primary alcohol. It is a colorless, odorless liquid, boiling at $170^{\circ}C$. and melting at $-10^{\circ}C$. It is soluble in all common organic solvents.

Due to the difficulty in preparing a pure sample of decanoic acid, the compound was prepared by the reduction of decanoic acid with lithium aluminum hydride in ether solution.

Stearic Acid

a) Crystal Structure

The compound chosen for this investigation was Stearic acid, $C_{17}H_{35}COOH$, a long-chain, fatty acid which forms monoclinic prismatic crystals. In these crystals the zig-zag hydrocarbon chains are parallel to the c-axis and inclined at an angle β to the ab plane. Several polymorphic forms are known, the two most stable being designated the B and C forms with long layer spacings 43.75\AA and 39.75\AA respectively (Francis, Collins and Piper, 1937). The two forms are readily distinguished by the differing interfacial angles between the (110) planes which are the closest packed planes and form the edges of the crystal rhombs, the B form having acute angle 74° and the C form, 56° .

Due to the difficulty in preparing pure, large crystals, only one complete X-ray analysis has been carried out, that by Muller (1927) on the B form who reported parameters $\underline{a} = 5.546\text{\AA}$, $\underline{b} = 7.381\text{\AA}$, $\underline{c} = 48.84\text{\AA}$, $\beta = 63^\circ 38'$ and hence $\underline{c} \sin \beta = 43.76\text{\AA}$. The lattice parameters of the C form have been determined by Schoon (1938) who found $\underline{a} = 9.46$, $\underline{b} = 4.96$, $\underline{c} = 49.15$, $\underline{c} \sin \beta = 39.85\text{\AA}$ and $\beta = 54.2^\circ$. Other forms with long layer spacings, $\underline{c} \sin \beta$, have been reported,

e.g., 41.5\AA° (Thibaud and Dupre la Tour, 1930), 46.6\AA° (Piper, Malkin and Austin, 1926) and 43.95\AA° (Dupre la Tour, 1936).

The fundamental difference between the B and C forms, and indeed between all the modifications reported in the literature, is the slope of the chains to the ab plane. The number of modifications reported and the slight discrepancies in the results of different workers examining the same modification suggests that the packing conditions for the molecules in the lattice are not rigidly defined but can be relaxed within certain limits.

The c-axial parameter of 48.84\AA° is approximately twice the length of a stearic acid molecule, this being due to hydrogen bond formation between the carboxyl groups in the molecules, the repeat unit thus corresponding to two molecules.

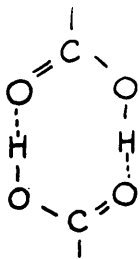


Fig. 1.

Schoon (1938) has shown that a monoclinic modification can be derived from the basic orthorhombic lattice of dimensions $\underline{a} = 4.95\text{\AA}$, $\underline{b} = 7.42\text{\AA}$, simply by displacing the hydrocarbon chains along the \underline{c} -axis, the perpendicular distance between the chains remaining the same. Displacement is possible either along the \underline{ac} or \underline{bc} planes of the original rectangular lattice and for minimum distortion the displacement must be an integral multiple of 2.52\AA .

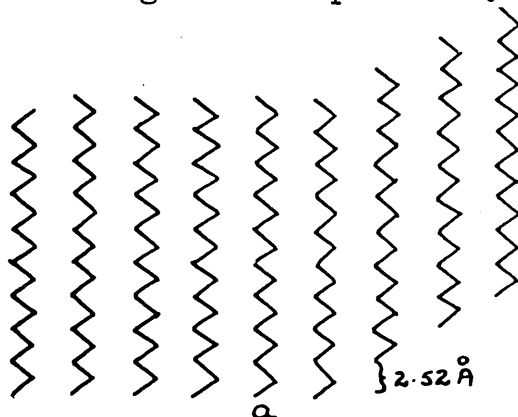


Figure 2 shows a displacement of 2.52 along the \underline{bc} plane. The resulting monoclinic modification has lattice parameters $\underline{a} = 5.6$, $\underline{b} = 7.42$. In a similar manner glide along \underline{ac} gives a modification with $\underline{a} = 4.95$, $\underline{b} = 9.02$, or, using the normal naming convention, $\underline{a} = 9.02$, $\underline{b} = 4.95$. The basic correctness of this hypothesis has been demonstrated by Shearer and Vand's (1956) measurements on the monoclinic form of n-hexatriacontane for which they obtained $\underline{a} = 5.57$, $\underline{b} = 7.42$. From the lattice parameters of stearic acid it can therefore be readily deduced that the B and C forms

arise by tilt of the chains in the fundamental orthorhombic lattice with respect to the a and b axes respectively.

Stearic acid crystallises in the monoclinic rather than in the orthorhombic form since the tilted chain arrangement of the monoclinic form gives greater volume for the accommodation of the relatively large hydrogen-bonded carboxyl groups.

b) Crystal Growth

The growth of crystals of stearic acid has received intensive study by two schools of workers, Anderson and Dawson (1953) using the electron microscope and Verma and Reynolds (1953) with the optical microscope. Both reported growth by the spiral growth mechanism, but whereas Verma and Reynolds measured steps up to four times the bimolecular length and observed many much larger, Anderson and Dawson produced evidence that dislocations initially of multiple strength, dissociated into bimolecular steps as growth proceeded. The wide discrepancies in the sizes and thicknesses of the crystals examined, however, made comparison of the results difficult, as completely different conditions would exist during the growth of Verma's large crystals and during the growth of Anderson's, of necessity, minute crystals.

Polytypism

Polytypism can best be described as a special case of

polymorphism in which only one lattice parameter is altered in the different polytypes. When a crystal grows by a spiral growth mechanism, the pitch of the screw and hence, the pattern in which the molecules repeat in the lattice, is determined by the Burgers vector of the original dislocation. Provided that the Burgers vector coincides with, or is an integral multiple of the lattice repeat unit, then the structure produced by the screw dislocation will be the same as the structure of the undislocated lattice. When this condition does not hold and the Burgers vector of the dislocation is not an integral in terms of the lattice repeat unit, then the pitch of the spiral growth form will likewise not be an integral multiple of the lattice repeat unit, and a structure differing from the perfect lattice will be produced. Such a structure is known as a polytype. For the growth of such structures the presence is necessary, in solution or vapour, of units which are not integral multiples of the repeat unit in the lattice.

In stearic acid, the dimeric unit in solution is identical to the c-axial repeat unit, hence, polytypism would not be expected unless in circumstances where single molecules are present in solution.

Related Monocarboxyl Acids

The growth of palmitic acid, $\text{CH}_3(\text{CH}_2)_{14}\text{COOH}$, a compound almost identical in structure to stearic acid, has been studied in detail by Verma (1953). As with stearic acid, he reported multimolecular steps, but in this case he also reported evidence of polytypism which he suggested was due to growth on a screw dislocation with Burgers vector an odd integral multiple of the molecular length. Such growth necessitates the presence of a reasonable concentration of unassociated molecules in solution.

Evidence for imperfect dislocations in stearic acid had been reported previously by Anderson and Dawson (1953), but their interpretation was that double not single molecules condensed on the dislocation, the resulting lattice misfit producing a hold-up in the growth pattern on one side of the dislocation. This interpretation was confirmed by the work of Amelinckx (1956) on eikosanic, behenic and lignoceric acids where similar misfits in growth patterns were observed.

Amelinckx did, however, report evidence of an unique form of polytypism and suggested it was due to stacking faults in the layers. From an analysis of growth patterns he concluded that a polytype could be produced in a monocarboxylic acid by a rotation of a layer through 180° as in Fig.3. Growth around a large dislocation containing such a

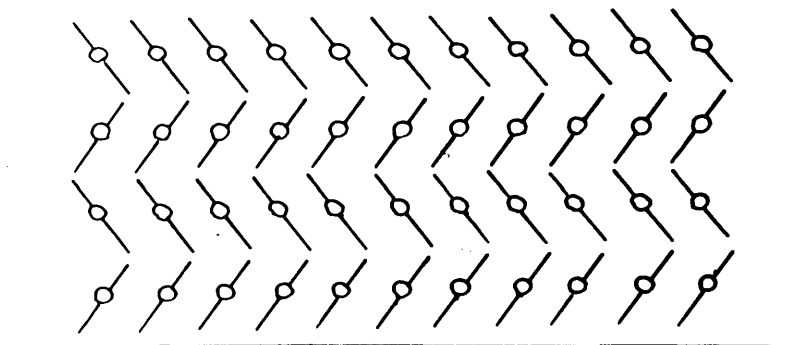


FIG. 3.

structure would result in a polytype, in the very general sense, without necessitating the presence of any unassociated molecules in solution, as the lattice repeat unit would be a multiple of the dimeric unit in solution.

A further observation of Amelinckx's was that, although the steps heights were usually bimolecular in accordance with Anderson and Dawson's results, in polytypic crystals the step heights were multimolecular. This was observed not only on monocarboxylic acid crystals but also on n-paraffins and n-alcohols. Now, if polytypism in long chain compounds is due to lattice rotations, then it is to be expected that step bunching will occur as it is possible that a step making an acute angle with the ab plane may be followed by several steps making an obtuse angle, these having faster growth rates. This observation does not, therefore, contradict Anderson and Dawson's conclusion that the step height

is dependent on the unit in solution, but rather tends to support it.

Replica Methods

a) General Considerations

Although the use of electrons instead of light as imaging media results in a hundred fold increase in resolving power, serious limitations are imposed on the nature of the specimen which may be examined. In modern electron microscopes the accelerating voltage is 60 or 80 K.V. and the high energy beam produced by such voltages results in energy transfer to the specimen during examination. This transferred energy may be sufficient to either melt the specimen or, in some cases, to break chemical bonds and thus cause decomposition. A related effect is the serious limitation imposed on specimen thickness. Thick specimens cause excessive scattering of the electron beam, with the result that very few electrons diffracted by the specimen reach the final imaging plane of the viewing screen and hence, surface definition and resolution are extremely poor.

Examination of surface detail in thick specimens is, however, possible by the use of replica techniques although the resolution obtainable is not comparable with that obtainable by direct observation of a similar, ideally thin specimen.

b) Types of Replica

Replicas, being impressions of the surface of a specimen, can primarily be divided into two classes, positive and negative. In a direct replica of a surface, the surface topography of the replica is the reverse of that of the specimen; such a replica is a negative replica. A positive replica, i.e., one in which surface topography of specimen and replica are identical, can be made by making a direct replica of a negative replica. In both these techniques the surface detail of the specimen is revealed by shadow-casting (Williams and Wyckoff, 1946) after the replica has been made, i.e., they are post-shadowed replicas.

A much more accurate technique for revealing surface detail was introduced by Mahl in 1940. This was the pseudo-replica or the pre-shadowed replica. Here the specimen is shadow-cast in the usual manner and the resulting metal film transferred to a supporting film. Provided this supporting film is of low atomic number, then the structure observed is that which would have been observed if the original specimen had been of negligible thickness and had been shadow-cast and viewed in direct transmission. Although this technique is by far the best in that the precision of the replica is in no way governed by the structure of the replicating medium, it has several disadvantages. Firstly, the metal film is

very difficult to remove from the substrate, usually glass; secondly, the metal film granulates in the electron beam, and thirdly, any substance to be replicated must be easily extractable.

c) Replicating Media

The first materials used for producing replicas were plastics (Mahl, 1940) and, in particular, formvar (Schaefer and Harker, 1942). Substitutes were soon found, however, since organic polymer molecules, being usually large, cannot replicate fine detail. Furthermore, distortion is easily introduced both in stripping such a film from glass and in the electron beam during examination. More accurate replicas can be obtained by using evaporated silicon oxides and metal oxides, but these are fragile both on handling and during electron bombardment.

The most suitable substance found so far for preparing replicas is carbon. The method of preparation was first described by Konig (1951) and later Bradley (1954) developed a modified technique which was much more successful. Carbon is an ideal material since it has a low atomic number. Very thin almost structureless films can be made by evaporation and, provided spectroscopically pure graphite is used, such films are fairly robust.

The most accurate replicas are therefore made by using the pseudo replica technique and supporting the metal film with an evaporated carbon film.

Crystal Preparation

Regular crystals of a suitable size, i.e., easily visible under an optical microscope, magnification 150x, were prepared by allowing one drop of a cooled 1% solution of stearic acid in benzene to evaporate slowly. If the solution was not sufficiently cool, irregular crystals were formed. In all preparations both the B and C forms were obtained and no method was found for controlling the ratio of forms produced.

Replica Preparation

The major difficulty in the pseudo replica technique is in stripping the supporting film from the substrate, usually glass, on which the material to be replicated had been deposited prior to shadow-casting. A simple method of avoiding this difficulty is to grow the crystals on electron microscope mounts which have been covered with a thin film of collodion. This preparation is shadow-cast with nickel-palladium and carbon is then evaporated onto the surface. The collodion substrate is dissolved away during the extraction of the crystals leaving a pseudo-replica already mounted for examination. This method has the added advantage of selectivity in that crystals can be followed through all stages of preparation to final viewing in the microscope.

The backing film used in this investigation was of carbon mainly because of its reputation for durability. It was prepared by the method described by Bradley (1954) in which a current of 25 amps at 12 volts is passed through the tips of two carbon rods lightly pressed together, this being carried out at as high a vacuum as possible. The carbon was in the form of spectroscopically pure Acheson graphite which gave rapid evaporation and a tough film.

Extraction

The extraction stage proved the most difficult in that more specimens were lost in this stage than in any other. Both collodion film and stearic acid crystals had to be extracted. Amyl acetate was the first solvent tried primarily because of its effect on collodion films and the extraction was carried out in the vapour phase by suspending grids on a silver gauze in the vapour of boiling amyl acetate. A beautiful clean extraction was always obtained presumably because the boiling point of amyl acetate is far above the melting point of stearic acid and, hence, the crystals must melt during the extraction. Unfortunately, most specimens thus extracted were covered in a deposit of some electron dense substance, a typical example being shown in Plate 1. The origin of this deposit was traced to free acetic acid present in the amyl acetate giving rise to copper acetate

PLATE 1.

Shadowed carbon replica of crystal of C-modification
of stearic acid, illustrating deposition of copper
and silver acetate over specimen. (x8,000)



and silver acetate in combination with the copper of the specimen mounts and the silver of the gauze in the extraction apparatus.

This free acid can most easily be removed by washing with distilled water, the last traces of acid being removed after five washings. Subsequent drying with P_2O_5 gives pure amyl acetate. This does not remain acid free, however, if exposed to the atmosphere and as even slight traces of acid cause these dense deposits to form on the specimens, and as it is exceedingly difficult to remove the last traces of moisture from an organic solvent, the use of boiling amyl acetate as an extraction agent was discontinued. It was found that cold, dry amyl acetate remained acid free over a long period and extractions carried out by floating specimens on the surface of this solvent gave replicas showing only very slight traces of contamination.

Several other organic solvents, e.g., benzene, ether and acetone, were tried as extraction agents both in the vapour and liquid phases. In most cases, the extraction was inefficient and did not compare favourably with cold amyl acetate as the collodion film appeared fairly resistant to such solvents. The majority of extractions were therefore carried out using cold, dried, acid-free amyl acetate.

Electron Microscopy

All replicas were examined in a Philips E.M. 100 electron microscope at low magnifications, not above 2,500x. When higher resolution was required, for example, for accurate step-height measurements, the replicas were examined in a Siemens Elmiskop 1 at a magnification of 10,000x.

large areas and

the other was the region

of the growth of the

the other was the region

the other was the region

the other was the region

the other was the region

the other was the region

RESULTS

the other was the region

the other was the region

the other was the region

the other was the region

the other was the region

the other was the region

the other was the region

the other was the region

the other was the region

the other was the region

the other was the region

the other was the region

the other was the region

Growth Patterns

Although over one hundred replicas were made, only a small number were found to have areas exhibiting multi-molecular steps when examined in the microscope. The majority showed complex growth centres of the type shown in Plate 1, but these centres did not necessarily produce multimolecular steps. As large crystals, with steps visible in the optical microscope, were often observed before replication began, the loss of such crystals must be due to a fault in the technique. The weakest link in the preparative chain was probably the carbon evaporation stage. Here, slight misalignment of the specimen from its position normal to the carbon source could cause a sizeable gap in a film at the edge of a very large step. Although this gap would be partly filled by deflection of carbon from apparatus and bell-jar, this area at the edge of a large step could still remain a weak point in the film, the larger the step the weaker the area. It is therefore not surprising that, after prolonged extraction, the replicas of such areas had broken up. A method of overcoming this would be to rotate the specimen in the vacuum chamber while evaporation was proceeding.

Two of the many examples of growth patterns arising from complex dislocation centres are shown in Plates 2 and 3, in Plate 2 the crystal being of C-modification and in Plate 3,

PLATE 2.

Replica of crystal of G-modification, showing
typical complex growth centre. (x14,500)

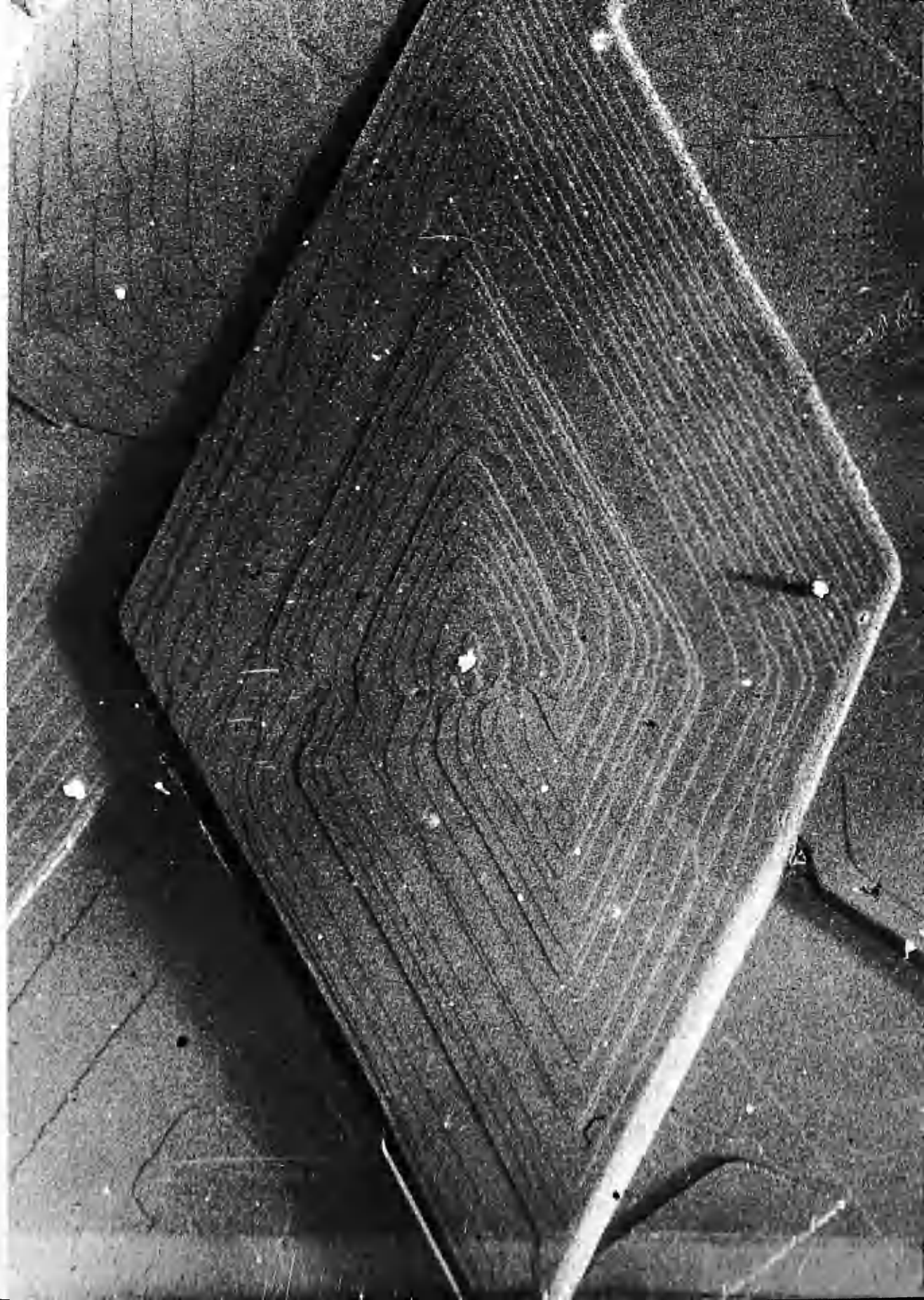


PLATE 3.

B-modification crystal. The growth pattern arising from the complex growth centre shows irregular bunching of the steps across the face of the crystal. These steps are serrated on one side of the bisector of the acute angle of the rhomb and smooth on the other.

(x21,000)



B-modification. In both cases there is an irregular spacing of the steps across the face of the crystal. This effect was common to all crystals with such growth centres and the only case observed of a fairly uniform pattern is shown in Plate 4. Here, there is an apparently four-fold dislocation centre with a fifth dislocation appearing to one side. An interesting feature of Plate 3 is the appearance of the steps which, on one side of the bisector of the acute angle of the rhomb, have a serrated appearance and, on the other, a smooth one. A more striking example is shown in Plate 5. This effect was reported by Verma and was attributed by him to the tilt of the molecule with respect to the basal plane. Figure 4 shows the crystallographic orientations of the B and C modifications.

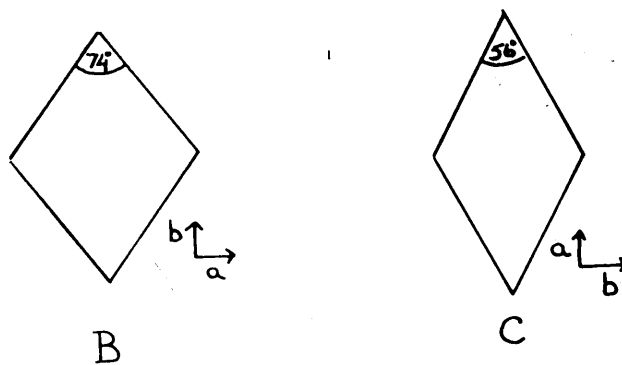


Fig. 4.

PLATE 4.

This replica of a crystal of the B-modification was the only example observed of a uniform growth pattern arising from a complex growth centre. (x12,300)

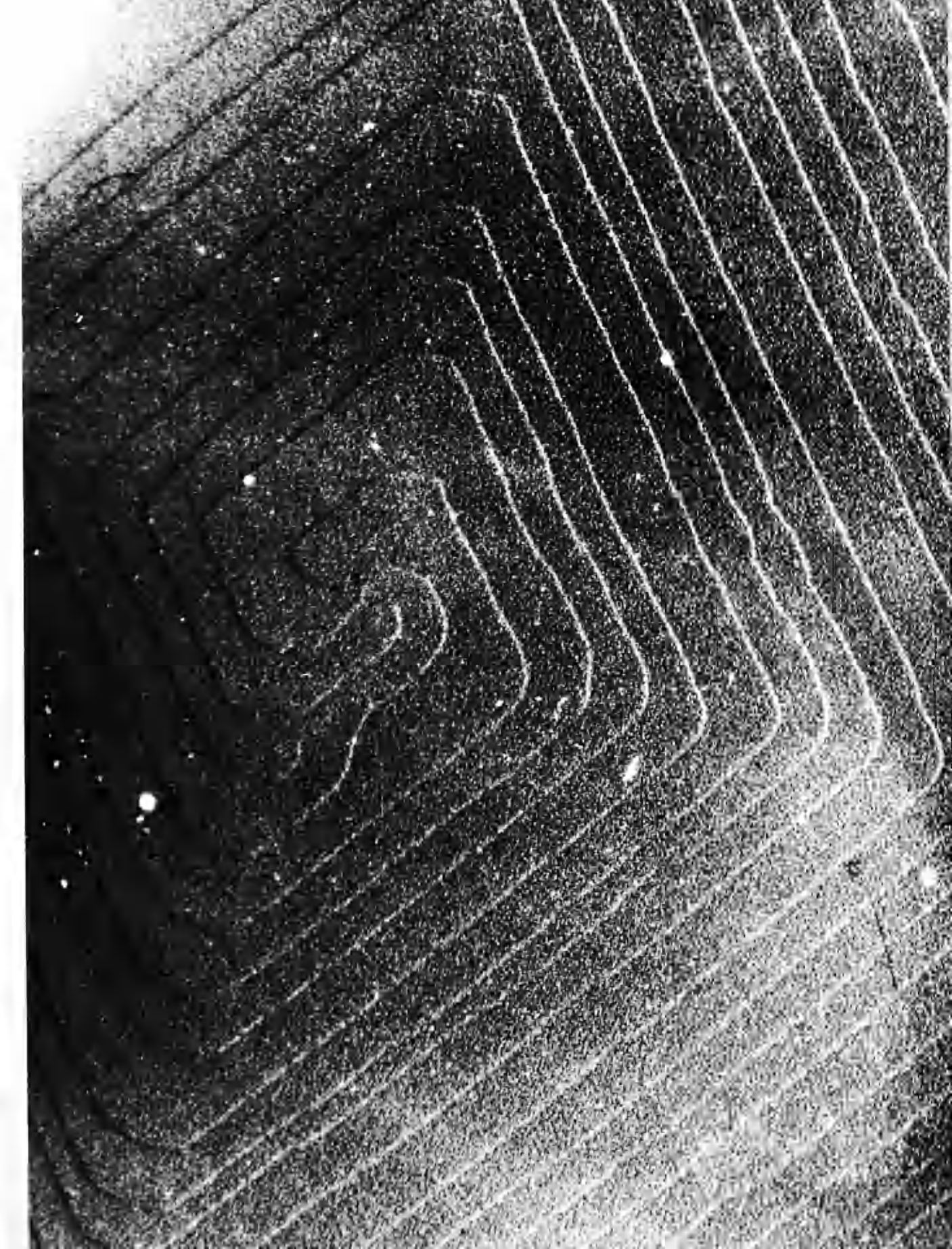


PLATE 5.

This micrograph clearly shows the different nature of the step edges on either side of the bisector of the acute angle of the rhomb.

(x17,300)



In the B-modification where the chains are tilted with respect to the a-axis, on one side of the b-axis, i.e., the bisector of the acute angle of the rhomb, the chains will make an obtuse angle with the basal plane and on the other side an acute angle. Step edges, even along (110) would therefore be expected to show different growth characteristics due to the difference in the solid angle available for the approach of condensing molecules. This is what is observed in Plates 3 and 5. In the case of the C-form, steps on either side of the obtuse angle of the rhomb should show this effect. An example is shown in Plate 6.

This differentiation in step etch enables an interesting deduction to be made from the growth pattern on the crystal in Plate 7. Here, the steps on the crystal, again of B-modification, are bunched in pairs. Consider these paired steps on either side of the bisector of the acute angle of the rhomb. In each case one of the steps of the pair is serrated and one is smooth and on crossing the bisector, the serrated step becomes smooth and the originally smooth step so serrated that it is almost invisible. There must therefore be a reversal of chain tilt as shown in Fig. (5).

PLATE 6.

In this replica, the crystal being of the G-modification, the nature of the step edges differs across the bisector of the obtuse angle. (x8,000)

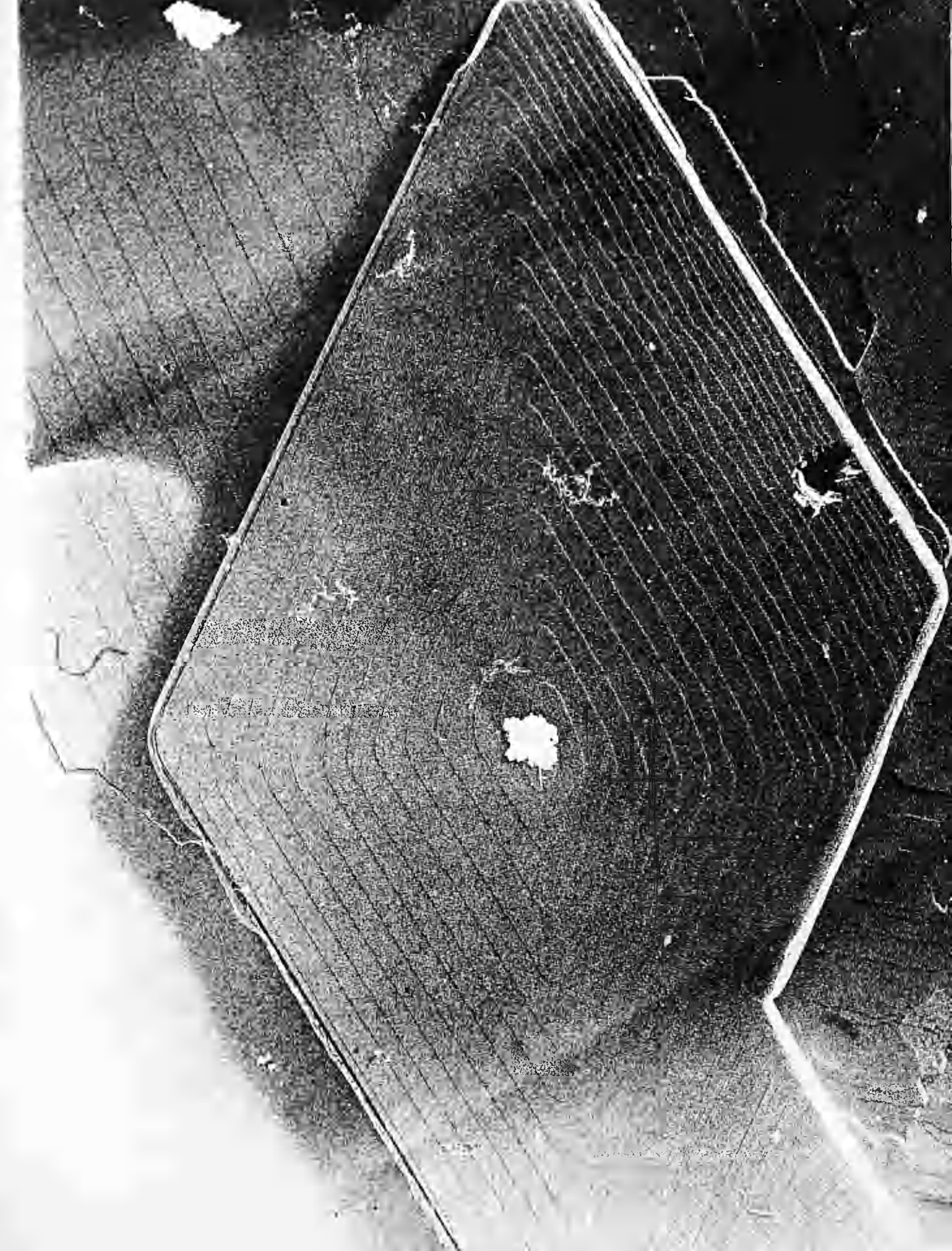
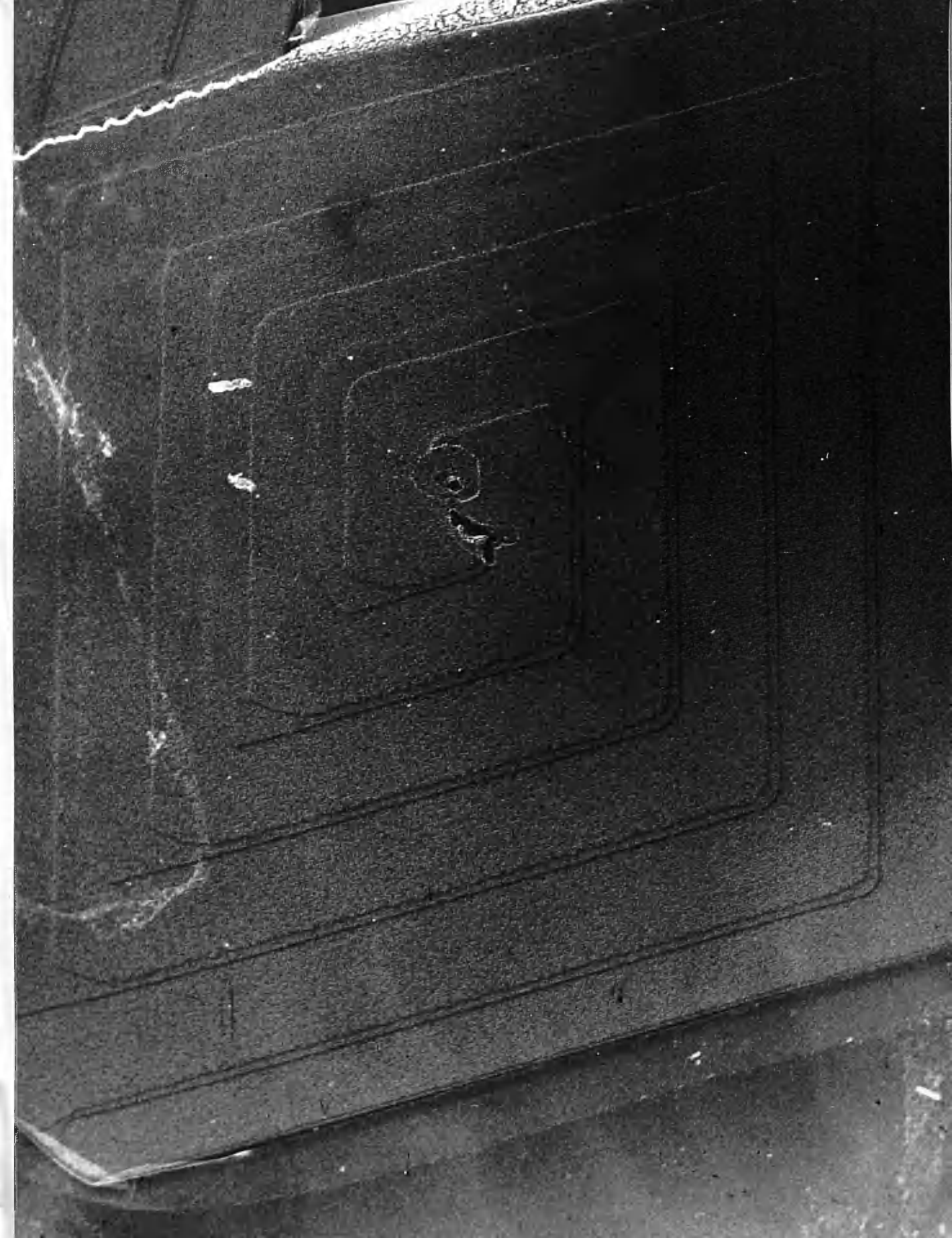


PLATE 7.

In this replica of a crystal of the B-modification the differential step etch is again obvious.

Here, however, one of the bunched pairs of steps is smooth while the other is serrated. (x12,700)



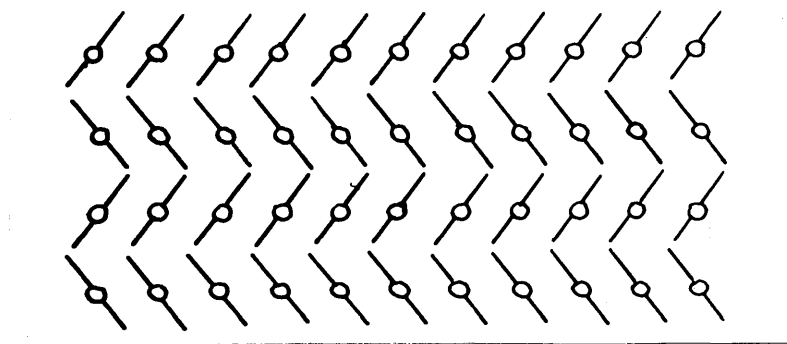


Fig. 5.

Multimolecular Steps

Although most of the replicas of crystals showing probable multimolecular steps were lost in preparation, a few were observed. Plate 8 shows an example of a B-modification crystal with two separate dislocation centres, one being of two dislocations of opposite sense, the other being the more usual single complex centre. This combination of growth centres gives rise to what appears to be several fairly large steps but, as the enlargement in Plate 9 shows, these multimolecular steps are clearly dissociated into smaller steps. A much larger crystal is shown in Plate 10 and here again there appear to be multimolecular steps, but here also, enlargement (Plate 11) shows them to be dissociated. A large crystal of the C-modification is shown in Plate 12. An artefact has here deposited on the steps and while this

PLATE 8.

Large crystal of B-modification showing apparently multimolecular steps arising from two distinct growth centres. (x3,200)

PLATE 9.

Enlargement of Plate 8. This clearly shows that even the step closest to growth centre is dissociated. (x10,400)

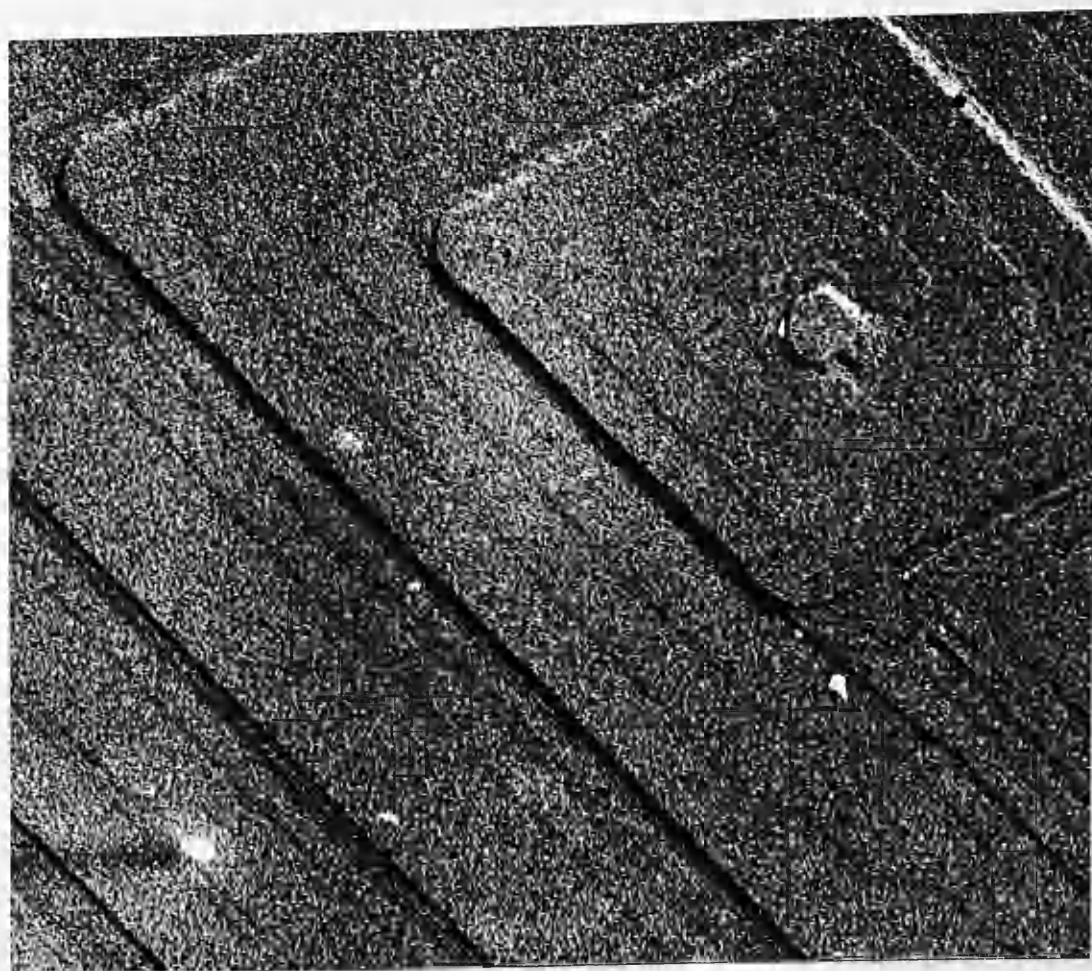
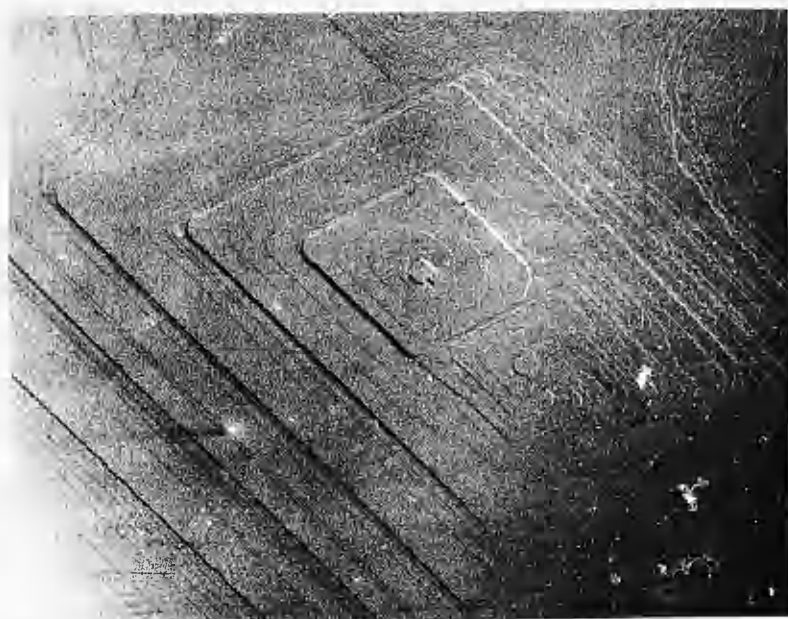


PLATE 10.

Large crystal of the B-modification with again apparently multimolecular steps evident. (x1,600)

PLATE 11.

Enlargement of small area of Plate 10. The multimolecular steps are all clearly dissociated. (x8,200)

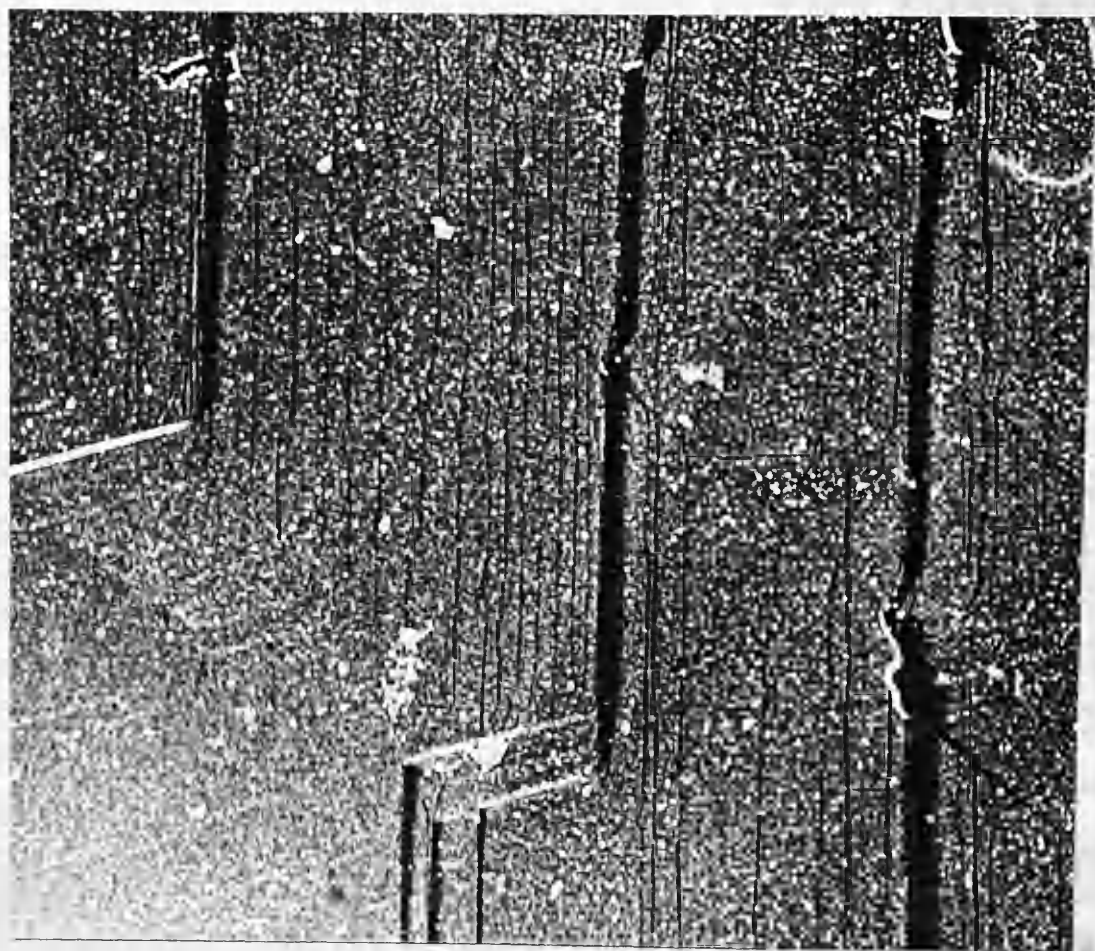
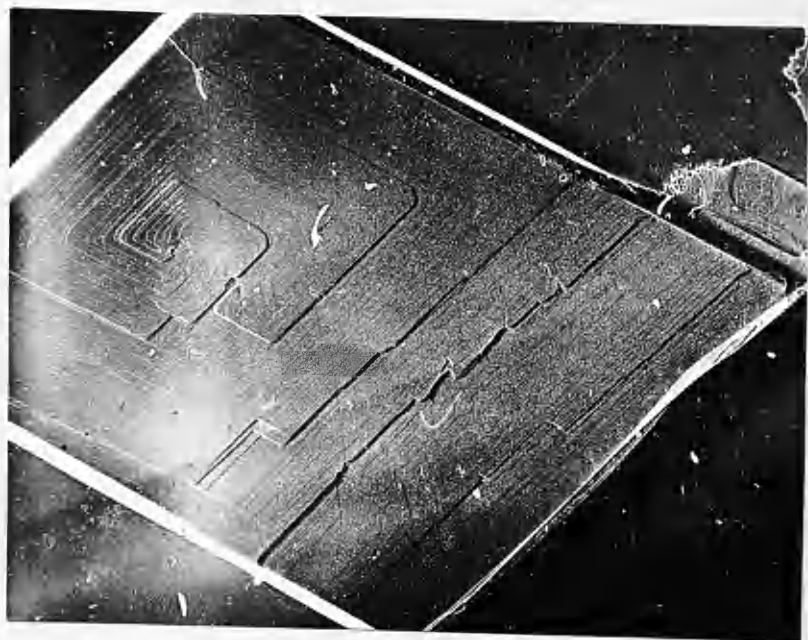


PLATE 12.

The growth pattern on this crystal of the G-modification is dominated by an apparently multimolecular single spiral step. (x1,600)



PLATE 13.

This enlargement of Plate 12 shows that the multimolecular step is again clearly dissociated. (x5,700)



outlines the growth patterns perfectly, in most cases it obscures the shadow-cast layer. What can be clearly seen, however, is that the step PQ which in Plate 12 appears multimolecular, is in Plate 13 a series of much smaller steps.

Step Height Measurements

As the main object of this investigation was to examine large crystals, the magnifications employed in the electron microscope were consequently as small as possible. The micrographs obtained were therefore useless for accurate measurements on growth steps. When such a measurement was required, the replicas were examined in the Siemens microscope at a magnification of 10,000x.

It was found that all clearly dissociated steps gave step heights which fell in the range $43 \pm 5\text{\AA}$. For the B and C forms, the $\frac{c}{\sin \beta}$ values are 43.76\AA and 39.85\AA respectively. The measured steps are therefore bimolecular.

Outgrowths

a) Geometry and Lattice Orientation

Although the observed number of replicas with entirely undissociated multimolecular steps in their growth patterns was small, large numbers of replicas were found to have one, or at most two, truly multimolecular, undissociated steps in a pattern which otherwise showed dissociation. An

example is shown in Plate 14. Here, a striking feature at the centre of the crystal is the very large incomplete step. Careful examination of the shadow, Fig.6, reveals another peculiarity of this feature - it must rise out of the crystal surface - although the shadowing also shows that at the point A in Plate 14 it is in contact with the surface plane. Cal-

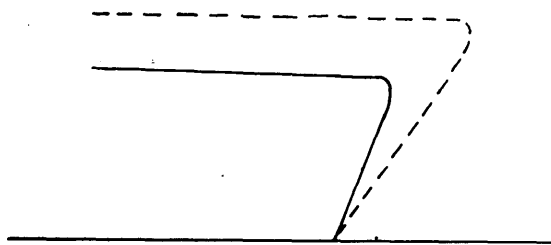


Fig. 6.

culations on the area of shadow illustrated in Fig.6 show that this area is rising at an angle of 13° out of the ab plane. Confirmation that these features are indeed rising out of the surface is shown in Plate 15 where one has been undershadowed, the step in this case being closed, and the angle of tilt being 11° . In these two cases, and in all cases observed, the edges of the outgrowths were parallel to those of the underlying lattice and the interfacial angles were identical to those of the underlying lattice.

PLATE 14.

This micrograph shows a crystal of the B-modification with an outgrowth arising at the centre and producing a very large step. The shadowing reveals that at the point A, the outgrowth is in contact with the surface. In the right hand corner, there has been a hold-up in the growth of the steps. (x11,200)

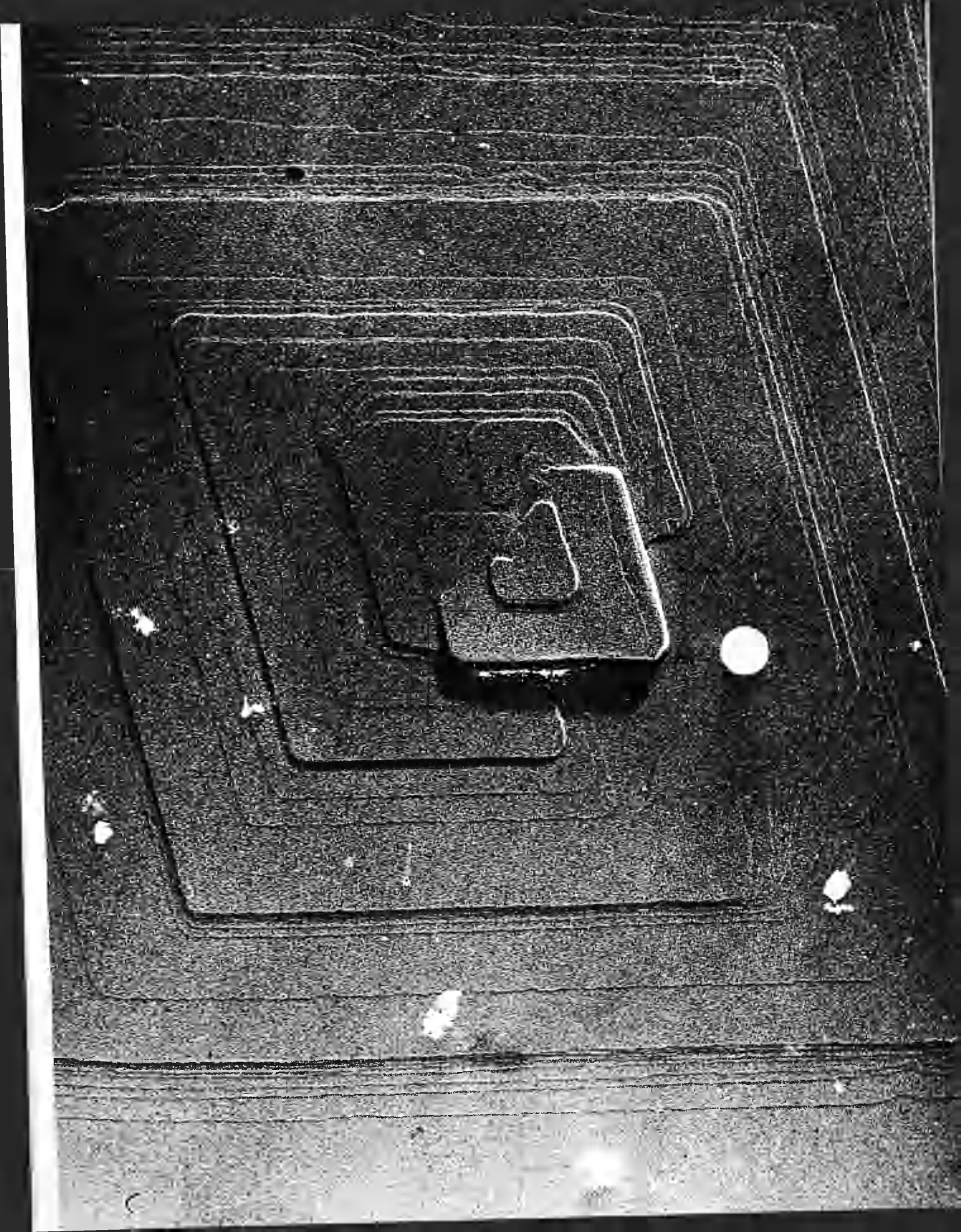
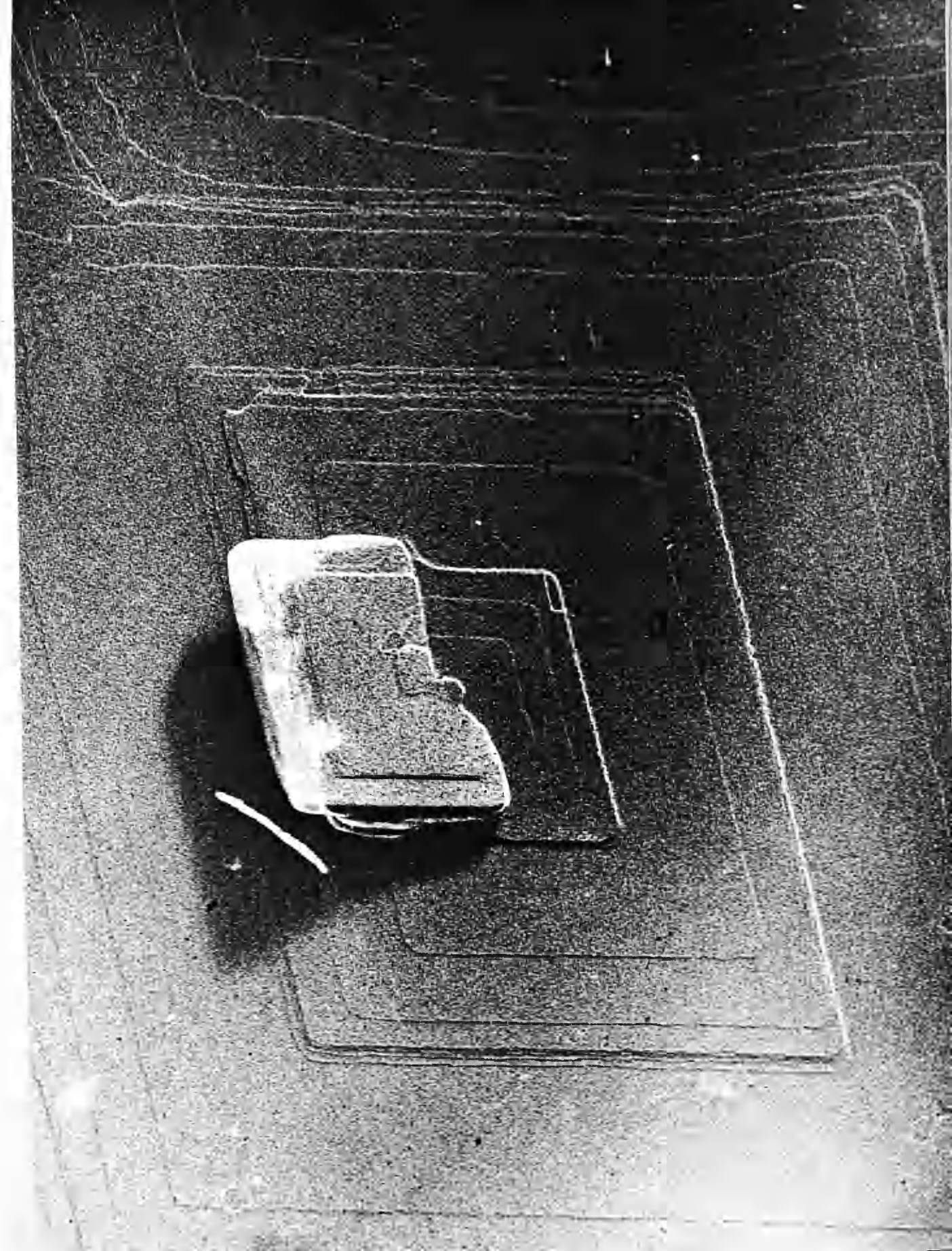


PLATE 15.

In this micrograph, the growth feature at the centre of the crystal has been undershadowed and must therefore be rising out of the crystal surface. (x13,000)



Plates 14 and 15 show different possible orientations of these outgrowths. In Plate 15 there has been growth on one side only of the b-axis, in Plate 14, on both sides, so that, in this case, the b-axis is the bisector of the acute angle of outgrowth. A similar example is shown in Plate 16, this being the largest angle of tilt observed, 14° , although here again the shadowing reveals that the outgrowth is in contact with the surface. These three examples of outgrowths are all at the centre of crystals and govern, to a certain extent, the growth pattern produced. Plate 17 shows that this is not always so, here the outgrowth appearing to have had little influence on the growth pattern produced by the underlying lattice. The replica in Plate 18 is included for two reasons; firstly, the outgrowth is growing in towards the centre of the underlying crystal; secondly, the outgrowth is rising out on either side of the a-axis in contrast to Plates 14 and 16. It is also noteworthy that the outgrowth here is in shadow - the angle of tilt must therefore be slightly greater than the shadowing angle of 15° . Most of the outgrowths were observed on crystals of the B-modification, but Plate 19 shows an example of an outgrowth on a crystal of the C-modification. This is the only example observed of two outgrowths arising closely adjacent to each other and growing in opposite directions.

PLATE 16.

This micrograph shows an outgrowth on a crystal of the B-modification. Growth has taken place on both sides of the b-axis. There has been condensation of molecules round the areas where the outgrowth joins the lattice and there is distinct discontinuity between the growth patterns on outgrowth and crystal. (x13,000)

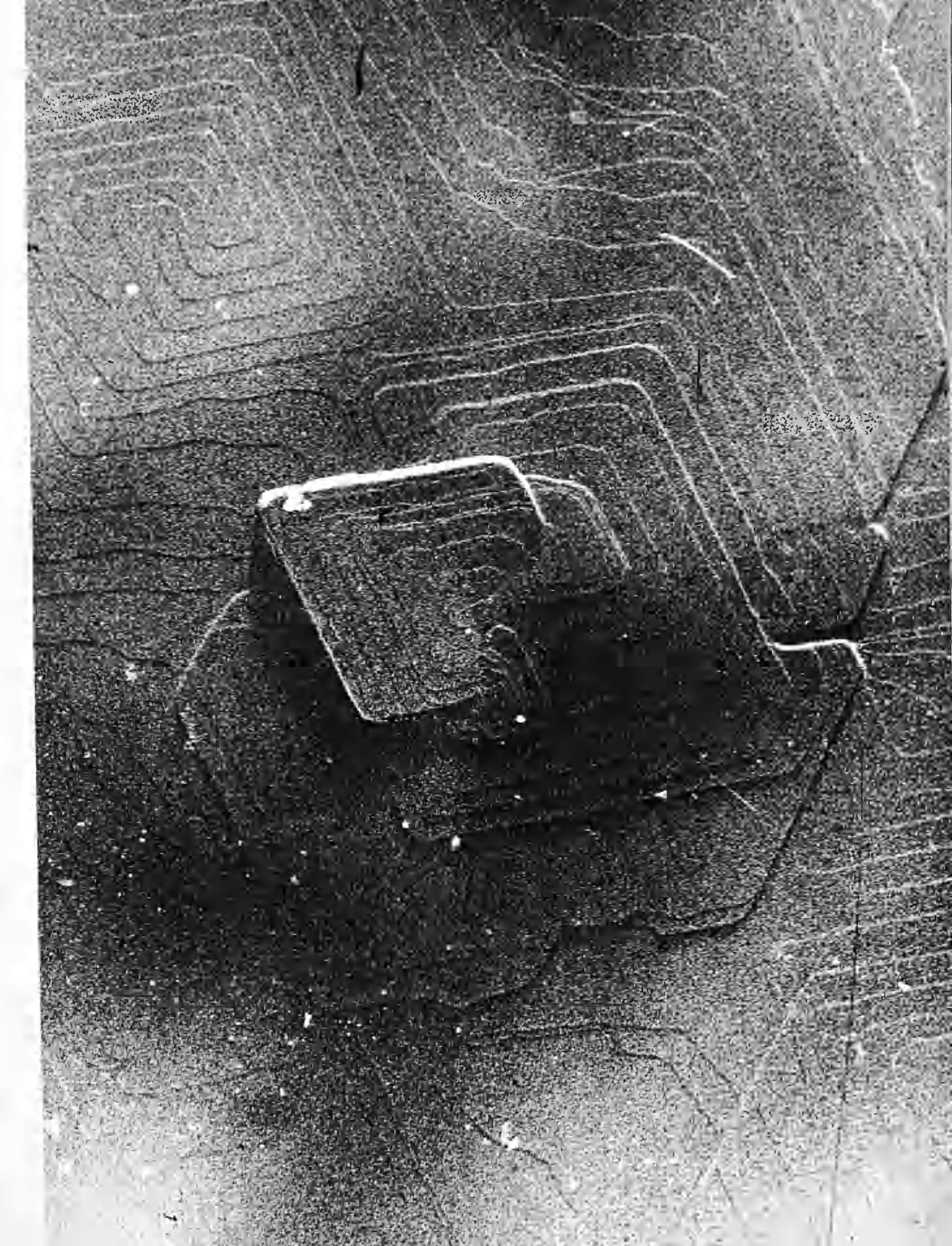
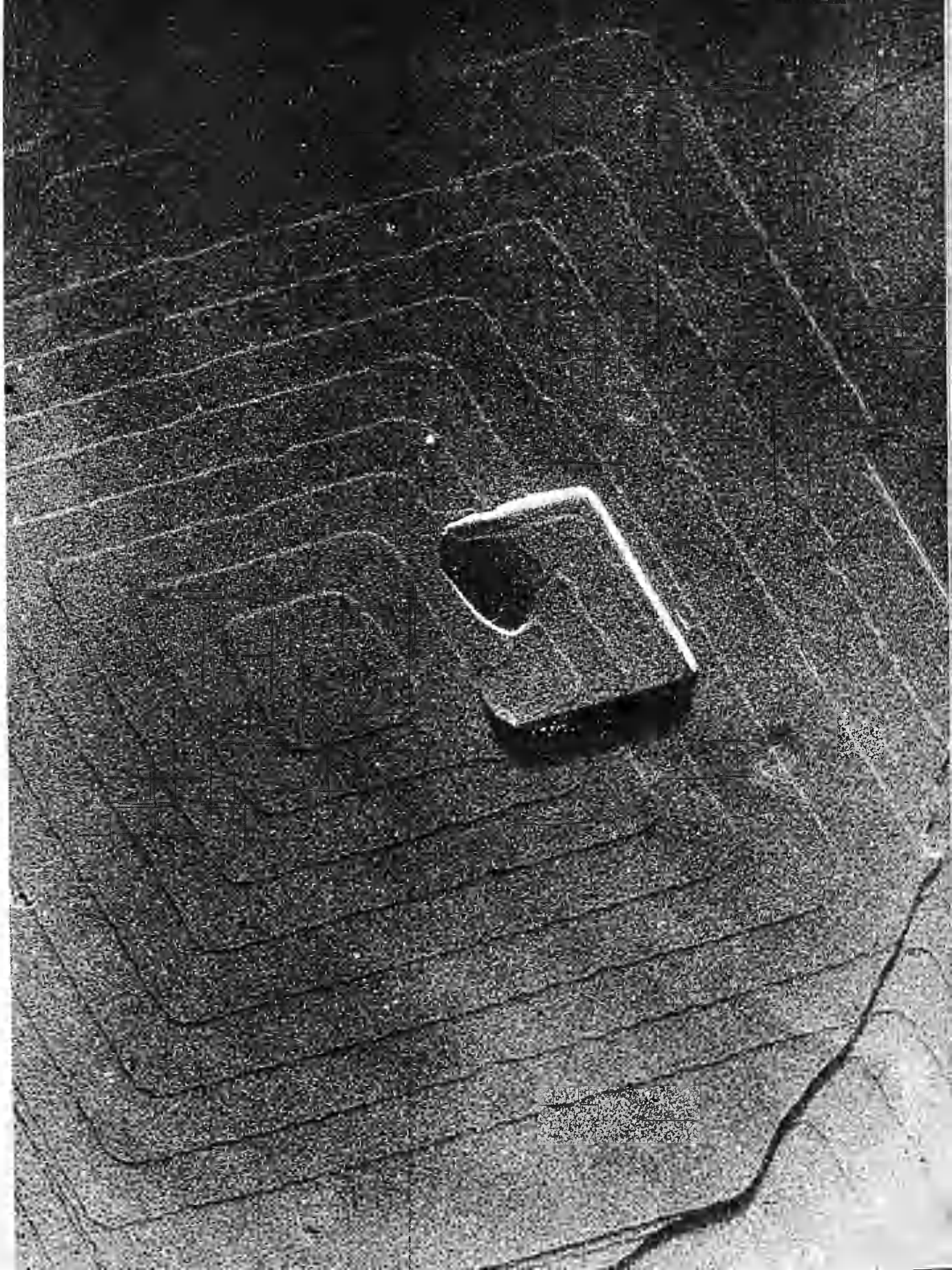


PLATE 17.

The outgrowth on this crystal has arisen on only one side of the b-axis and has, in this case, had a negligible effect on the growth pattern. (x17,200)



b) Influence on Growth Pattern

The most illuminating feature of the growth pattern surrounding the outgrowth in Plate 13 is the discontinuity in the symmetry in the right hand corner. This indicates that early in growth there was an obstacle to growth in this direction, the obstacle here being the outgrowth. The bunching of the steps in this pattern in groups of eight also indicates that there is a dislocation centre of this strength present. To produce such a pattern, the dislocation centre must be on the far side of the outgrowth from the dissymmetry in the pattern and, furthermore, to give rise finally to closed loops, there must have been two dislocations of opposite sense active.

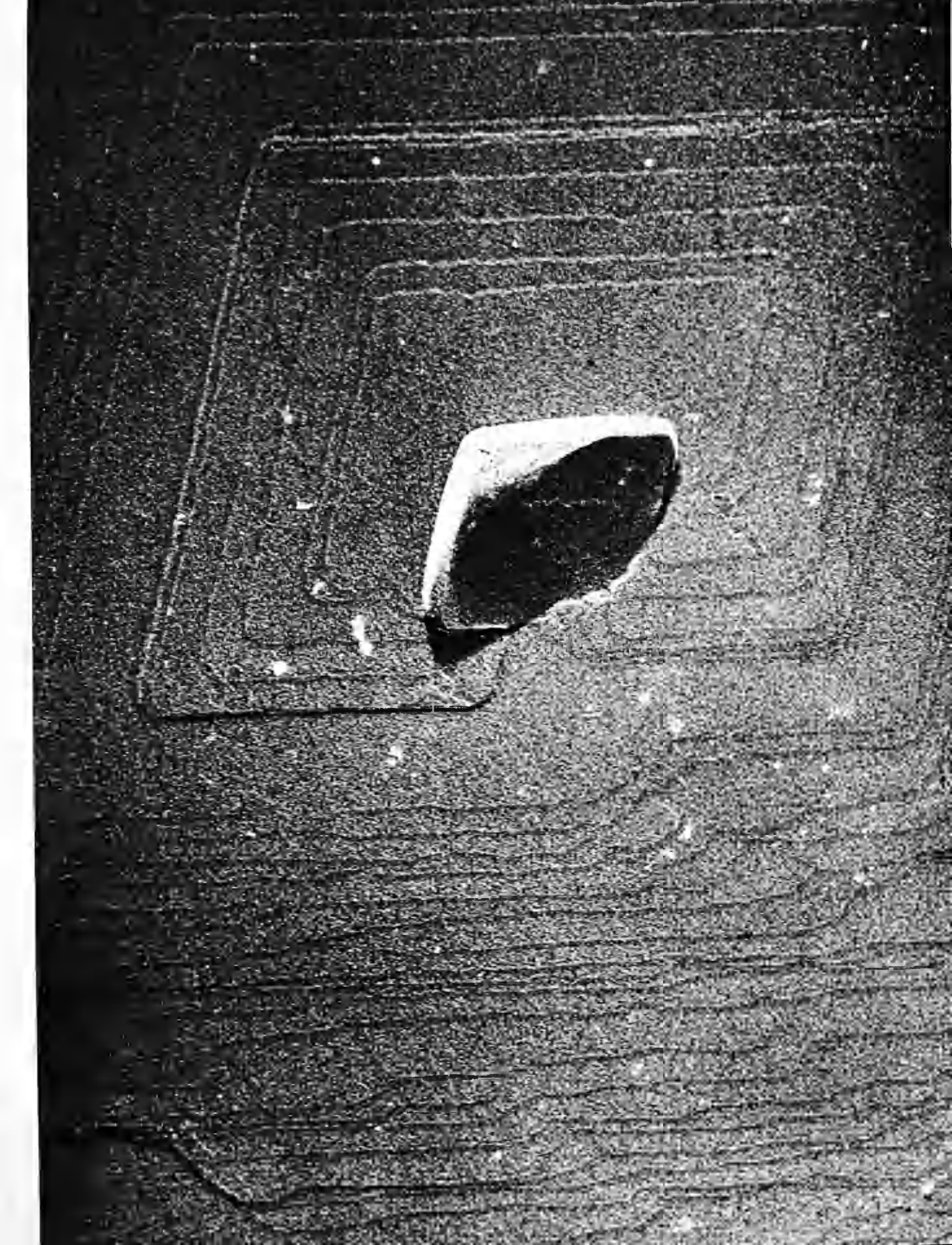
Illustrated in Plate 16 is another notable feature of several of these outgrowths; there is no continuity between the growth pattern on outgrowth and on underlying crystal. Similar effects can be seen on Plates 14 and 15.

Another interesting feature of Plate 16 is the condensation of molecules which has occurred round the areas where the outgrowth joins the lattice. Such effects are not observed on Plates 14 and 15, presumably because here large growth centres are active whose steps engulf those produced by the condensation sites and incorporate them in the crystal. Complete elimination of all traces of this condensation has also taken place in Plates 17 and 18. A

PLATE 18.

The outgrowth in this micrograph is unique in that it is growing in towards the centre of the crystal and has also grown on either side of the a-axis. A hold-up in the growth step pattern is evident in the right-hand corner.

(x15,400)



low magnification

Figure 19. A micrograph showing a crystal of the C-modification.

The crystal is surrounded by a layer of outgrowths.

The outgrowths are of the C-modification.

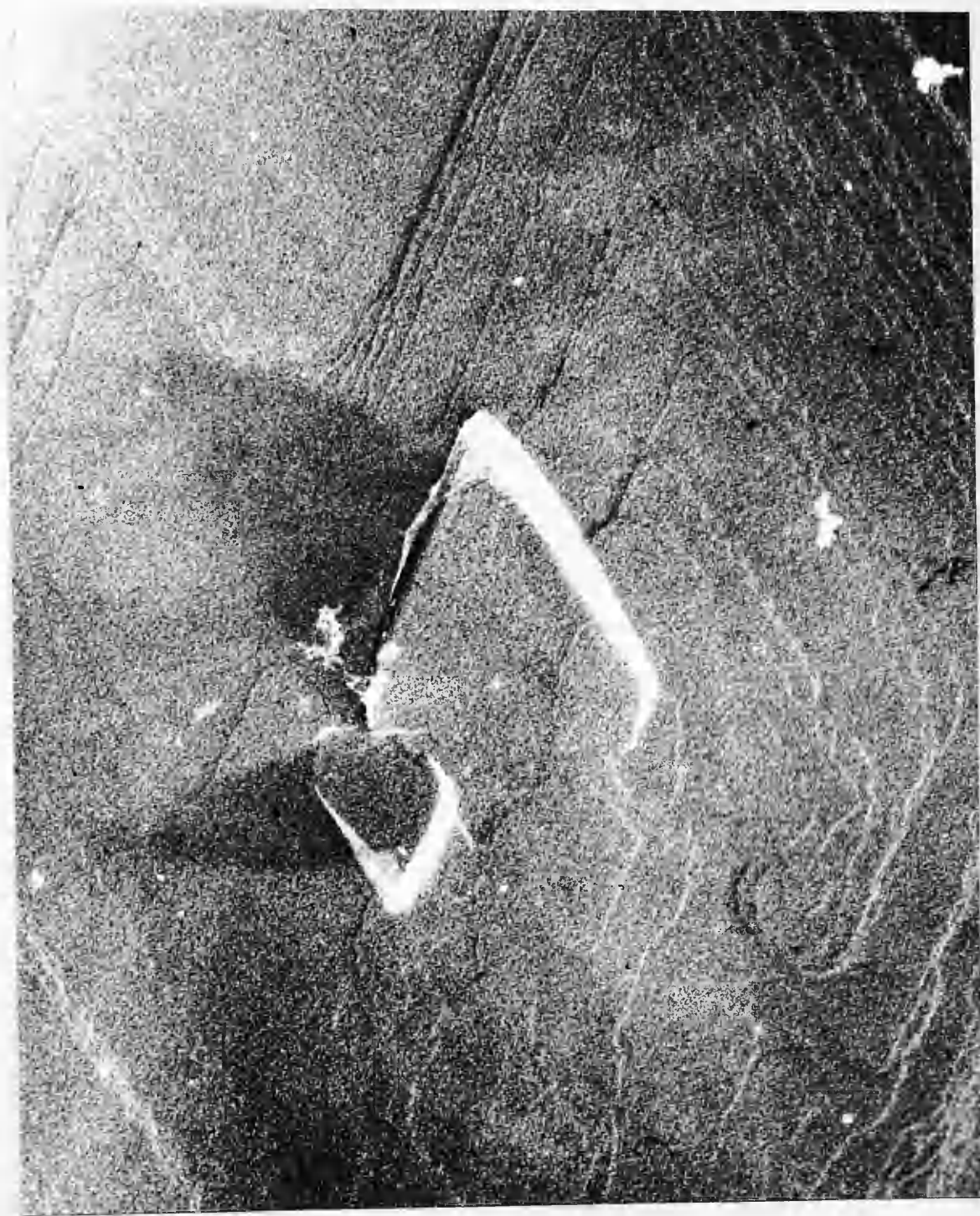
PLATE 19.

This micrograph shows one of the few examples observed
of outgrowths on crystals of the C-modification.

(x13,500)

possible explanation is that these outgrowths arose very early in growth and the condensation layers have thus been engulfed.

Plate 17 is remarkable in that there has been almost no delay produced in the growth pattern by the outgrowth. However, the shadowing shows that the central monolayer is completely circular indicating growth by surface nucleation not by spiral mechanism. Growth in regions beyond the outgrowth is not therefore entirely dependent on the arrival of steps from a spiral and hence there is little hold-up in the growth pattern. The obvious hold-up in Plate 18 and the flat surface of the topmost monolayer would tend to indicate that, in this case, growth was by two dislocations of opposite sense which, by collapse on to the substrate, cancelled out by the punch through effect described by Anderson and Dawson (1953).



1. Growth Centres

Although many of the replicas of the largest crystals were lost in preparation and the crystal replicas observed were not comparable to Verma's in size, the failure once again to observe truly multimolecular steps in the electron microscope would seem to indicate that in stearic acid, at least, multimolecular steps are not formed at an early stage in crystal growth and that, when formed by a secondary process at a later stage, begin to dissociate immediately into bimolecular steps. Excepting the replicas of outgrowths, even the largest spiral growth terrace observed (Plate 13) shows strong dissociation from the tip of the spiral to the edge of the crystal rhomb. All cases of growth arising from dislocations of smaller Burgers vector have produced steps which, although often grouped in bunches of two or three across the crystal face, are always clearly dissociated.

The majority of the growth patterns show step dissociation even at the growth centre, and where the steps are associated at the centre (Plate 3) these dissociate very quickly as growth moves outwards. The obvious conclusion is that the dislocation is itself dissociated, i.e., when formed, its exposed surface is not a single crystal plane.

Now, in large crystals, Frank has postulated that dislocations are formed by a buckling and subsequent slip in the lattice due to stresses in solution and non-uniform distribution of impurities. If such gross slip occurs in one plane then a single, multimolecular step will be produced on the face of the crystal. However, if the slip is spread over a series of planes, then a series of much smaller steps will be produced as shown in Fig.7. The growth pattern formed from this dislocation would be a series of regularly spaced concentric spirals, as, for example, Plate 4. Fig.8 shows the other possibility where there is an uneven spread of the slip over the lattice planes. Again a series of concentric spirals would be produced but, in this case, the steps would be irregularly bunched across the crystal face, as, for example, in Plate 3. Support for this view is given by the fact that almost all the growth patterns observed arose from a series of dislocations of the same sense. Similar growth patterns observed on carborundum by Verma (1951) were explained by Frank (1951) as being due to a similar mechanism to the one suggested above.

The staggered dislocation is necessary to explain the observed growth patterns, but the question now arises as to whether it is necessary only in the case of stearic acid or whether it can arise in the growth of any crystal.

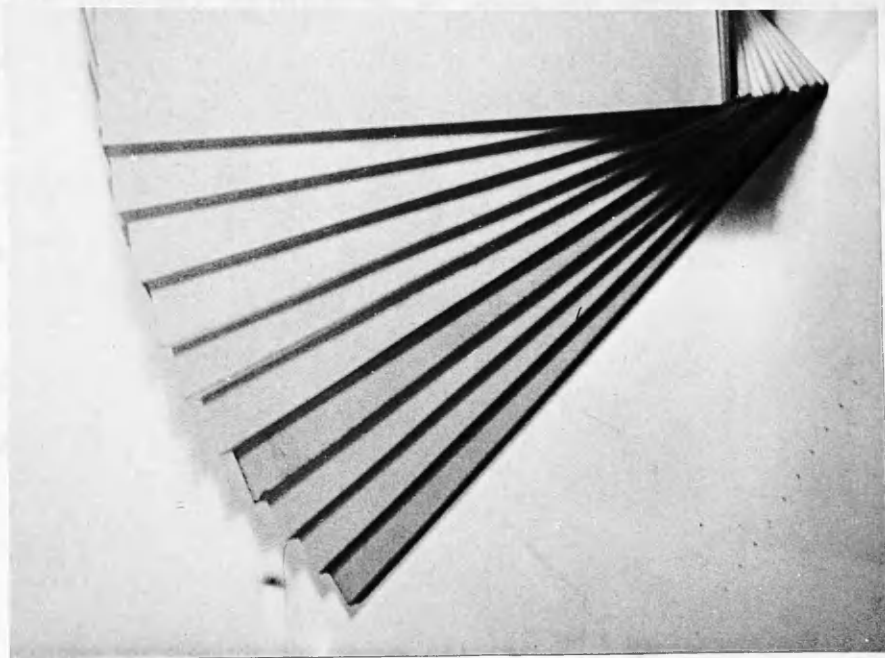


FIG. 7.

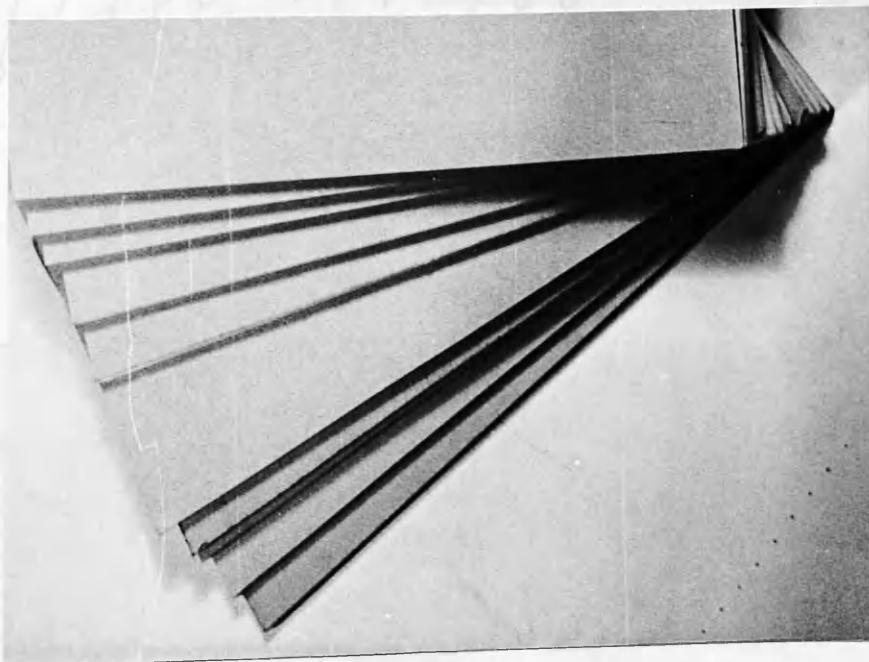


FIG. 8.

The crystal structure of stearic acid is governed, as has been discussed, by the size and position of the hydrogen bonded carboxyl groups. If gross slip occurred in the (hko) direction, as indicated by the arrow, it would be necessary for many of these groups to pass each other. However, if each group acted as a stop for the one above, then slip would have to be continued in an adjacent plane as illustrated in Fig.9.

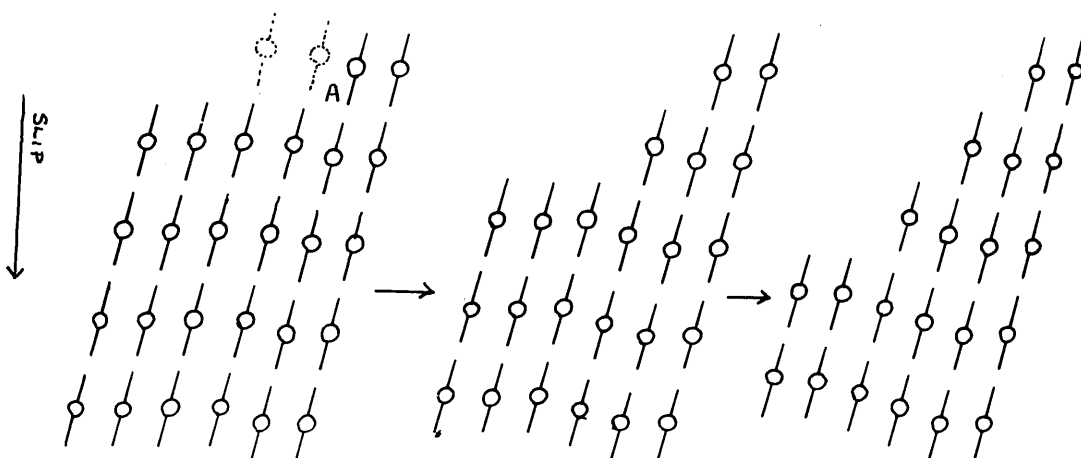


Fig. 9.

As this mechanism is assuming there is resistance to dimers passing each other, then, in the slip planes, these dimers must be aligned in twin positions to the unslipped lattice. This will have little effect on growth, however, as, after

the first dimer has condensed at position A, the lattice produced by further condensation will be identical to the unslipped lattice. Successive slips need not be in adjacent planes nor need there be any regular pattern in a gross slip. Staggered dislocations of the type shown in Figs.7 and 8 will thus be produced.

The mechanism suggested above therefore limits this type of growth to stearic acid and any other compound where there is resistance to slip. Since even only slight resistance is necessary because the slip would be expected to take the path of least resistance, this mechanism may be applicable to a large number of compounds.

Polytypism

Only one example of a crystal exhibiting a polytypic formation was observed, that shown in Plate 7. The growth step pattern here indicates an alteration in chain tilt in successive layers. Amelinckx's theory of the formation of polytypes in long chain compounds is therefore substantiated by this evidence. Amelinckx used optical techniques exclusively and was unable to observe fine differences in etch in growth steps, relying exclusively on growth rate measurements on growth patterns. This new evidence, therefore, confirms and supplements the earlier evidence.

2. Outgrowths

The outgrowths in Plates 13 to 19 are unique in that no similar features have been observed on any growth pattern on any crystal. Their three most outstanding properties are firstly, the fact that they grow out of the crystal; secondly, their thickness; and thirdly, their random orientation. Any proposed mechanism of growth must adequately explain these three characteristics.

a) Growth Mechanisms

(I). Twinning

As the edges of these outgrowths are exactly parallel to those of the underlying lattice and as the interfacial angles of both are identical, it would appear that the outgrowth is a twin of the original lattice. A twinning position which could give rise to outgrowths in a monoclinic lattice is shown in Fig.10.

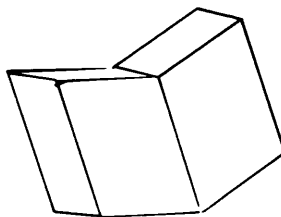


Fig. 10.

This mechanism can be rejected for two reasons. The angle of tilt, 52° would be much greater than any observed and the outgrowths would show preferred orientation, e.g., in the B-modification, the orientation would be as shown in Fig.11a with the a-axis the bisector of the acute angle of the outgrowing lattice.

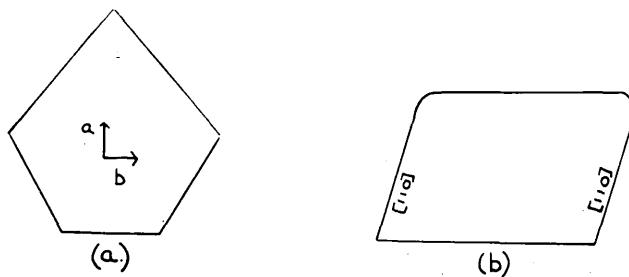


Fig. 11.

Only one example of this type was observed, in the remainder, the b-axis being the bisector. In addition, another type of outgrowth was observed, Fig.11b, indicating that the lattice change must take place along a diagonal and not an axis.

(II). Change in Modification

The way in which a monoclinic form may be derived from the basic orthorhombic lattice has already been discussed

and with a simple extension of Schoon's idea, it is possible to derive one monoclinic form from another or a triclinic form from a monoclinic form.

In a monoclinic lattice, the chains are tilted towards the a-axis, so that in the bc plane they are vertical. Application of Schoon's idea of displacement of chains to the b-axis will therefore produce a triclinic formation. Fig.12 illustrates how this can occur in the B-modification of stearic acid, the chain displacement being 1.26\AA .

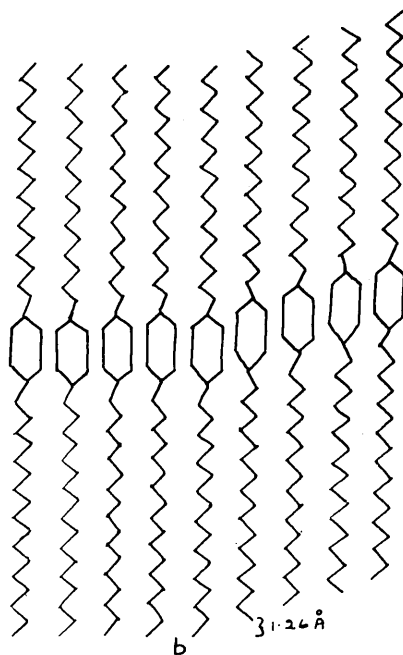


Fig. 12.

To maintain the symmetry of the adjacent chains, each dimer has to be rotated with respect to its neighbour. The angle of tilt of the outgrowth lattice is $9\frac{30}{4}^{\circ}$, a displacement of

1.26⁰Å being the only one to give an angle of tilt near the observed values.

b) Growth from a Diagonal

One reason for rejecting the twinning mechanism was that it involved growth from (010) or (100) rather than (110), the plane most commonly observed. This objection also applies to the above argument and should therefore be rejected. Before doing so, let us first consider what happens when growth takes place from a diagonal.

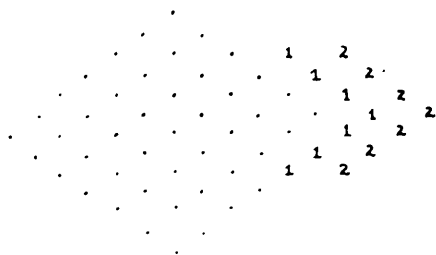


Fig 13

The figures (1) and (2) represent molecules in the first and second rows which have added on out of position. It is readily seen that such growth necessitates a change in stacking along the a-axis as well as along the b-axis. The way in which a displacement of 1.26⁰Å could occur along the a-axis is illustrated in Fig.14.

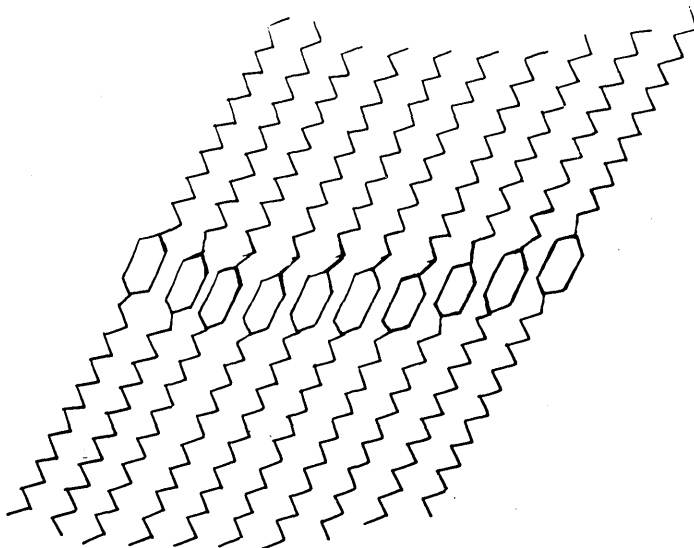


Fig. 14.

c) Angle of Tilt

As all measurements of angles of tilt on micrographs were made along diagonals, the theoretical calculations must also be made across the diagonal of the unit cell. In the B-modification of stearic acid, for a chain displacement of 1.26\AA along both axes, the calculated angle of tilt along the (110) direction is 14° agreeing well with the observed angles of from 11° to 15° .

d) Lattice Parameters of Outgrowths

Two objections can be immediately raised to the above mechanism. Firstly, the lattice parameters of the

outgrowths will differ from those of the underlying lattice and consequently the interfacial angles and the direction of the (110) planes should likewise differ. Now, in the electron microscope, the specimen is held perpendicular to the electron beam. The final image or diffraction pattern, therefore, gives no information on structure perpendicular to the surface of the specimen. What is viewed on the final screen is a projection of the specimen structure, in this case, a projection of the outgrowths. Hence, provided these outgrowths are derived from the underlying lattice simply by vertical displacement of the chains, then their projections will naturally have edges parallel to, and interfacial angles the same as, those of the original lattice.

The second objection is that when a dimer adds on to the obtuse angled side of a lattice of tilted chains, then the steric strain between adjacent carboxyl groups must increase. To answer this it is necessary to carefully consider why stearic acid only crystallises in monoclinic forms.

If stearic acid existed as an orthorhombic modification it would have parameters $a = 4.95$, $b = 7.42$ as shown in Fig.15.

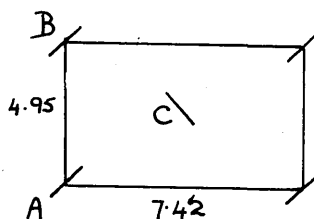


Fig. 15.

Now the position of closest approach is not between A and B but between A and C and is equal to 4.46\AA . Consequently, this must be too close for stable lattice packing. By tilting the chains, the distance AC is increased, e.g., in the B and C modifications $AC = 4.64\text{\AA}$ and 5.34\AA respectively. Although, therefore, it would appear that, by postulating addition at the obtuse angle, steric strain would occur, the corresponding tilt along the other axis will maintain AC at approximately its value in the original lattice.

It must be emphasised that, as the exact orientation of the tilted chains cannot be determined, it is not known how often, if at all, such addition occurs.

(III). Growth of Outgrowths

a) Extent

One remarkable feature of these outgrowths was the

distance they had grown out from the original lattice. For this to occur, condensation of molecules must have taken place on to the open edge of a lattice and not on to a hollow in a close-packed layer, and this is only possible very early in growth when the supersaturation is very high. Forty (1952) has produced evidence that dislocations arise late in growth, and hence these outgrowths should have an observable effect on the growth step pattern from the dislocations. Such an effect is indeed observed, all micrographs showing a delay in the step pattern indicating that the outgrowths arose before the dislocations.

Early growth on a crystal sheet, before the formation of dislocations, takes place by surface nucleation. In such a case, several nuclei are formed on the crystal surface and it is quite possible that misalignment of the molecules could occur approximately along a diagonal facing in towards the centre of the crystal or along opposite facing diagonals of two adjacent nuclei. This would account for the formation of the outgrowths in Plates 18 and 19.

On several micrographs, a discontinuity was observed between the growth step pattern on outgrowth and crystal. This is to be expected, however, if there has been an alteration in the lattice packing, as along the (110) direction, the packing in outgrowth and underlying lattice will be

slightly different giving rise to different growth rates along these directions.

b) Thickness

The one remaining problem, that of the thickness of these outgrowths, is readily explained. In extent, these outgrowths are, in most cases, relatively small compared to the size of the underlying crystal, an early limit to their size being put by the rapid fall in supersaturation during growth. Consequently, firstly, any heightening of the original crystal plate, although often not observed on our replicas, the crystal edges being outside the field of view in the microscope, will be evident on the outgrowth. Secondly, in a case where an active growth centre has arisen closely adjacent to the outgrowth, the total number of steps from the growth centre to the edge of the underlying crystal plate will be bunched into one large step at the edge of the outgrowth. The latter case is best illustrated by Plate 13, the former by Plate 16.

Another possible means whereby these outgrowths can thicken is afforded by the presence of the narrow angle between the outgrowth lattice and the underlying crystal lattice. This will act as a condensation site and there would seem an equal likelihood of molecules condensing on the outgrowth lattice as on the crystal lattice. Eventually,

when growth is proceeding by the spiral growth mechanism and the outgrowth has therefore ceased to increase in extent, the angle will become completely filled with condensed molecules both from direct condensation and from steps generated by a growth centre. This may not happen in every case, being dependent on the extent of the outgrowth, and thus several cases are observed where these outgrowths have been undershadowed.

c) Continued Growth

It is interesting to speculate on what would happen if growth continued beyond the point reached in this case. Presumably molecules would first condense at the edge of the multimolecular step which would therefore advance across the crystal face turning back on itself at the points where it joined the underlying lattice. Continued growth would generate a closed loop with an open multimolecular step on its surface. This is exactly what occurs when growth takes place from two dislocations of opposite sense and, indeed, growth features similar to those in Plates 13 to 18, but on a much smaller scale, can be seen at the centre of many of the growth patterns exhibited in the literature. This outgrowth, therefore, provides a spiral ramp from one layer in the lattice to, not the next layer, but to a surface thirty or more layers higher up. In so doing, it provides an

alternative to the Frank mechanism for the production of multimolecular dislocations and hence of multimolecular steps in the growth of crystals.

All outgrowths observed were at or near the centre of the underlying crystal and hence continued growth would generate a series of closed multimolecular steps. Only if an outgrowth terminated at the edge of the underlying lattice, as in Fig.16, would a multimolecular spiral step be generated by continued growth.

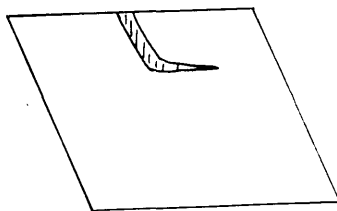


Fig. 16.

As these outgrowths can only increase in extent by condensation on to open lattice edges at high supersaturation, similar condensation must be occurring at the edges of the underlying crystal at the same time. Hence, while the outgrowth is rising from the surface, the underlying crystal is increasing in size laterally and thus crystals similar to Fig.16 will only be very occasionally produced. However, confirmation that such crystals are produced has been obtained

from the optical microscope, several examples having been noted in crystal preparations on glass slides.

The observation of these outgrowths on crystals grown on a glass substrate indicates that the outgrowths observed by replica methods were not caused by unique growth conditions introduced by growing the crystals on a collodion substrate on specimen mounts.

d) Cause of Outgrowth Formation

No growth features resembling these outgrowths have been reported on any compound examined under optical or electron microscopes. It would appear, therefore, that the lattice of stearic acid is especially suited to this type of modification. The distance of closest approach of two adjacent chains in the hypothetical orthorhombic form is 4.46\AA . In the B-modification it is 4.64\AA , and the C-modification, 4.95\AA . As the orthorhombic form is so markedly unstable as to be nonexistent, the B-modification with an increase of only 0.18\AA in the chain separation must just achieve a stable lattice packing of the carboxyl groups. Consequently, this form would be expected to show misalignment of adjacent chains much more frequently than the C-form, a fact confirmed by these observations, only very few examples of outgrowths arising from a C-modification crystal being found. Moreover, in the early stages of crystal growth,

when the supersaturation is high and molecules are arriving at lattice sites in large number, it is very probable that some will take up positions involving the least possible steric strain and hence give rise to outgrowths.

The displacement of $1.26\overset{\circ}{\text{\AA}}$ in the packing of the hydrocarbon-type chains, postulated as the mechanism whereby these outgrowths can rise out of a crystal, requires that each dimer in the new lattice is rotated with respect to its neighbour. Crystallographically there is no reason why this should not occur, and as the dimer molecules will be rotating in solution and as their condensation position will be determined more by the carboxyl groups than by the chain symmetry, there is also no objection from growth considerations.

Production of Dislocations by Impurities

A mechanism which is in some ways similar to the above has been proposed by Cabrera and Vermilyea (1958) for the production of dislocations in impure crystals. They suggest that bunching of steps could occur behind a region of greater than average impurity content and that subsequent overriding of the impurity by the entire bunching will give rise to a dislocation in the crystal. This has been illustrated diagrammatically in Fig.17.

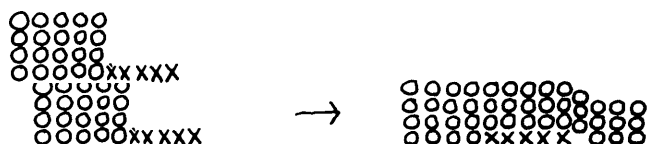


Fig. 17.

In the case of stearic acid the 'impurity' is much thicker, more extensive and self-produced.

Application to Other Compounds

Again the question arises, is this mechanism peculiar to stearic acid. It would seem, with the outgrowth being due to the symmetry of the hydrocarbon chains and the packing of the carboxyl groups, that it must be so, but nevertheless the twinning mechanism originally considered should be applicable to all monoclinic crystals. As more than half the crystal structures elucidated by X-ray analysis have monoclinic space groups, such a mechanism would have wide applicability.

PART TWO.

1911

Graphite

Structure

a) Single Crystal

Graphite was one of the first substances examined by the technique of X-ray analysis, but due to the difficulty in obtaining good crystals, its structure was not fully elucidated until the investigations of Bernal, and Hassel and Mark in 1924. The graphite structure and basal projection are shown in Figs.(1) and (2), the unit cell, outlined in red, having dimensions $a = 2.46\text{\AA}$, $c = 6.709\text{\AA}$ (Trzebiatowski, 1937). The regular, planar, hexagonal networks of carbon atoms, with C-C distance 1.42\AA , are not aligned perfectly in the c -axial direction but are displaced alternately so that an atom in one net is situated either over an atom in the net below or over the centre point of a hexagonal ring in the net below, as illustrated in the basal projection. An ABAB type of layer stacking is therefore produced. With a distance of 3.35\AA between layer nets any bonding can only be by very weak van der Waals forces and hence these layers can easily slip over each other accounting for the well-known lubricating properties of graphite.

To account for several anomalous lines in X-ray diffraction spectra of graphite, Lipson and Stokes (1942)

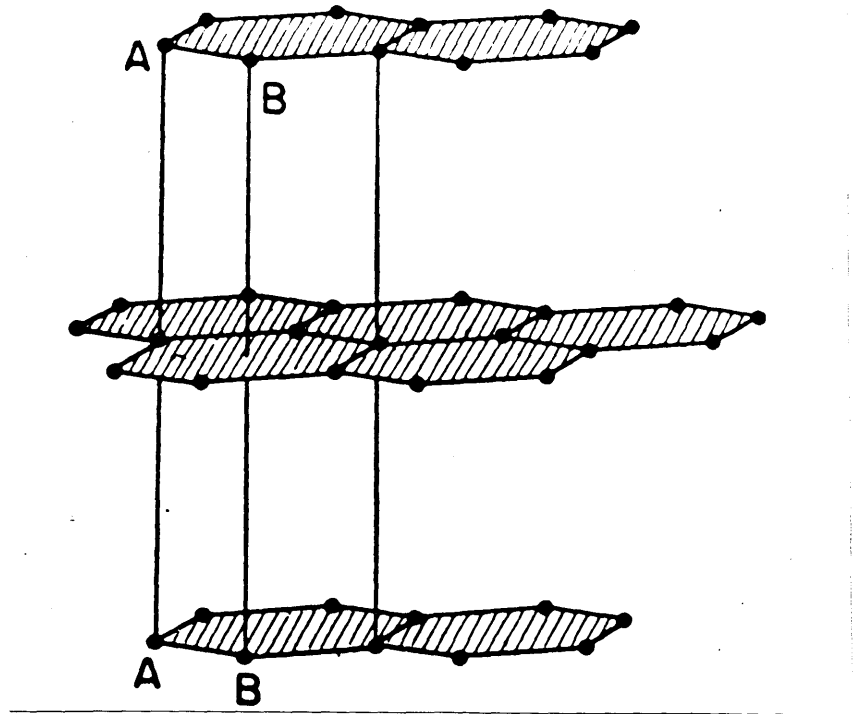


Fig. 1.

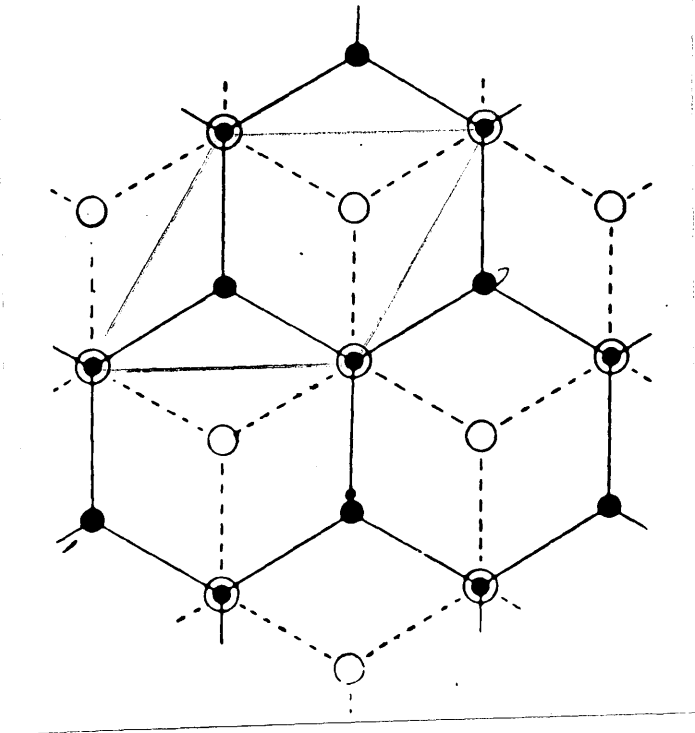
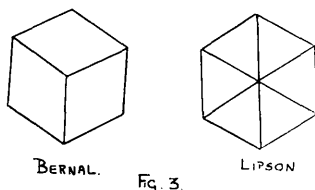


Fig. 2.

put forward an alternative structure which they suggested was present to the extent of 14% in ordinary graphite. The essential difference between the two forms is that Lipson and Stokes' structure has an ABCABC type of packing, the third hexagonal layer net being symmetrically related to the other two.



This is clearly illustrated in the basal projections in Fig.(3). The C-C distance and the interlayer distance are unaltered, the c dimension of the unit cell increasing to 10.064⁰Å. As it is possible to describe the structure in terms of a basic rhombohedral lattice, it is usually described as the rhombohedral form.

Natural Graphite

Single crystals of graphite are very rare, graphite in its natural form being a polycrystalline material. The dimensions of these crystallites vary from sample to sample,

a well crystallised sample having layers of diameter 74u and thickness many times this value.

Synthetic Graphite

During the past fifteen years intense interest has developed in the study of synthetic graphite. This is due to the use of thousands of tons of this material in nuclear reactors. All power producing reactors in use and under construction at the present time are graphite moderated. Almost all known physical properties of synthetic graphite have been evaluated under normal conditions and after irradiation and similar studies have been made on its reactions with the various gases used as coolants. In all this intense activity structural studies have also received attention.

The preparation of synthetic graphite is fundamentally the transformation of disordered carbon, in the form of coke, into its ordered, allotropic modification, graphite. This is done by baking coke together with a 'binder' such as pitch, at temperatures of up to 3000°C. The transformation and the relationship between the various grades of graphite have been studied by X-ray methods by Franklin (1951).

Carbons can be divided into two classes, graphitic and non-graphitic. Non-graphitic carbons have been defined by Franklin to be those whose diffraction patterns show only

(00 l) reflexions and two dimensional (hk) bands. These latter spectra indicate that the carbon contains small layer planes of graphite-like structure which are packed in parallel groups but are not otherwise mutually oriented, i.e., their structure may be defined as a 'random layer structure' (Biscoe and Warren, 1942). In these carbons the interlayer distance is constant at $3.44\overset{\circ}{\text{\AA}}$.

With increasing graphitization, the (hk) bands deform and (hkl) reflexions appear, indicating a three dimensional ordering in the lattice. This is paralleled by a gradual decrease in the interlayer spacing from $3.44\overset{\circ}{\text{\AA}}$, a fact first noted by Rooksby (1942) and first accurately measured by Bacon (1950). Franklin (1951) has shown that this interlayer spacing in graphitic carbons is a mean value, the groups of oriented and disoriented layers in the carbon retaining their own interlayer spacings of $3.35\overset{\circ}{\text{\AA}}$ and $3.44\overset{\circ}{\text{\AA}}$ respectively. Some perturbation of the disorientation spacing may be caused by the presence of the closely packed oriented groups resulting in the first disoriented layers on either side of each oriented group having an intermediate spacing. Bacon (1951) has suggested that in low graphitization samples there may also be a reduction in the spacing of the second layer adjacent to an oriented group. The packing of these different layers is shown in Fig.(4). It has been

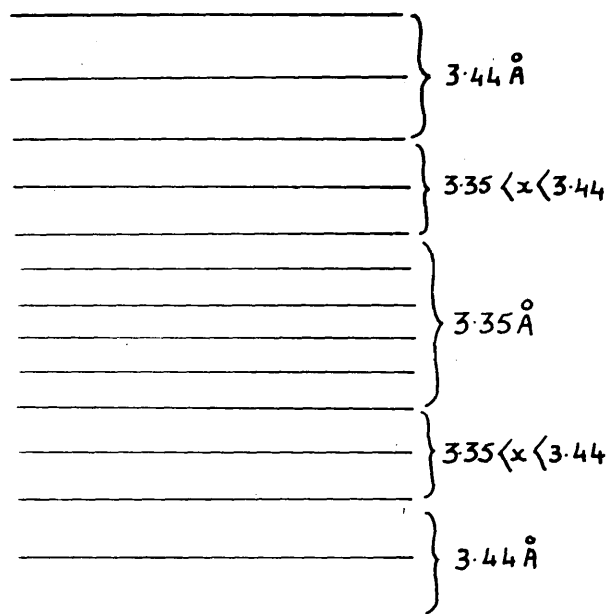


Fig. 4.

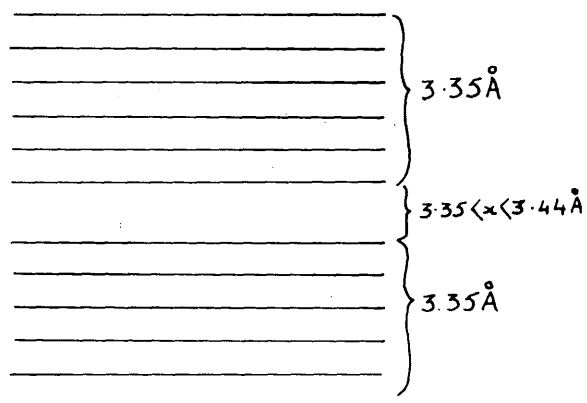


Fig. 5.

further postulated by Franklin that a doubly reduced spacing may be present between two oriented groups as shown in Fig.(5). The distribution of disoriented layers in a stack of parallel layers has been shown by Franklin and Bacon to be random.

As the decrease in interlayer spacing parallels the increase in graphitization, the difference between the oriented spacing of 3.35\AA and the observed spacing should be a measure of the proportion of disoriented material present. An equation, whereby the proportion of disoriented layers, p , present in any carbon can be evaluated, has been derived by Franklin and Bacon. For reactor graphite, p has a value of 0.16 (Bacon, 1957).

A study of synthetic graphite used in reactors has been made by Bacon and reported in a number of papers. In general, his powder photographs show several distinctive features. Firstly, the $(hki0)$ reflexions are sharp, indicating a large extension of the crystallites in directions parallel to the layer planes. Bacon reports an average crystallite diameter of 600\AA for reactor graphite. Secondly, the $(000l)$ reflexions are less sharp, the height of a group of parallel layers being therefore less than its width - 300 to 400\AA in reactor graphite. Thirdly, general $(hki\ell)$ reflexions are very diffuse. This is because in these 400\AA

stacks, there are random rotations between small groups of perfectly aligned layers as in Franklin's graphitic carbons. These misorientations occur, on average, once every six layers in reactor graphite and, as a result, increase the observed value of the interlayer spacing, giving the p value mentioned previously.

Pore Structure

a) Pore Volume

In synthetic graphite, the crystallites are not packed together in any regular pattern but are randomly oriented, and this distribution implies the presence of pores in the structure. Synthetic graphite has therefore an appreciable pore volume. This pore volume has been classified into two distinct categories by Dresel and Roberts (1953). Using organic liquid and helium gas displacement techniques, these workers found that 20% of the total pore volume calculated from X-ray data was inaccessible. They accordingly differentiated between what they called open pore volume and closed pore volume. Moreover, reducing the particle size of the synthetic graphite to 70 microns opened up an appreciable fraction of the closed space and they therefore concluded that the inaccessible pores must be widely distributed throughout the material. Accessibility was also improved by oxidation of the graphite at 430-500°C.

A similar result has recently been reported by Walker and Rusinko (1958); in their case, a closed pore volume of 20% in a total of 5.6% decreased to 9.5% on oxidation at 900°C.

b) Pore Size

Macropores

It is only recently that quantitative data has become available on the pore sizes in synthetic graphite. The results obtained by Loch, Austin, Harrison and Duckworth (1957), Walker and Rusinko (1958) and Walker, Rusinko, Rakszawski and Liggett (1958) show that synthetic graphites have an appreciable macropore volume at pore diameters between 10,000 and 100,000⁰Å. These are assumed by these workers to be pores between the original coke particles. Loch et al. found that only two of their graphites had appreciable volumes of open pores between 140 and 5⁰Å in diameter.

Micropores

It has been observed by several workers that although powdering synthetic graphite decreases the closed pore volume, there is always a certain volume completely inaccessible to even helium gas. These micropores have been defined by Loch et al. to be equivalent to "inaccessible voids". In an earlier paper, Loch and Austin (1956) reported that

the smaller the crystallite size, the higher was the closed pore volume. Subsequently, Loch et al. found that the micropore volume also increased with decreasing crystallite size, suggesting that the pores forming the closed pore volume and the micropores are the result of small separations between adjoining crystallites. From their data on micropore volume and crystallite size, Loch et al. were able to arrive at a value for the average space between crystallites, this varying from 3-15 \AA , agreeing with the fact that these micropores are closed to liquids and relatively inaccessible to helium gas.

Defect Structure

As X-ray analysis is essentially a statistical technique, it can provide no information on structural defects within each sub-crystallite. However, spiral hexagonal growth step patterns on natural graphite have been reported by Horn (1952), showing that screw dislocations exist in the graphite lattice. Furthermore, a method of revealing dislocations in natural graphite has been developed by Tsuzuku (1958) who, by etching large graphite flakes with silicon vapour at 2500 $^{\circ}\text{C}$, produced holes at reactive sites in the flake. Diffraction evidence showed these holes to be in the layer net planes. A dislocation density of $10^8/\text{cm}^2$ was estimated by Tsuzuku for his material as against $10^4/\text{cm}^2$ by

Horn. No evidence has been reported of dislocations in synthetic graphite, but the investigations of these workers, especially those of Tsuzuku, illustrate the importance of dislocations in the chemical reactivity of the material.

Reactivity

Although a large volume of data has been collected on the reactions of synthetic graphite with air, oxygen and carbon dioxide, under normal conditions, after periods of irradiation, at different gas flow rates, at various temperatures and pressures, etc., little attempt appears to have been made as yet to relate structure and reactivity.

Lattice Edges

Due to the microcrystalline structure of synthetic graphite and the presence of pores between the crystallites, a small but by no means negligible proportion of the surface atoms will be situated at the edges of the individual lattice planes. Such atoms are less strongly bonded than the majority and hence would be expected to be more reactive.

Now, carbon black has a structure in some ways similar to synthetic graphite, but much more disordered, and it has been shown by Smith, Thornhill and Bray (1941) and Emmett and Gines (1947) that carbon becomes porous on oxidation. This development of porosity they attributed to a preferential

attack of oxygen atoms on high energy sites on the carbon surface, these sites being associated with the edge atoms of the quasi-graphitic parallel layer groups composing the fundamental particles of the carbon black. A detailed investigation of the reaction between steam and carbon dioxide with charcoal led Long and Sykes (1948) to a similar conclusion, these workers further suggesting that two types of reactive site were present as illustrated in Fig.(6).



Fig. 6.

Type 1, with one orbital available for interaction with other molecules, is most likely to be found at the edge of the aromatic ring systems, while sites of the second type, capable of forming two extra bonds, are more likely in incomplete benzene rings, although a few might be present at lattice edges. Long and Sykes suggested that the former sites were specific to steam and the latter to carbon dioxide.

Basal Planes

In 1955, Amberg, Spencer and Beebe reported that graphitization of carbon black removed high energy sites from the surface, their conclusions being based on adsorption measurements. This was confirmed by Smith and Polley (1956) who showed that the surface of the graphitized carbon black was almost completely composed of basal plane structure which had a much lower reactivity than the ungraphitized material where a high percentage of the surface was composed of crystallite edges. A qualitative correlation between the reactivity of graphitized carbon plates and the fraction of the surface composed of basal planes was obtained by Walker et al. (1958), their results once again confirming that, compared to the crystallite edges, the basal planes have a very low reactivity.

That the results obtained from graphitized carbons also apply to natural graphite has been demonstrated by Hennig, Dienes and Kosiba (1958) in electron microscope and associated studies on natural graphite crystals. Although mainly concerned with irradiation effects, their paper did show that the basal planes in natural graphite were much less reactive than the lattice edges.

Object of Work

When this work was begun in 1958, all available information on the structure of synthetic graphite had been obtained from X-ray data. The object of this work was, therefore, to confirm this structure and to supplement it with information on the structure within the crystallites, inaccessible by X-ray analytical techniques. It was also hoped to obtain data on boundary width and distribution and on pore size and distribution. As the crystallite diameters measured by Bacon were only 600\AA , high resolution electron microscopy is the only technique which can reveal these crystallites in sufficient detail to allow study of their internal structure.

The Observation of Molecular Detail

The Need for Electron Microscopy

It has long been realised that the inability of the human eye to distinguish fine detail in optical microscopes was due, not to a defect in it or in the instrument providing the magnified image, but to the nature of the medium, light, used to image the object. The ultimate resolution obtainable in any optical microscope, no matter how great the magnification, is governed by the wave-length of light, the lower limit of resolution being around 0.2λ . To image

molecular structure, therefore, even in giant protein molecules, it is necessary to use an imaging medium with a wave-length more comparable to the dimensions of the structure being imaged. Such a medium was provided in 1897 with the discovery of the electron, beams of which can be focussed by electrostatic and magnetic fields in the same way as a glass lens focusses light.

In modern electron microscopes, the electron beam is produced by an accelerating potential of up to 100K.V. giving the electrons a wave-length of 0.05\AA . It should therefore be possible to directly observe lattice structure. At the present time, however, the highest direct resolution reported has been 6.9\AA by Bassett and Menter (1957). The reason for this wide discrepancy between the theoretical and practical values lies with the constructors and operators of the microscopes and not with the imaging medium. Only one type of electron lens can be made, a convergent type, and hence aberrations in an electron lens cannot be corrected as simply as in a glass lens. Nevertheless, the extension of vision produced by the rapid development of the electron microscope in the last thirty years, has resulted in major advances in the fields of biology, metallurgy and crystallography.

Molecular Resolution

Electron microscopy is a field dependent, probably more than any other in Science, on the development of new techniques, not only of instrumentation but also of specimen preparation. The first major advance in the latter category was made by Williams and Wyckoff (1946) with the introduction of shadow-casting. Using this technique, Markham, Smith and Wyckoff (1947) were able to observe for the first time individual protein molecules present in a tobacco necrosis virus crystal, the diameter of the molecule being 240\AA° . Similar studies have also been made on several other virus protein crystals, e.g., tobacco mosaic virus, the minimum molecular dimension observed in this case being 150\AA° .

A further example of the power of this technique was provided by Dawson and Vand in 1951 with their micrographs of single crystals of n-hexatriacontane, $\text{C}_{36}\text{H}_{74}$. Not only did their results confirm Frank's screw dislocation theory of crystal growth, but they also showed that it was possible to resolve on the surface of a crystal, growth steps corresponding to the length of one molecule. Since that time shadow-casting has been used both directly and indirectly via pseudo-replica techniques, to reveal finer and finer detail, until recently Bradley (1959), with a modified

technique, has resolved a step of 6\AA height on a sucrose crystal.

Direct Lattice Resolution

The next important break-through in electron microscopy was an instrumental one, the development of the Siemens Elmiskop 1, with a resolution better than 8\AA . With this instrument, Menter (1956) showed that it was possible, but only in very specific instances, to resolve lattice planes in a crystal. For this to be attained, certain rigid conditions must be fulfilled. Firstly, the crystal must be extremely thin; secondly, the planes to be resolved must be almost parallel to the electron beam; and thirdly, the planar spacing must be within the resolution of the instrument. All these conditions can be satisfied by platinum phthalocyanine crystals where the $(20\bar{1})$ planes with spacing 11.94\AA lie in a suitable orientation for diffraction.

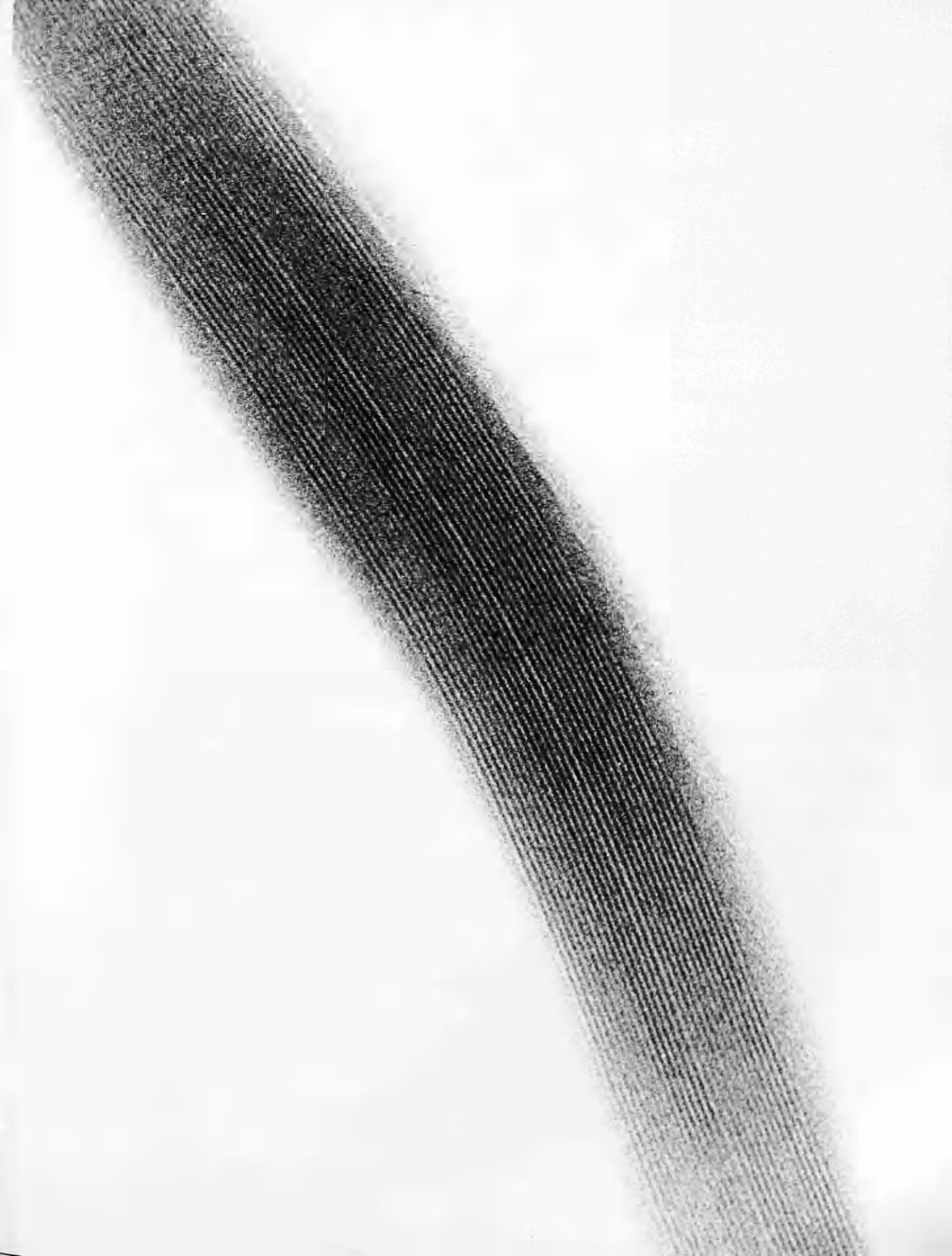
Menter's micrographs of the needle shaped crystals showed a series of regularly spaced lines parallel to the long axis of the needle and with spacing 12\AA , comparing very favourably with the $(20\bar{1})$ spacing. Of just as great importance as the magnitude of the resolution was the fact that these images revealed for the first time edge and screw dislocations in lattice planes.

The isomorphous copper compound was also examined by Menter and, in this case, planar spacings of $10.3 \pm 0.3\text{\AA}$ and 13\AA were observed. An exhaustive study of the various modifications and crystal habits of copper phthalocyanine was carried out by Suito and Uyeda (1957), who reported several possible spacings, the most common being the (001) and (20 $\bar{1}$) with dimensions 12.6\AA and 9.63\AA respectively. A micrograph similar to those of Menter and Suito and Uyeda is shown in Plate 1, the crystal being the β modification of copper phthalocyanine. The spacing is here 12.7\AA approximating to the (001) spacing resolved by Suito and Uyeda.

Although these compounds contain a heavy atom, it was suggested by Menter (1956) that this was not a necessary condition for resolution. This was confirmed by Labaw and Wyckoff (1957), who observed periodic lines on crystals of indanthrene scarlet R, an indanthrene dye. As no X-ray data on this compound was available, crystallographic indices could not be assigned to the imaged planes. Further proof that heavy atoms are unnecessary for lattice resolution has been afforded by a paper by Dawson and Watson (1959) on crystalline ribonuclease. In this case, a periodic spacing of 18\AA was observed which could be related to the amino acid residues present in the crystal.

PLATE 1.

Transmission micrograph of thin crystal of the β modification of copper phthalocyanine. A spacing of 12.7\AA has been resolved corresponding to the (001) planes. (x1,210,000)



Limitations on Lattice Resolution

Of the three conditions stipulated by Menter for resolution of lattice planes in platinum phthalocyanine, the most important, when considering further possible compounds, is that concerning the orientation of the planes to be resolved. Many compounds have prominent planar spacings greater than 6\AA , but it has proved impossible to grow such crystals thin enough, and to deposit them on a microscope specimen mount in a suitable orientation for resolution. Before the potential of high resolution microscopes can be fully exploited, therefore, a goniometer specimen stage will have to be developed.

Indirect Lattice Resolution

The Moiré Pattern

Crystals of a great variety of chemical compounds can be prepared thin enough and small enough for examination in the electron microscope. Provided such crystals are stable under bombardment by the electron beam, useful information on lattice dimensions and structure can often be obtained from selected area diffraction patterns. Only in compounds of the type mentioned above can further information be obtained directly. However, in recent years, a classical technique has been applied to give indirect information on the

lattice structure of such crystals. This is known as the 'moiré magnification' technique. Moiré patterns are familiar optical phenomena and occur when any two regular arrangements of diffracting material are rotated through a small angle with respect to each other. These arrangements may be series of lines, systems of dots, meshes, such as silk, etc. Interference effects then produce an 'image' which has exactly the same arrangement as the component material but a much enlarged periodicity.

In 1948, Green and Weigle realised that crystals, with their regular atomic arrangements, would provide ideal components for the formation of moiré patterns and hence, that it would be possible to 'image' individual atoms in the electron microscope. It was not until 1951, however, that a moiré pattern was observed in the electron microscope and it was not until 1958 that the possibilities of the technique were fully realised and utilised by Bassett, Menter and Pashley. In the intervening years, moiré patterns were regarded more as curiosities than as aids to lattice resolution.

Historical Development

Rotational Moiré Patterns

The first interference fringes observed in the electron microscope were reported by Mitsuishi, Nagasaki and

Uyeda (1951) in an examination of graphite crystals. They interpreted the fringe pattern as being due primarily to the presence of a wedge angle between two pieces of overlapping crystal, this permitting a diffracted beam from the first crystal to be diffracted again in the opposite sense by a different set of lattice planes in the second crystal. Under such conditions it is possible to produce a doubly diffracted beam which is almost parallel to the undeviated beam. Interference between these two beams was suggested by Mitsuishi et al. to be the cause of the observed fringes. An explanation also involving double diffraction was put forward by Seki (1953) as to the origin of fringes on sericite, this author showing conclusively that the fringes arose from two overlapping crystal sheets, rotated with respect to each other. That fringes on crystals were similar to moiré patterns was first suggested by Hillier (1954) who observed fringes on iron oxide and suggested that they represented regions of matching and mismatching between two rotated overlapping crystals. This problem of the interpretation of fringe patterns on electron micrographs was finally resolved in 1956 by Dowell, Farrant and Rees. These workers showed that neither double diffraction nor a moiré effect was solely responsible for the production of fringe patterns but that both were combined, the fringes being

indeed moiré patterns whose production was dependent on double diffraction. From purely crystallographic considerations, Dowell et al. derived a relationship between the fringe spacing, S , the lattice spacing, d , and the angle of rotation, α , showing that $S = \frac{d}{\alpha}$. Hence, even a lattice spacing of 1\AA will become resolvable if it is overlapped by a second lattice rotated through an angle of 0.1 radian.

Although applicable to any crystal stable in the electron beam, this technique of indirect resolution has been of limited value since no technique has been devised for accurately placing and rotating one crystal over another. All moiré patterns, produced by rotation, reported in the literature are due to fortuitous overlap of two or more crystals.

Parallel Moiré Patterns

In 1957, Pashley, Menter and Bassett showed that a moiré pattern could be obtained from two overlapping lattices in parallel orientation if the lattices had a small difference in spacing. The relationship between the spacing S , of this parallel moiré pattern and the spacings, d_1 and d_2 of the contributing lattices is given by

$$S = \frac{d_1 \cdot d_2}{d_2 - d_1}$$

In this case, provided $d_2 - d_1 \ll d_2$, the fringe spacing, S , will be within the resolution limits of the microscope and the lattice will be indirectly resolved. Specimens exhibiting this phenomenon can be prepared by evaporation of one metal onto another and, in this way, Bassett, Menter and Pashley (1958) were able to study the atomic array in metal lattices.

Imaging of Dislocations

Although of great theoretical interest, moiré patterns had little real practical value until in 1957 Hashimoto and Uyeda, using overlapping copper sulphide crystals, and Pashley et al., using parallel moiré patterns from metal crystals, showed that the extra terminating half-plane associated with an edge dislocation could be imaged in the moiré pattern. In their 1958 paper, Bassett et al. pointed out that screw as well as edge dislocations are made visible as extra half-lines. Moiré patterns, therefore, provide a means of studying dislocation density and distribution in crystal lattices whose spacings are well below the resolution limits of present day electron microscopes.

Formation of Moiré Pattern

Geometrical

The simplest illustration of the formation of a moiré

pattern is shown in Fig.(7) in which two line gratings have been rotated through an angle, their matching and mismatching producing the fringe pattern AB etc. From such a simple geometrical illustration the direction of the moiré fringes relative to the component gratings, and the relation between the fringe spacing, S , the angle of rotation α , and the grating spacing, d , can be easily derived.

Let MN be the bisector of the angle α at Q and let PR and PS be perpendiculars onto the component gratings through Q. A circle can therefore be drawn on PQ as diameter and MN will be a tangent to this circle. Hence, $\hat{MQR} = \hat{QPR}$. But, $\hat{QPR} + \hat{RQP} = 90^\circ$. Therefore, $\hat{MQR} + \hat{RQP} = 90^\circ$. The direction of the moiré pattern is therefore perpendicular to the bisector of the angle between the rotated lattices. In the parallel case, the fringe pattern is parallel to the component lattice directions.

It can easily be shown that $\hat{QEF} = \hat{FEP} = \frac{\alpha}{2}$.

Now, from $\triangle PRE$, $\sin \alpha = \frac{PR}{PE}$ i.e., $= \frac{d}{PE}$

and, from $\triangle EFP$, $\cos \frac{\alpha}{2} = \frac{EF}{PE}$ i.e., $= \frac{S}{PE}$

$$\text{But, } \sin \alpha = 2 \sin \frac{\alpha}{2} \cos \frac{\alpha}{2}$$

$$\text{Therefore, } d = S \cdot 2 \sin \frac{\alpha}{2}$$

or, for small angles,

$$d = S \cdot \alpha$$

$$\text{i.e., } S = \frac{d}{\alpha}$$

Crystallographic Considerations

That a fringe pattern identical to the moiré pattern discussed above could be produced by double diffraction was first shown by Dowell, Farrant and Rees (1956) from consideration of the conditions for reflexion of a crystal lattice.

The diagram, Fig.(8), represents a reciprocal lattice construction for two parallel crystals with a small rotational disorientation, α . If AO is the incident beam, the reflexion C $(hk0)_1$ will be produced when the sphere of reflexion ACO passes through a reciprocal lattice point C. If double diffraction is to occur, then this beam will have to be diffracted again by the second crystal. Therefore, consider now BC as the direction of the incident beam; draw EO//BC; on EO as diameter draw a second sphere of reflexion. If this sphere passes through a reciprocal lattice point, say F, then the beam will be reflected to give an emergent ray GF. Draw BD//GF and equal to it. Since BC is equal and parallel to GO and this also applies to GF and BD, then OF is equal and parallel to DC. But OF is a reciprocal lattice vector and therefore CD is also a reciprocal lattice vector; i.e., D is a reciprocal lattice point.

$$\text{Now, } n\lambda = 2d \sin \theta$$

$$\text{i.e., } \sin \theta = \lambda / 2d$$

$$\text{But, } \sin \theta = \frac{CO}{AO} = \frac{CO}{2}$$

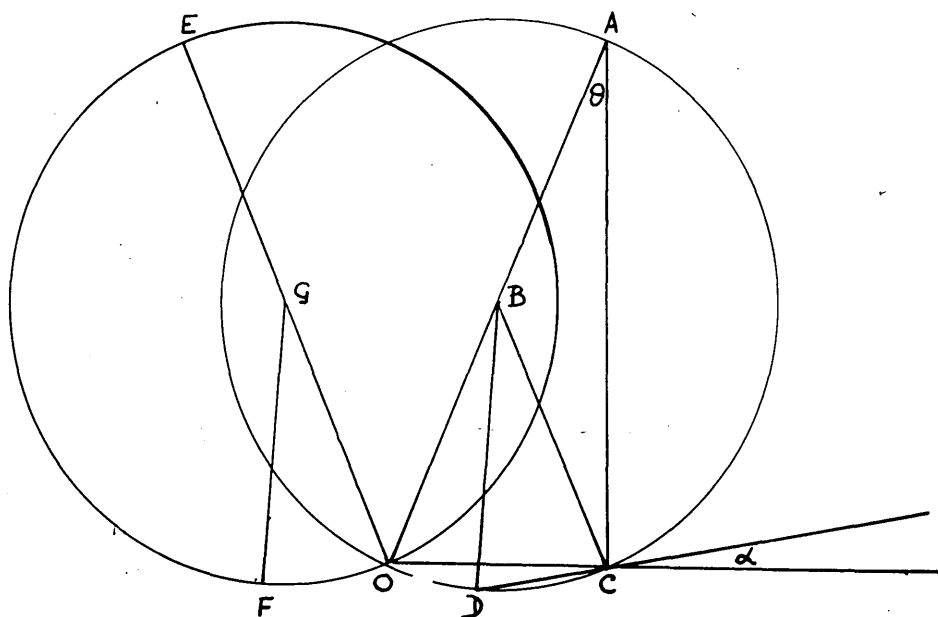


Fig. 8.

$$\text{Therefore, } CO = 2\sin \theta = \lambda/d$$

For very small angles, $CO \approx CD$

$$\text{Therefore, arc } OD = \frac{\alpha \cdot \lambda}{d} \quad (\text{arc} = r\theta)$$

$$\text{But, } OB = 1$$

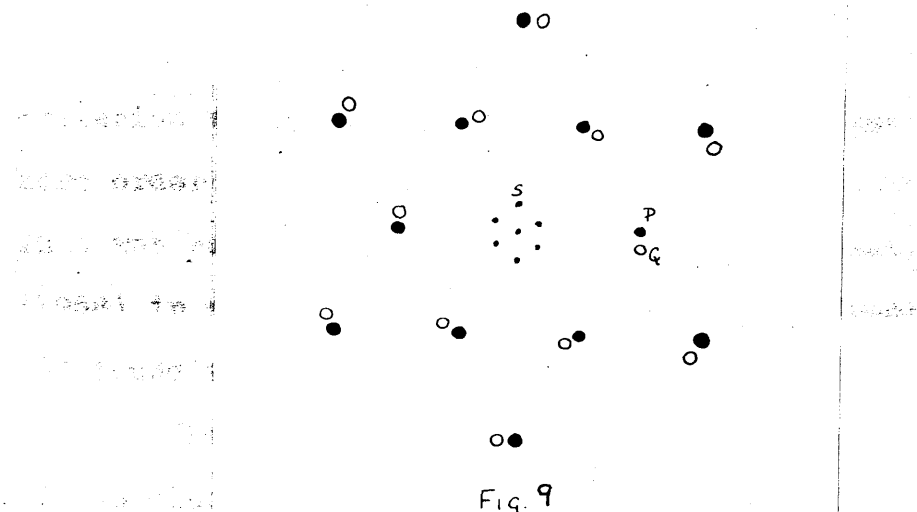
$$\text{Therefore, } \hat{OBD} = \frac{\alpha \cdot \lambda}{d}$$

For interference between two rays inclined at a very small angle, $\lambda = n\alpha$, where α is the angle between the rays and n an integer. Using this condition we get,

$$n = d/\alpha$$

$$\text{i.e., the fringe spacing } S = d/\alpha$$

Doubly diffracted beams such as BD appear on diffraction patterns as low angle reflexions close to the central undeviated beam. An illustration of this was given by Dowell, Farrant and Rees in their 1956 paper. In their study of moiré patterns in metal films, Bassett, Menter and Pashley (1958) were able to relate the spacing associated with these low angle reflexions directly to the spacing of the moiré patterns, in this case the patterns being of the parallel type. The diffraction pattern to be expected in the rotational case was, however, discussed in the paper and is illustrated in Fig.(9), the pattern being from two superimposed face-centred cubic crystals with $[111]$ parallel to the electron beam.



The large open and closed circles represent primary diffraction spots, the smaller dots, double diffraction spots. The reflexion Q can be considered as rising from diffraction by the $(2\bar{2}0)$ planes in the uppermost crystal, the beam passing undeviated through the second crystal. Part of the beam, however, may be diffracted again by the $(2\bar{2}0)$ planes in the second crystal to give rise to the doubly diffracted beam which produces the spot S. Application of this construction to all $(2\bar{2}0)$ reflexions produces a hexagon of spots round the central spot. Now, Menter (1956) has shown that for resolution of periodic objects

in the electron microscope, the Abbé condition must be fulfilled, i.e., both the zero order and the first order beams must contribute to the image. In case of moiré patterns, Dowell et al. (1956) showed that a similar criterion was necessary, here the imaging beams being the zero order and the first order doubly diffracted beams. This was substantiated by experiments by Bassett et al. (1958) in which they cut out the doubly diffracted beams and found that the moiré pattern disappeared.

The principal factor limiting the resolving power of the electron microscope is the spherical aberration of the objective lens, caused by the power of the lens being greater at the periphery than at the centre. A point in the object is thus imaged as a disc whose diameter depends on the degree of aberration. This defect can be partially overcome by only selecting the central beams for image formation by using apertures. A quantitative relation between aperture size and the lattice dimensions of the image forming beams has been derived by Menter (1956) in which he shows that the use of a 50 μ aperture effectively removes all beams of less than $4.2\overset{\circ}{\text{\AA}}$ spacing from the imaging pencil. For very high resolution even smaller apertures are necessary, hence, for most crystals, and in particular, graphite, the image forming beams in a moiré pattern can only be the zero order beam and the doubly diffracted beams.

Interpretation of the Moiré Pattern

The Lattice Image

The simplest interpretation of a moiré pattern is that it is an imperfect image of one of the component lattices. This concept arises from consideration of the diffraction pattern. In Fig.(9) the doubly diffracted reflexions round the central spot have exactly the same symmetry as the surrounding reciprocal lattice and therefore can be considered to give rise to an enlarged image of the lattice planes producing the reciprocal lattice. If diffraction conditions were theoretically perfect, a complete reciprocal lattice would be produced round the central spot, but normally only the strongest reflexions give observable doubly diffracted beams. The moiré pattern is therefore an imperfect image of only the planes giving rise to the doubly diffracted beams present in the diffraction pattern. This limitation has been considered in detail by Agar, Frank and Kellar (1959) who showed that, for polythene, combination of a doubly diffracted ($hk0$) beam with the undeviated beam produced a line grating and that combination of a doubly diffracted ($hk0$) beam, any other doubly diffracted beam except ($\bar{h}\bar{k}0$), and the undeviated beam produced a two dimensional pattern, an imperfect image of the lattice.

Limitations of the Image Interpretation

In general, the faithfulness of an image is very dependent on the nature of the imaging medium. With moiré patterns we are trying to image one lattice by using a second lattice as medium. It was first pointed out by Bassett et al. (1958) that, although the terminating half-planes associated with dislocations could be imaged in the moiré pattern, if a dislocation extended through both superposed lattices, then no extra half-line would be produced in the moiré pattern. In Fig.(10)a two line gratings containing an extra half-line have been rotated through a small angle - no half-line is visible in the moiré. Now, in Fig.(10)b one of the gratings has been rotated through 180° - two extra half-lines are now visible. In neither case is the moiré a faithful image of either component grating. Unless it is known, therefore, that one component is crystallographically perfect, the moiré pattern cannot be referred to as an image of the lattice.

The Patterson Projection

The formation of moiré patterns from superimposed thin crystals has been studied theoretically by Cowley and Moodie (1959). It had been shown earlier by Dowell, Farrant and Rees (1956) that in certain limiting cases the moiré

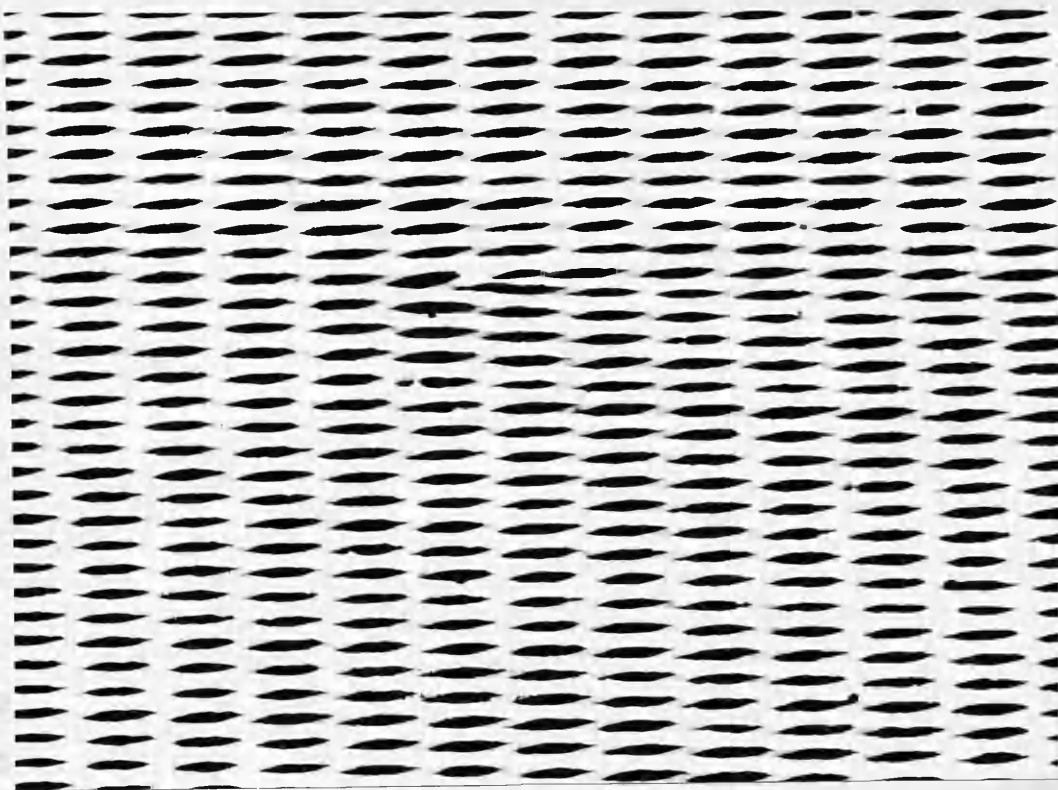


Fig. 10a.

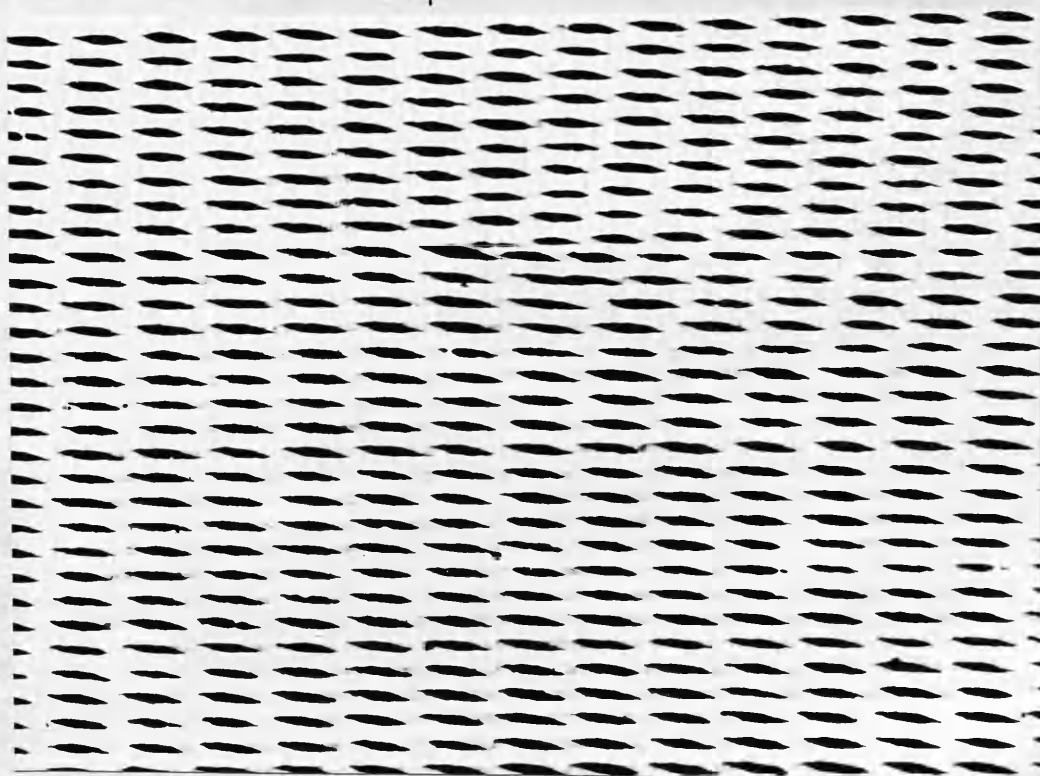


Fig. 10b.

pattern could represent the Patterson function of the crystal projection. Cowley and Moodie studied several general cases and also determined the electron optical requirements for the formation of moiré patterns, considering in detail the effect of a limiting aperture in the observing system, and effects produced by focussing. In the case of thin identical crystals superimposed with rotation, they concluded that the pattern produced would represent the Patterson function of the crystal projection.

All cases of moiré patterns reported in the literature have so far been in compounds where the lattice projections and the Patterson distribution of the lattice projection are indistinguishable. Consequently a two dimensional moiré pattern must be considered either as an image of the lattice projection which would be produced by considering only those planes which give doubly diffracted beams or as a Patterson distribution of the lattice projection.

Application to Graphite

The basal planes in graphite, as we have seen, are composed of a hexagonal arrangement of C-atoms separated by a distance of 1.42\AA , and the strongest diffracting planes, $\{11\bar{2}0\}$, have a spacing of 1.23\AA . Direct resolution is therefore impossible. However, Bacon's investigations on

reactor graphite show that numerous rotations occur in a stack of layer net planes, indicating a possible formation of moiré patterns. As moiré patterns had been reported on natural graphite, it was decided such patterns might provide a method of studying the structure within the crystallites composing synthetic graphite, as defects in the structure would, in most cases, be imaged in the moiré pattern.

Thin-sectioning

Microtomes

The rapid advances made in the application of electron microscopy to biology and medicine in the past ten years have been possible primarily by the development of ultra-microtomes capable of cutting sections of less than 250⁰Å thickness. Early ultra-microtomes were adapted versions of the ordinary microtome used to cut sections for optical microscopy, the commonest technique being to cut a wedge-shaped section so that, at one end, there was an area thin enough for viewing in the electron microscope. This technique was first reported by von Ardenne (1939) and was later improved by Richards, Anderson and Hance (1942). As only a very small area was thin enough to be useful, little information could be gained from these sections.

The earliest attempts to produce sections the entire

areas of which were thin enough for electron microscopy, were carried out with high speed microtomes. Microtomes with cutting speeds of 40,000 cuts/minute were employed by O'Brian and M^CKinley (1943) and later by Fullam and Gessler (1946). Although providing useful information on fixation, embedding and handling of specimens, this method was discarded when more reliable techniques became available.

In 1948, Pease and Baker demonstrated that using standard histological techniques and a suitably modified standard microtome, it was possible to cut sections thin enough for electron microscopy, the minimum feed on their machine being 0.1 μ . Several improvements were made to this machine by Hillier and Gettner (1950) who, using for the first time a section floating trough so that as sections were cut they floated onto a liquid surface, were thus able to consistently produce uniform sections 0.2 μ thick.

A new method for controlling the specimen feed was introduced by Newman, Borysko and Swerdlow in 1949, in their microtome the advance of the specimen towards the knife being controlled by thermal expansion, in comparison to the mechanical methods of previous microtomes. In present day microtomes, both methods are employed, a good example of the thermal advance type being the Sjostrand microtome (1953), and of the mechanical advance type, the Porter-Blum (1953) instrument. With both these instruments, it is

possible to cut a continuous series of sections 250\AA thick.

Embedding

The biggest single difficulty which held back early microtomists was the lack of a suitable embedding material. The standard early material, paraffin wax, was not hard enough and although mixtures of it and other substances, notably collodion (Pease and Baker, 1948), met with some success, it was not until Newman, Borysko and Swerdlow introduced the methacrylates as embedding materials in 1949, that a significant advance was made. On polymerisation, however, these substances considerably contract (up to 20% for n-butyl methacrylate) and it was shown by Borysko (1956) that this causes severe damage to tissue. To overcome this, Borysko suggested the use of a partially polymerised syrup and embedding at higher temperatures.

A new embedding material which does not have the disadvantages of methacrylate was introduced by Glauert and her collaborators in 1956. This was 'Araldite', an epoxy resin which, as it is in a highly associated state before setting, has a volume shrinkage of only 2%. It also has the added advantage of being stable in the electron beam, in comparison to methacrylate which degrades, contaminating apertures in the machine and thus destroying the resolution.

Knives

The first sections examined in the electron microscope were cut with the metal knives used in ordinary microtomes. It soon became apparent, however, that these were unsuitable, becoming rapidly blunt, and requiring considerable time for resharpening. The introduction of the glass knife by Latta and Hartmann (1950) was a significant advance in this field. Glass knives are cheap, easily made and, provided care is taken in their selection, capable of cutting sections down to the thickness limits of modern ultra-microtomes. They have, therefore, completely replaced sharpened metal edges for thin sectioning, but they have one disadvantage - the cutting edge rapidly deteriorates. Diamond knives are now being increasingly used for microtomy as their cutting edge lasts for several months without resharpening. The possibilities of diamond as a material for microtome knives were first demonstrated by Fernandez-Moran (1953) and, using such a knife, it has been proved possible to cut very hard materials such as bone and metals.

As only one example of a moiré pattern from graphite was shown in the literature and, as it was not known if the patterns in synthetic graphite would be suitable as regards extent and contrast for a study of structure, and, in particular, the defect structure, a specimen of colloidal Acheson graphite was first prepared. Examination of this material, as can be seen from Plate 2, revealed good moiré patterns but only in the thinnest areas. This method of observing structure was therefore practicable and now a technique had to be found for preparing thin flakes from the synthetic graphite.

Scraping

The synthetic graphite, Calder A quality, which was supplied by Dr. D.M. Donaldson, U.K.A.E.A., Dounreay, was in the forms of blocks of assorted shapes and sizes, the smallest being 2" x $\frac{1}{2}$ " x $\frac{1}{2}$ ". The first technique tried was simply to scrape a very fine powder from the surface of the block with a razor blade, suspend it in benzene, allow the gross material to settle, and evaporate one drop of the remaining fine suspension on a formvar covered specimen mount. A typical example of the material obtained thus is shown in Plate 3. A moiré pattern is visible, but it is rather confused and indefinite. Most of the material on such a

PLATE 2

Specimen of colloidal Acheson graphite showing
numerous moiré patterns. -(x150,000)

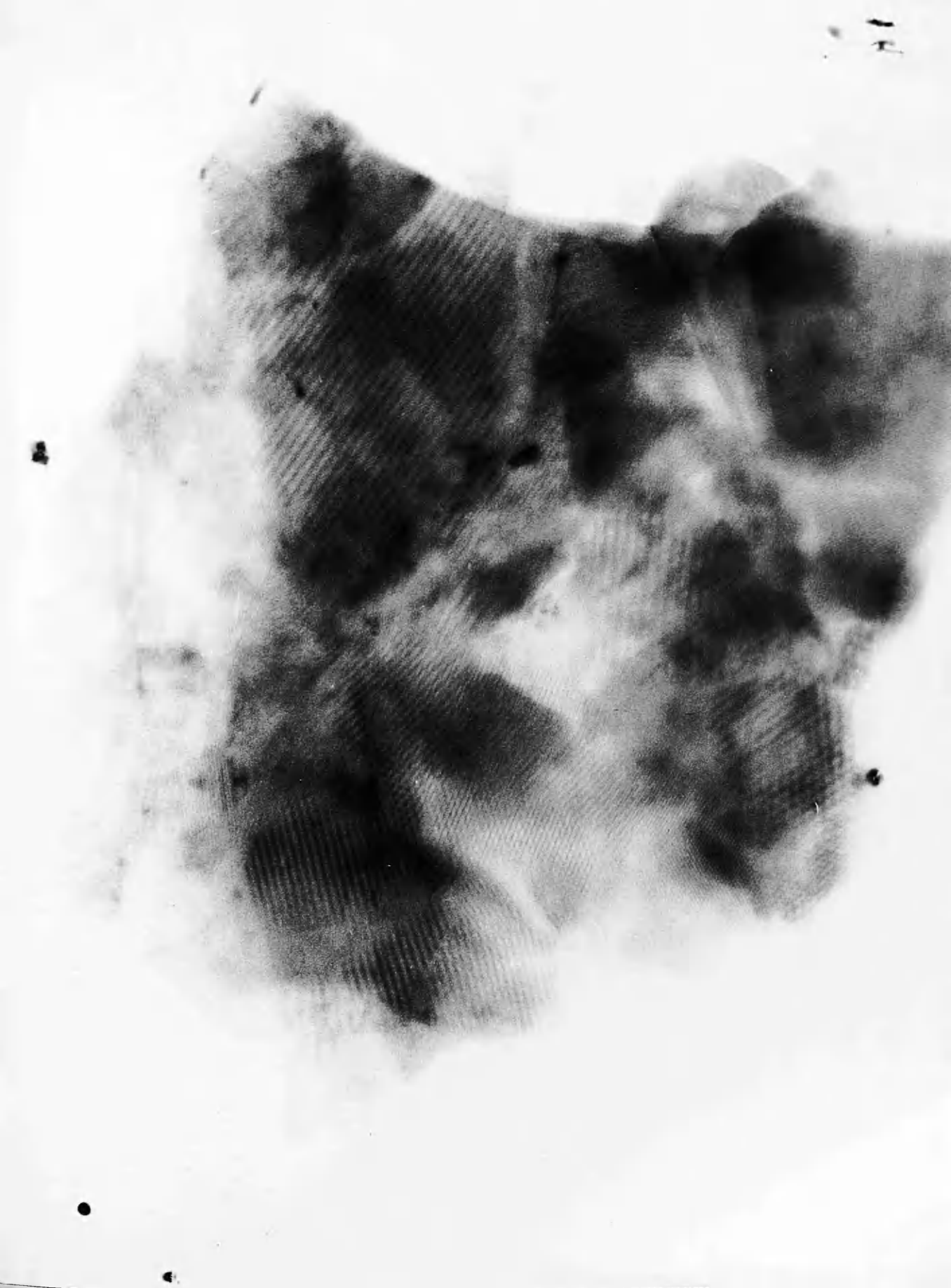
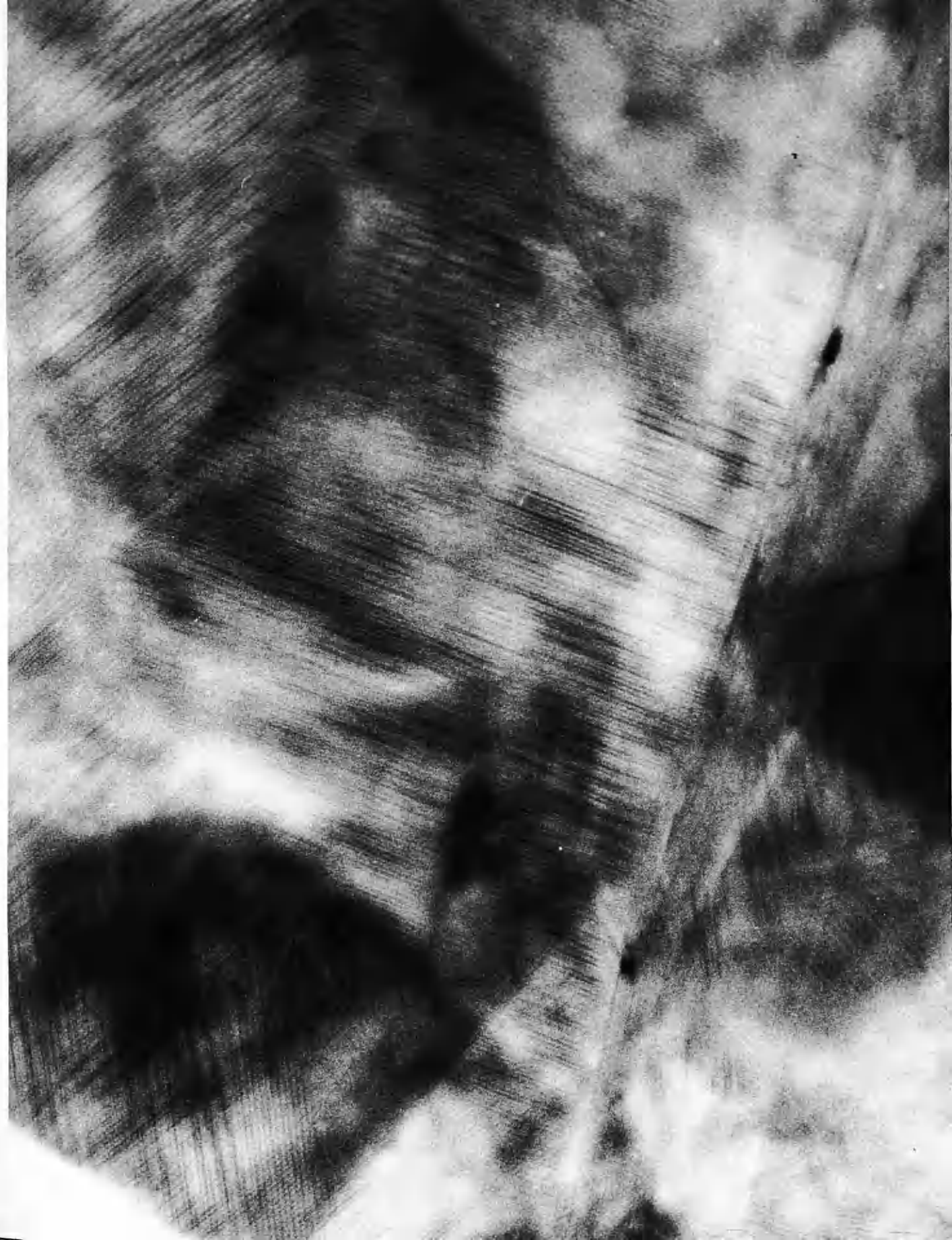


PLATE 3.

Specimen obtained by scraping technique.

(x259,000)



specimen was much too thick and bombardment by the electron beam caused break up of the surrounding film and hence, destruction of the specimen.

Rubbing

The second method tried, mainly in an attempt to reduce the amount of opaque material in the specimens, consisted of rubbing a small area of the block on the surface of a clean glass slide. Continued rubbing removed fine material from the surface of the block to the slide, which was then covered with a collodion or formvar film and both film and graphite floated onto a water surface. Areas of this film were then easily mounted on specimen grids. The example shown in Plate 4 is typical in that clear moirés were observed, but also a large amount of debris, seen in the right hand corner, presumably produced by the continued rubbing.

A variation of this technique was to scrape fine material from the surface of the block and grind it between two glass slides. Although there was an improvement in the standard of the specimens, it was not marked enough to justify further work on this technique.

Although these two methods did provide some material of the required standard, they were considered to be unsatisfactory for a rigorous quantitative examination of synthetic

PLATE 4

Typical specimen prepared by rubbing technique.

Debris evident in right hand corner. (x290,000)



graphite for several reasons. Neither method gave any indication of the precise location in the parent block of graphite of the flakes examined in the microscope. The specimens were not reproducible, and all information regarding the structure in the region between flakes was lost during preparation. The thickness of the material could not be controlled. Moreover, since both methods involved grinding, which has been shown by Bacon (1952) to affect the normal structure of synthetic graphite, the possibility of some modification in the structure during preparation could not be excluded.

Thin-Sectioning

The principal requirement of any preparatory technique was that it had to provide a large number of areas thinner than $500\overset{\circ}{\text{\AA}}$ and free from artefact. As there was at that time in the laboratory a microtome reputedly capable of cutting sections less than $250\overset{\circ}{\text{\AA}}$ in thickness and as graphite has well defined cleavage planes, it was decided to try cutting the material and, in this way, overcome at least the thickness problem discussed above.

Embedding

As no guide was available as to procedure, the well-tried technique for embedding biological specimens was first followed. However, as the water content of the synthetic

graphite is negligible compared to that of a biological specimen, the various stages for removal of water were omitted. Accordingly, 1 mm. cubes of the graphite were placed in 00 size gelatin capsules which were filled with an embedding mixture of 95% n-butyl methacrylate, 5% methyl methacrylate and 1% benzoyl peroxide catalyst. Heating at 48° in an oven overnight gave sufficient hardness for cutting. The specimen was prepared for sectioning by dissolving away the gelatin in warm water and trimming the face of the block under a binocular microscope to a size of approximately 0.1 mm².

The recently introduced epoxy resin Araldite was also used as an embedding agent but, in this case, heating of the capsules had to be prolonged for several days at 60° to ensure thorough hardening.

An early problem encountered in the embedding procedure was the formation of bubbles in the polymer, especially round the graphite block. These were formed exclusively in the polymerised methacrylate. This, however, is a fairly common phenomenon in methacrylate polymerisation and is due to local overheating or boiling, the graphite block playing the same role as porous chips or bubbling stones. It was found that bubbling could be most simply overcome by holding the temperature at 40° overnight before raising it

to the polymerisation temperature, 48° ; this assuring almost 100% success in a series of samples.

Synthetic graphite has a considerable pore volume and for efficient embedding it is necessary to remove as much of the air in these pores as possible. A vacuum embedding technique was developed for these samples using the apparatus illustrated in Fig.(11). During evacuation the monomer is cooled with liquid air. After 15 mns. pumping the graphite can be transferred to tube B simply by raising A. Complete degassing of the graphite can be further

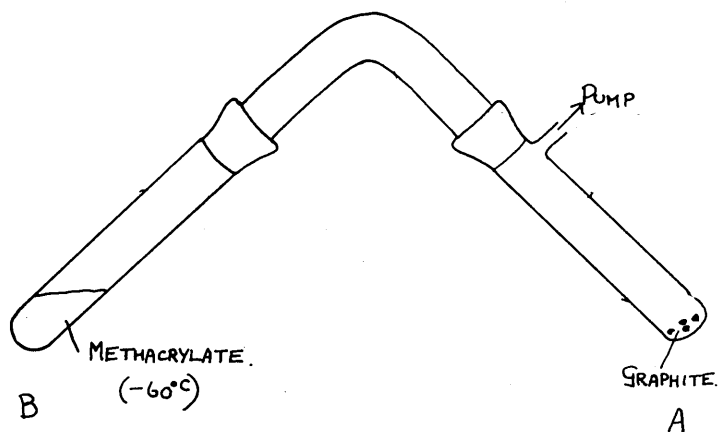


FIG. 11.

ensured by heating it to a low temperature, but this was found to have little effect on the efficiency of the embedding.

In the case of Araldite, vacuum embedding was more difficult as, once made, the embedding mixture must be maintained at 60°C. The apparatus shown in Fig.(12) was therefore used.

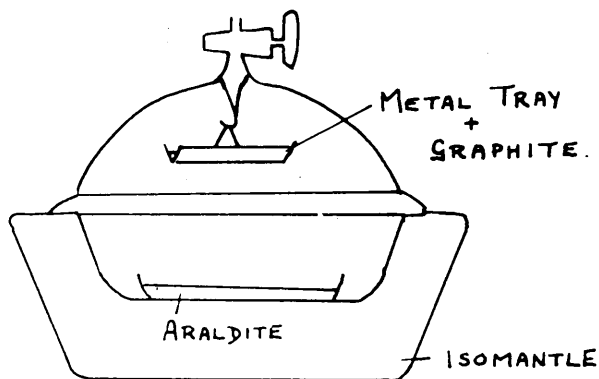


FIG. 12.

A calibrated, thermostatically controlled isomantle maintained the temperature at 60°C and, after a suitable vacuum was obtained, the graphite was dropped into the Araldite by raising one side of the metal tray with a magnet. Much shorter pumping times were used than for methacrylate as it was feared that, at the higher temperature, constituents of the Araldite mixture would distil off. In spite of this, vacuum embedding proved far more efficient than the normal technique.

Sectioning

Preparation of Knives

Two types of knife were used in this work, glass and diamond, the former being easily made and expendable, the latter commercially made.

Large numbers of glass knives can be conveniently made by diagonally scoring strips of plate glass, as shown in Fig.(13),

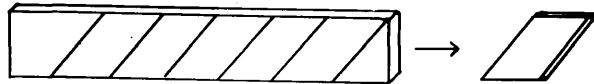


Fig. 13.

and then breaking the strip mechanically into small rhombs, the acute angles forming the cutting edges. Upon this cutting edge depends the quality of the section produced, the efficiency of embedding being of only secondary importance. Accordingly, great care must be taken in the selection of the knife which must have a perfectly straight edge, no serrations along the edge and no traces of fault lines near the edge. These conditions result in the rejection of up to 70% of the knives broken. Although great

time and trouble may therefore be taken in the selection of a good knife, the working life of a glass knife is very short, deterioration being detected in this work after 15 minutes. This deterioration of the cutting edge is due primarily to attack by the atmosphere, accelerated by the water-acetone solution also present and hence, nothing can be done but to begin again with a new knife. This defect in glass knives has been circumvented by many workers who use instead diamond knives which provide a tougher, more durable cutting edge. Such a knife was tried with some success in this work.

Microtome

The microtome used in this investigation was the Porter-Blum instrument, a mechanical advance type, the advance being by fractions of the pitch of a screw thread, with the smallest advance an indicated $250\overset{\circ}{\text{\AA}}$. Controlled by this mechanism is the advancement of a cantilever arm at the end of which is a chuck holding the embedded graphite specimen. A major problem in early microtomes was that the specimen block, on the upstroke, picked up the section previously cut on the down-stroke. To avoid this, the movement of the block in this microtome follows a parallelogram, thus enabling the specimen block to by-pass the knife on the return stroke, and eliminating any

possibility of damage to the face of the block or the section.

Section-cutting

Glass Knives

When a good knife has been obtained it is sealed into a brass trough with dental wax and the position of the trough and knife carefully adjusted with respect to the specimen block. Ideally, the front edge of the knife should form a tangent to the arc of the circle described by the specimen block. Gross deviations can cause damage to, or wetting of the block, while even slight deviations produce "juddering" a phenomenon easily recognised in biological specimens by the corrugated nature of the section, but very difficult to observe in graphite. Whenever glass knives were used, all sections were floated onto a 30% acetone-water solution.

The sections of graphite produced by this technique are hardly sections in the biological sense. They are not continuous, in only very few cases is their thickness uniform overall, and they stretch neither on the acetone-water solution nor on exposure to chloroform vapour. All sections, as they were cut, had therefore to be perfectly flat. The production of such sections depends on two factors, the sharpness of the knife and the angle of contact

between the knife and the solution in the trough. Fortunately, the acetone-water solution used has a very low surface tension and the contact angle between glass and 30% acetone-water must be very small. It was noted, however, that once the solution level in the trough had been raised to the knife edge, it had to be kept there, as any drying of the edge greatly increased the contact angle. To further aid in maintaining the graphite sections flat, several knives were broken with 30° angles at the cutting edge instead of the more usual 45° . Although such knives would no doubt be an improvement, it was found impossible to obtain a straight, serrationless edge with the smaller angle.

This inability to stretch graphite sections after cutting made the conditions for obtaining good sections even more exacting than in the case of biological specimens and it was only when these were most favourable that sections worth examining in the microscope were produced.

Diamond Knife

The prime object in purchasing a diamond knife was to see if graphite could be cut in directions other than along the cleavage planes and, in particular, in a direction perpendicular to the cleavage planes. The knife was supplied with a special collecting bath and had only to be

sealed into this with a ribbon of wax. Although possessing many advantages compared with the glass knife, the diamond knife has one disadvantage, its surface is hydrophobic and the contact angle between it and an acetone-water solution is consequently very large. On cutting, this results in a crumpling of the sections, but this is no trouble in biological material which can be easily flattened. With graphite, however, this is impossible, the section remaining crumpled.

Two different approaches were tried in an effort to overcome this difficulty. Firstly an attempt was made to change the nature of the diamond surface by evaporating various metals and non-metals onto it. In no case, however, could sufficient adherence be obtained between film and diamond to permit prolonged operation. The second technique is used by many biological workers and consists of adding a very small amount of wetting agent to the solution in the collecting bath. Unfortunately, in this case, if sufficient were added to provide a favourable contact angle, the graphite sank. It did prove possible, using this technique, to cut some very good sections shown in Plates 17 and 19, but such areas were so few and far between that it was decided to reject the diamond and concentrate on perfecting the glass technique.

Even when flat sections have been cut and are floating on the surface of the collecting bath, a further difficulty arises in transferring them to the specimen mount. Two methods can be used to do this. Either a specimen mount covered with a suitable supporting film can be held under the sections and the solution level dropped until the sections settle on the mount or, the mount can be lightly laid on top of the solution surface, covering the sections, and then quickly removed, the sections adhering to the supporting film. In this work, the latter technique was used as the areas cut were so small that use of the former technique would have resulted in the sections being at the edge of the specimen grid and they would not have been observed in the Siemens microscope.

Throughout this investigation formvar was used as a supporting film in preference to collodion and carbon. Collodion, it was found, was very unstable at high beam intensity, and carbon was not tried as it was feared ambiguity would occur when interpreting a diffraction pattern of graphite on a carbon substrate.

Microscopy

Transmission

Only in the very early stages, in the investigation of possible specimen preparation techniques, was the

Philips E.M. 100 microscope used. After the sectioning technique had been established, the Siemens Elmiskop 1 was used exclusively. This microscope has two systems of illumination known as single condenser and double condenser after the lenses employed. The essential difference between the two systems is that the double condenser uses a very small area of the beam emitted by the tungsten filament to illuminate the specimen, while the single condenser system uses a much greater area. With double condenser illumination, the beam passing through the specimen is therefore almost parallel and resolution is at its maximum, in this case $\sim 8\text{\AA}$, while with single condenser illumination the resolution is probably around 14\AA . Now, with the Siemens microscope, it is also possible to carry out selected area diffraction. Unfortunately, during the first year of this work, this could only be done when single condenser illumination was employed and therefore micrographs taken during this period do not represent the ultimate in resolution. Modifications to the power supplies have since taken place and it is now possible to take a diffraction pattern of an area just photographed under double condenser illumination.

Diffraction

The use of electron diffraction in this work, although it would seem superfluous in an investigation involving the one type of material, proved of great value in that it provided information on the structure in the c direction of the lattice which otherwise would have been unavailable. In obtaining a diffraction pattern in the electron microscope, a small aperture is used to select the area from which a diffraction pattern is desired. If the diameter of the aperture is D , the diameter of the area selected, d , is given by

$$d = 0.043D.$$

In this investigation two aperture sizes have been used, 20μ and 10μ , giving selected areas of diameter 0.86μ and 0.43μ and hence, areas of $0.58\mu^2$ and $0.145\mu^2$. The diffraction pattern obtained is calibrated by taking, immediately afterwards, a diffraction pattern from an evaporated thallium chloride specimen, and using the maxima of this pattern, whose spacings are known from the A.S.T.M. index, as standards.

subject, however, it must be noted that the
order of the alphabet is not the same as the
order of the alphabet in the English language.
The order of the alphabet in the English language
is as follows: A, B, C, D, E, F, G, H, I, J, K, L, M, N, O, P, Q, R, S, T, U, V, W, X, Y, Z.
The order of the alphabet in the English language
is as follows: A, B, C, D, E, F, G, H, I, J, K, L, M, N, O, P, Q, R, S, T, U, V, W, X, Y, Z.
The order of the alphabet in the English language
is as follows: A, B, C, D, E, F, G, H, I, J, K, L, M, N, O, P, Q, R, S, T, U, V, W, X, Y, Z.

RESULTS.

The introduction of the new alphabet into the
English language is a very important step in the
history of the English language.

Notes-Sections

For reasons already mentioned, the new alphabet
is used almost exclusively. As the alphabet is
used in an alphabetical order, the order of the
alphabet is as follows: A, B, C, D, E, F, G, H, I, J, K, L, M, N, O, P, Q, R, S, T, U, V, W, X, Y, Z.
The order of the alphabet in the English language
is as follows: A, B, C, D, E, F, G, H, I, J, K, L, M, N, O, P, Q, R, S, T, U, V, W, X, Y, Z.
The order of the alphabet in the English language
is as follows: A, B, C, D, E, F, G, H, I, J, K, L, M, N, O, P, Q, R, S, T, U, V, W, X, Y, Z.

Embedding

Although the epoxy resin "Araldite" was initially tried for this work, methacrylate was used in the later stages. In the graphite sections there was hardly enough polymer present to cause serious contamination of microscope apertures if degradation took place. The advantage in using methacrylate is due to this degradation, which removes most of the polymer and greatly improves contrast in the specimen. With "Araldite" there is always the chance that a very thin area of specimen will be obscured by a layer of the resin.

The introduction of vacuum embedding produced a marked increase in the areas of section thin enough for transmission microscopy.

Thin-Sections

For reasons already discussed, glass knives were used almost exclusively. As the orientation of the crystallites in an embedded block can be taken as random, a knife edge, on cutting through this block, will only very occasionally cut parallel to the basal plane. In most cases, the edge will be at an angle to these planes and it appears that then the knife crushes rather than cuts, as no extensive area of section was ever observed with the basal planes parallel to the electron beam. If such crushing takes

place in the first few hundred angstroms of the knife's traverse through the block, the debris produced will have a detrimental effect on the cutting of the remainder of the block. To try and offset this, the area cut was kept as small as practicable. As a further consequence of this crushing effect, the continuous areas of section observed were only a small fraction of the area cut, and hence, no information could be gained on the size and distribution of macropores in the material.

Observation of Moiré Patterns

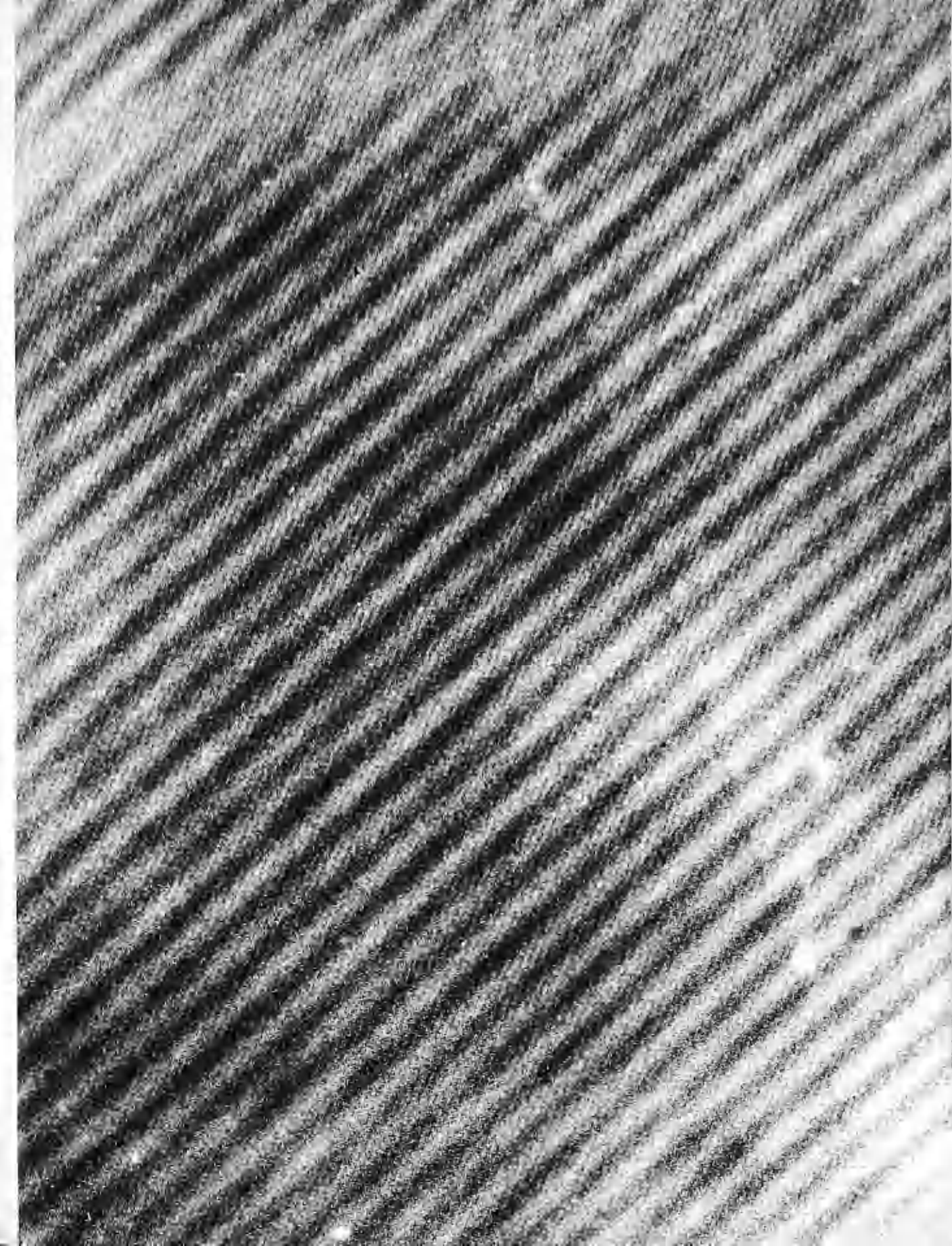
The moiré patterns observed on thin sections were far superior to those observed on material obtained by the scraping and rubbing techniques and proved suitable for an investigation of the structure of the crystallites composing the synthetic graphite. Five distinct types of moiré pattern were observed.

a). Line Moiré

Plate 5 shows an example of a line moiré pattern, here a fine pattern being crossed at a large angle by a coarser pattern. This is typical of all the patterns observed in that hardly ever was a single pattern seen, two or more moirés usually being combined in the one area. These line patterns are produced when only one set of planes in each of the two component crystals is oriented for double diffraction.

PLATE 5.

This micrograph is typical of the many line
moiré patterns observed. The spacing of the
fine moiré is 29\AA . (x543,000)



b). Spot Moiré

The most extensive example observed of a spot moiré pattern is shown in Plate 6. Such a pattern arises when more than one set of planes is in a suitable orientation for double diffraction. The arrangement of the spots in such patterns was always hexagonally symmetrical.

c). Double Line Moiré Pattern

This type of pattern, illustrated in Plate 7, was fairly commonly observed, although it has not been reported in the literature. It consists of two basic line patterns, one coarse and one fine, the fine pattern being inclined at a very small angle to the coarse pattern. Now, to produce two patterns at such a small angle, a minimum of three lattices is required, A, B and C. A small angle between A and B will produce a coarse moiré ($S = d/\alpha$) and the fine pattern could arise from a large angle between B and C. However, another pattern will be produced by A and C and, hence, three separate moirés should be observed. If now the angle between A and B is small enough ($< 1^\circ$), then the fine spacings produced by BC and AC will be very similar and, in addition, the angle between them will be very small. Provided there is a close enough similarity in the fine spacings - a difference of not more than 10\AA - then it is unlikely that the spacings would be resolved separately, either only the spacing from the stronger

PLATE 6.

This thin section shows a hexagonally symmetrical
spot pattern over an extensive area. (x270,000)



PLATE 7.

This micrograph shows an example of a double line moiré pattern, the coarse pattern being crossed at a very small angle by a fine pattern. (x412,000)



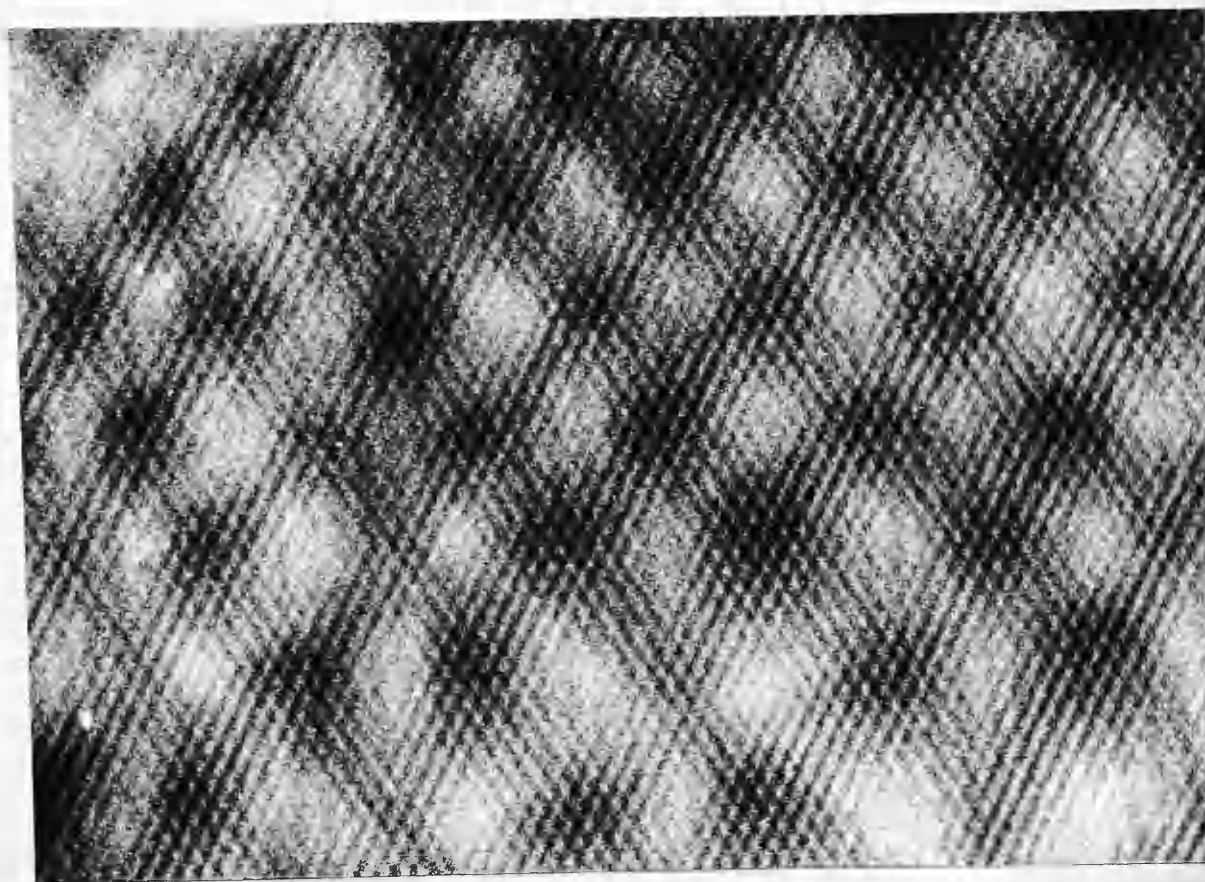
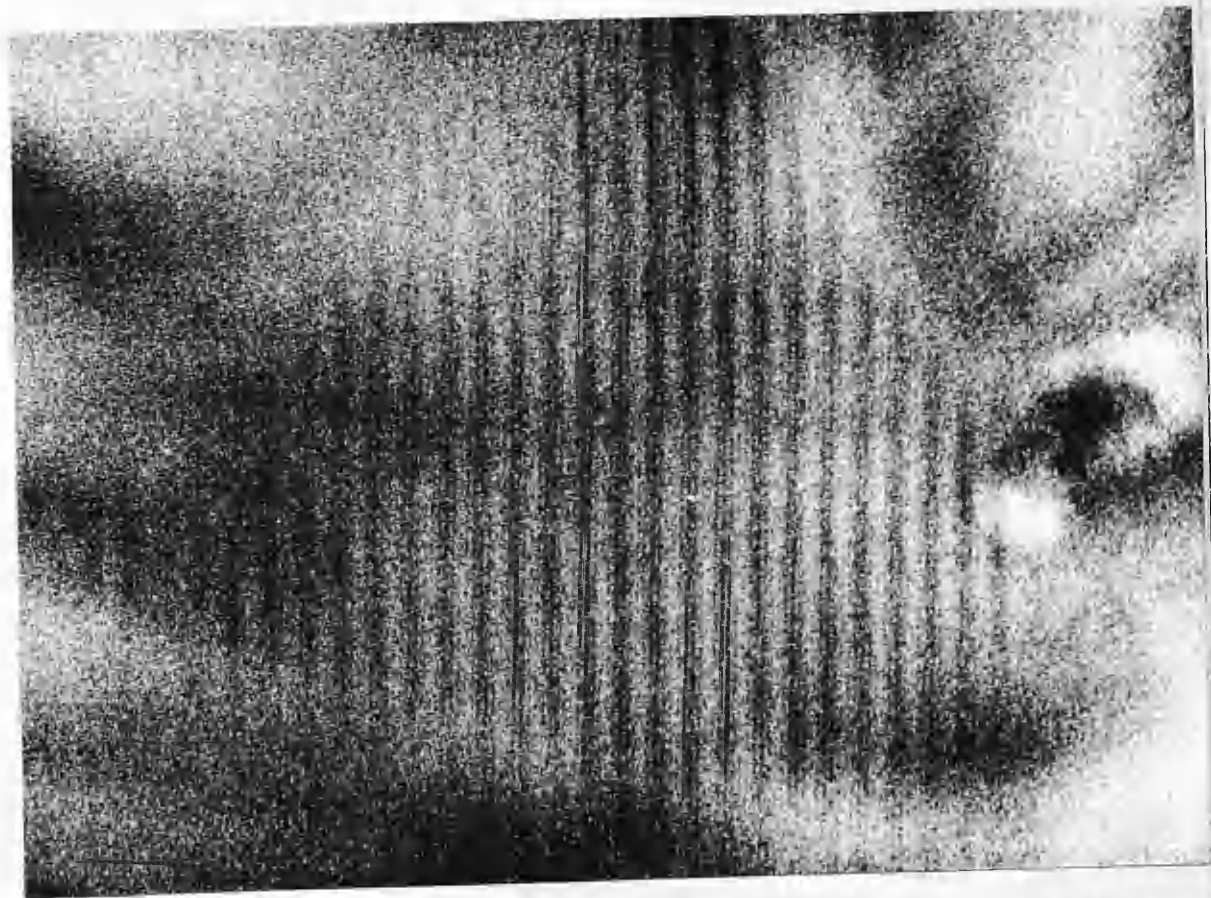
The micrograph displays a complex interference pattern. It features a series of broad, parallel, light-colored bands that are slightly tilted. Overlaid on these bands is a much finer, more regular grid-like pattern. The combination of these two patterns creates a moiré effect, resulting in a series of smaller, more intricate sub-patterns within the larger bands. The overall appearance is that of a high-magnification view of a crystalline or layered material.

PLATE 8.

In this micrograph several sets of planes have been imaged giving rise to a double spot pattern. Within each large diffuse spot is a hexagonal arrangement of smaller spots. (x409,000)

This micrograph shows a pattern of large, irregular, light-colored spots or regions of diffuse light. These spots are distributed across the field of view. Within each of these larger spots, there is a distinct, more organized pattern of smaller, darker spots. These smaller spots are arranged in a hexagonal lattice, which is a characteristic feature of certain types of crystalline structures. The overall image has a grainy, high-magnification quality typical of electron microscopy.



diffracted beam being resolved or a combination of the two. This is why only two patterns appear in this type of moiré although occasionally the fine spacing can be further resolved at various points in the pattern.

When the angle between the A and B lattices is almost zero, then the fine spacings produced by BC and AC can be taken as parallel. The spacing of the coarse pattern can then be related to the fine patterns by the formula derived for parallel patterns by Bassett, Menter and Pashley (1958)

$$S = \frac{d_1 d_2}{d_2 - d_1}$$

As these authors have shown that, for small angles of rotation, the effect on a parallel pattern of lattice rotation is principally a large angular magnification of the rotation, then the formula above can be applied to all cases of double line patterns. The coarse spacing is therefore, a moiré of the two fine moiré patterns.

d). Double Spot Moiré Pattern

As with a line moiré, a double spot moiré can be produced when more than one set of planes is contributing to the pattern. An example is shown in Plate 8. Within each large spot there is a hexagonal arrangement of smaller spots produced by the fine spacings. Both large and small

spots always exhibited hexagonal symmetry.

e). Rectangular Moiré Pattern

Plate 9 shows a pattern completely unexpected from a hexagonal lattice. It is a double line pattern and two sets of fringes have been produced, but these fringes are at 90° to each other. The inequality in the spacings of the two sets produces a rectangular pattern. Assuming that the planes contributing to this pattern are in the same lattice, then they must be at right angles and, furthermore, their spacings must be in the ratio of the fringe spacings. On the few such patterns observed, the ratio of the spacings was 1.72 ± 0.06 .

Electron Diffraction

1. Diffraction Patterns from General Areas.

a). Wide Angle Reflexions.

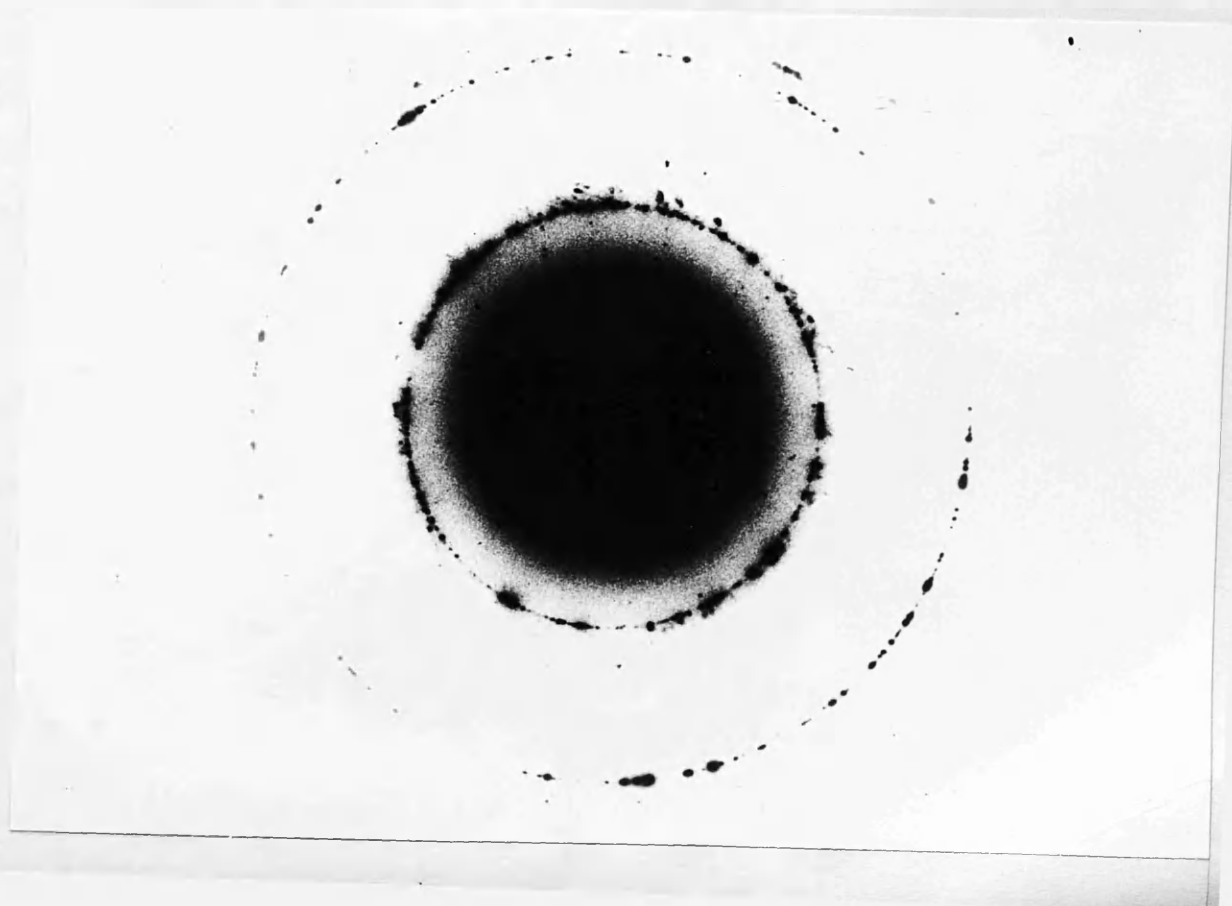
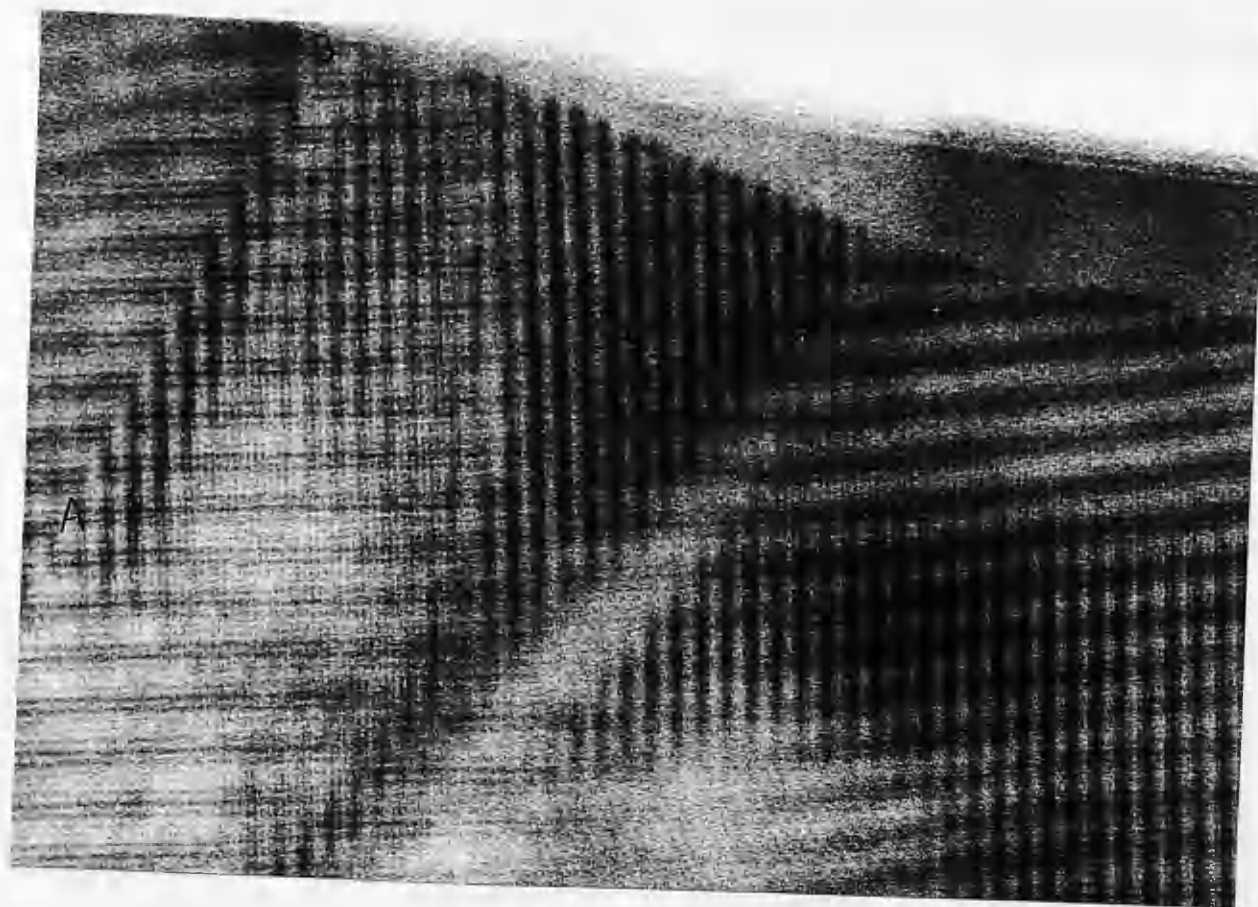
A typical diffraction pattern from a thin area of graphite section is shown in Plate 10. It can immediately be deduced from the distinct reflexions on the rings that the area examined was composed of numerous small crystal-lites rotated with respect to each other. The mean values of the d spacings of the most prominent rings are shown in Table 1.

PLATE 9.

This micrograph shows one of the few observed examples of a rectangular pattern, the planes imaged in the moiré here being at right angles. In the left-hand corner, the coarse moiré is out of register along AB indicating a slip in the lattice. (x295,000)

PLATE 10.

Selected area diffraction pattern from thin section of synthetic graphite. (100u aperture)



No. of Plates examined	No. of Plates showing reflexions	d spacing	Index
50	50	2.10	$10\bar{1}0$
50	41	1.22	$11\bar{2}0$
50	9	1.15	$11\bar{2}1$
50	2	3.34	0002

Table 1.

In the vast majority of cases, the diffracting planes are the $(10\bar{1}0)$ and the $(11\bar{2}0)$. Hence, the areas examined must consist of basal planes, the hexagonal layer nets being perpendicular to the electron beam in the microscope. As many of these diffraction patterns were taken with a very short exposure in an attempt to show double diffraction spots close to the central spot, the number of observed $(11\bar{2}0)$ and $(11\bar{2}1)$ spacings may be low, these reflexions being farthest from the centre. A converse argument applies to the (0002) reflexions, and hence the observation of reflexions on only two plates indicates that in sections of graphite the layer net planes are never extensively aligned perpendicular to the plane of the section. This diffraction evidence therefore shows that, in the microscope, the image produced is an image of the layer net planes.

b). Crystallite Size.

The unit cell of the graphite lattice is hexagonal. Therefore, a diffraction pattern from the layer net planes

will be hexagonally symmetrical. Accordingly, measurement of the number of spots in a 60° arc of the $(10\bar{1}0)$ diffraction ring will give the average number of crystallites in the area examined. These measurements were only made on plates from areas showing extensive uniform moiré patterns, as it was hoped, in this way, to isolate a single crystallite, laterally as well as vertically.

Using a 20μ aperture to select the area required, an average value of 11 was obtained. As the area selected by this aperture proved rather greater than the average lateral dimensions of a crystallite, a 10μ aperture was tried. The average number dropped to 9.6. This remained appreciably unaltered (9.5) when a 5μ aperture was used.

In parallel with this diffraction investigation, the thickness of the sections was measured. Calculations on over twenty areas gave an average value of 150\AA , only the thinnest areas being measured as only these give good moiré patterns. The interlayer spacing in graphite is 3.35\AA , and hence, a section of 150\AA will contain 46 layer nets. With an average of 9.5 crystallites per section, this gives a crystallite depth of approximately 5 layers. It can therefore be concluded that, in a large stack of graphite layer nets, there is a twist or stacking fault, on average, once every five layers.

2. Diffraction Patterns from Moiré Patterns.

Low Angle Reflexions

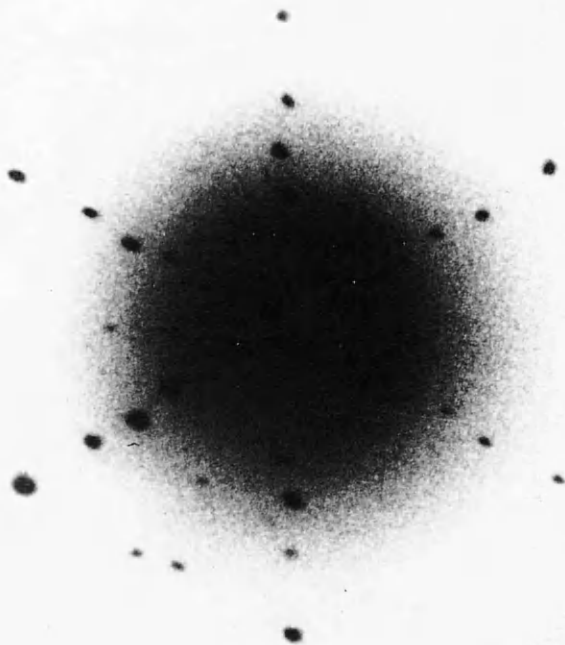
The selected area diffraction patterns from areas exhibiting strong moiré patterns were characterised by the presence of low angle reflexions close to the undeviated beam. The spacings of these reflexions could be related to the spacings of the moiré patterns as these reflexions are the doubly diffracted beams responsible for the formation of the patterns. Plate 11 is an enlargement of the central region of the pattern obtained from the area shown in Plate 12. Like the moiré pattern, the low angle reflexions show hexagonal symmetry, each arm of the hexagonal star consisting of four strong reflexions. The spacings of these spectra are 10\AA , 14\AA , 17.5\AA and 24\AA , the last being closest to the centre. This illustrates a difficulty when trying to correlate the diffraction spectra with the moiré pattern. Only very high resolution moirés can be used as all spectra with spacing above 35\AA are usually undetectable. The low angle reflexion pattern in Plate 10 is unique in that the four spectra along each arm are almost colinear. In this case, therefore, conditions are almost perfect for the formation of parallel type moiré patterns from these various spectra. Naming the reflexions a, b, c and d (10 — 24), the possible combinations are given by ab, ac,

PLATE 11.

Enlargement of central region of diffraction pattern obtained from area shown in Plate 12. Numerous reflexions arising from doubly diffracted beams are visible.

PLATE 12.

Moiré pattern formed from combination of undeviated beam and doubly diffracted beams in Plate 11, spacing, 39\AA . (x410,000)



From the left picture the object is seen from the right side.



ad, bc, bd, cd. The spacings of the resulting moiré patterns calculated from the formula derived by Bassett et al. (1958) are 35\AA , 23.5\AA , 17.2\AA , 70\AA , 33.5\AA and 65\AA . The actual spacings observed on the micrograph were 39\AA and 70\AA , the finer patterns probably being obscured by the coarser patterns. The point illustrated by this diffraction pattern is, however, that, even although the moiré spacings initially produced may be below the resolution of the microscope, it is still possible to obtain a resolvable pattern by combination of the various spectra.

This concept of the formation of a moiré pattern from moiré patterns has already been suggested as an explanation of the formation of double line patterns. Two diffraction patterns from moiré patterns of this type are shown in Plates 12 and 13. In both cases, there are examples of spectra very close together and almost colinear with the centre, e.g., at A in Plate 12 and B in Plate 13. The spacing of the coarse moiré pattern was found, in each case, to be exactly equal to that calculated from these reflexions by applying the formula.

In Table 2 are listed the low angle reflexions measured on several plates and the moiré spacings observed on the corresponding micrographs. Where the moiré pattern is formed from other moirés, the component spacings are shown in brackets. A further measurement was also made on

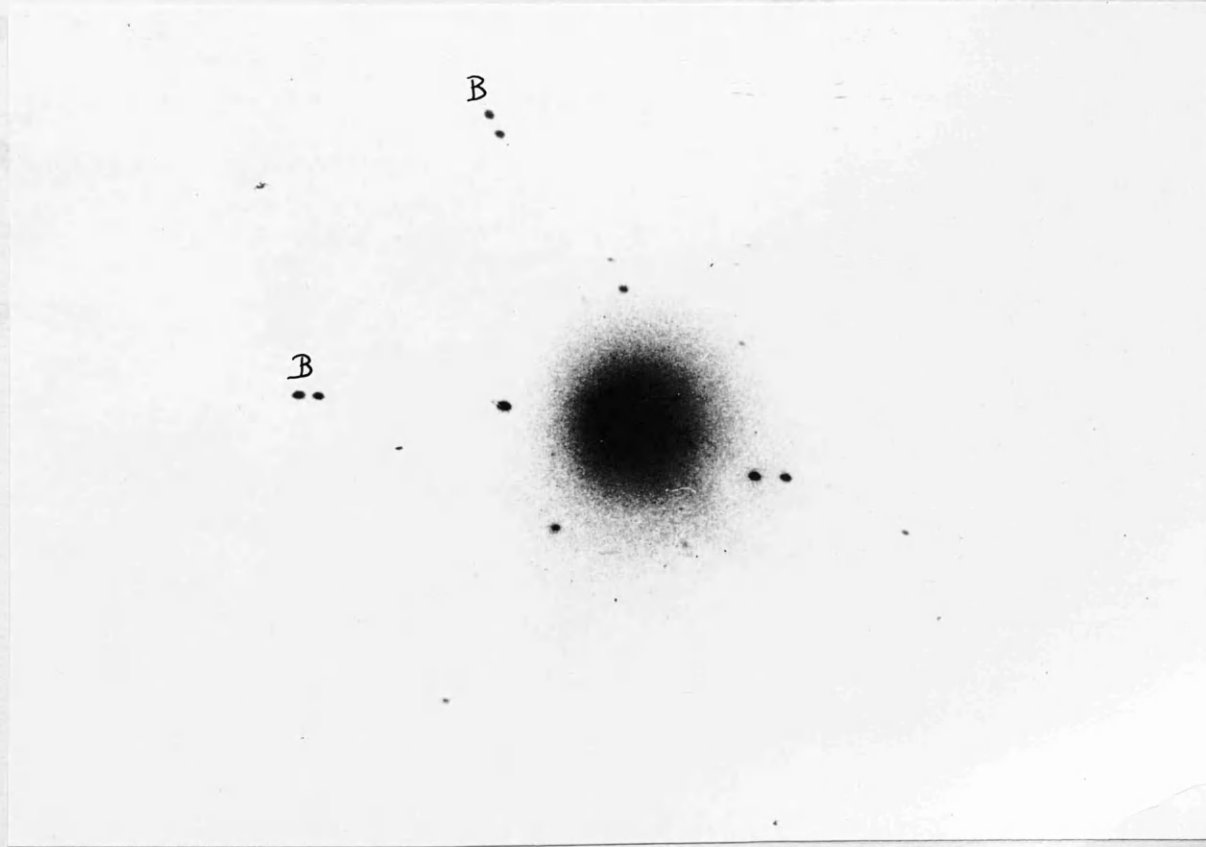
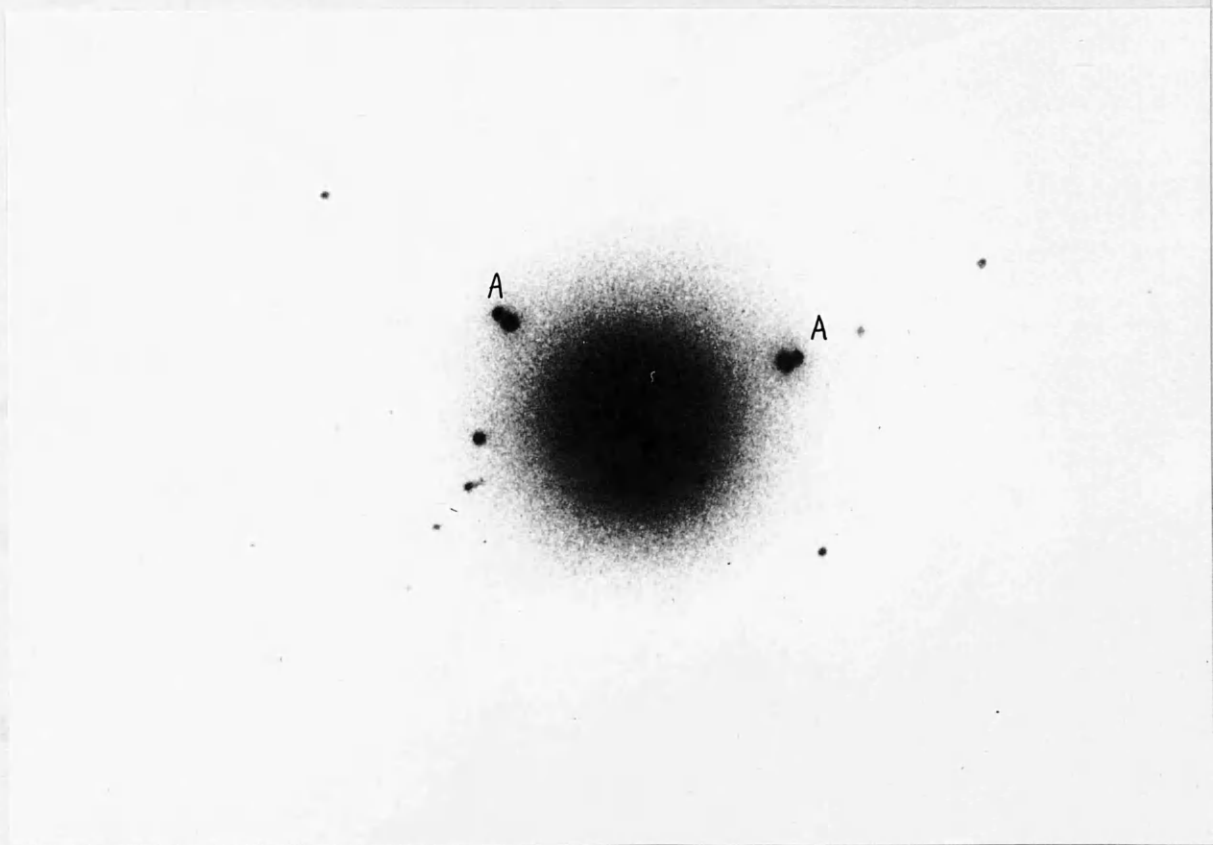
PLATE 13.

Diffraction pattern from double line moiré pattern.
The two reflexions at A have almost coalesced.

PLATE 14.

A further diffraction pattern from a double line moiré pattern. Here, the closely grouped (B) reflexions are slightly separated.





each plate; the average number, N , of low angle reflexions in a 60° sector. The number, n , of crystals contributing per 60° arc is also shown.

Plate No.	No. of crystals / 60° arc n	Average No. / 60° sector N	Low angle reflexions	
			Spacing $\overset{\circ}{A}$	Moiré Spacing $\overset{\circ}{A}$
G, S59/366	16	26	10.4	34
			13.2	49 (13.2, 10.4)
			20	
			34	
G, S59/404	9	14	3.9	
			4.3	44 (4.3, 3.9)
			7.9	136 (8.3, 7.9)
			8.3	14
			14.3	
G, S59/407	10	17	20	
			18.5	19
			40	40
G, S59/417	11	21	240	240 (20, 18.5)
			10	
			14	39 (14, 10)
			17.5	70 (17.5, 14)
G, S59/456	12	26	24	
			9.9	26
			11	97 (11, 9.9)
			23.5	
			29	

Table 2.

In a stack of n crystallites, a moiré pattern can be produced by a rotation between any two. The total number of possible patterns is hence given by nC_2 . Now each moiré pattern will produce, in the hexagonal case,

from one to six doubly diffracted low angle reflexions, depending on the orientation of the planes to the electron beam. At a rough estimate, therefore, $N \approx nC_2$. In the above examples, the values ranging from 14 to 26 found for N give values of n ranging from 6 to 8 as against the observed values of from 9 to 16. This can be considered fair agreement as errors in N and n are very likely from two causes. Firstly, too brief an exposure will give low values of N due to failure to record all doubly diffracted beams. Secondly, inadequate screening, i.e., use of too large a selecting aperture, will give high values of n , because of the intrusion of extra reflexions from neighbouring microcrystals; e.g., in the measurement of crystallite depth a value of 9.5 for n was obtained using a 5μ aperture. The range here, 9-16, for n is therefore high, a 20μ aperture being used.

Planes giving Rise to Low Angle Reflexions

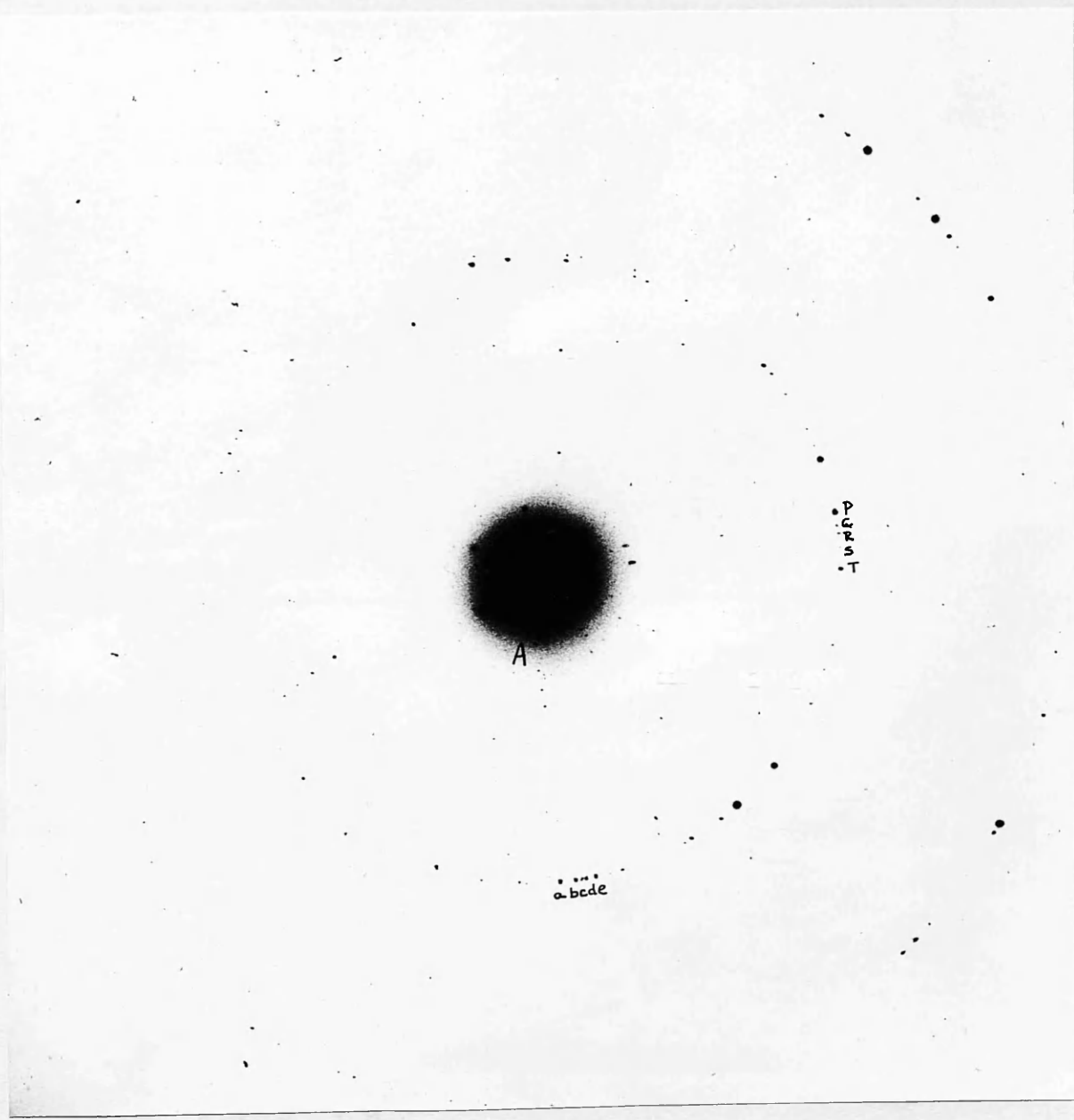
All the diffraction patterns from areas exhibiting moiré patterns show evidence of two prominent scattering planes, $\{10\bar{1}0\}$ and $\{11\bar{2}0\}$. The question now arises as to whether one or both is responsible for the low angle reflexions which give the moiré pattern. Plate 15 shows the entire diffraction pattern whose central region was shown in Plate 11. Now, the direction of a moiré pattern is

PLATE 15.

Complete diffraction pattern whose central region
was shown in Plate 11.

perpendicular to the plane of the paper

most likely group of reflections of the



ratio of the area of the

ratio of the area of the

between the

perpendicular to the planes producing it and hence, the most likely group of reflexions on the $(10\bar{1}0)$ ring which could produce the arm A of the inner star is that marked P, Q, R, S, T. One method of checking this is to measure the angles between the reflexions and compare their ratios to the ratios of the spacings of the low angle reflexions. In this case, the ratios did not compare favourably, e.g., the ratio of the two largest angles was 1.3, whereas that of the two smallest spacings was 1.4.

Immediately opposite the arm A is a closely bunched group of reflexions marked a, b, c, d, e. As the arc of the circle on which they are grouped is so small, no significant error is introduced if the distance between the spots is taken as a measure of the angle. These distances and their ratios and those of corresponding low angle reflexions are shown in Table 3.

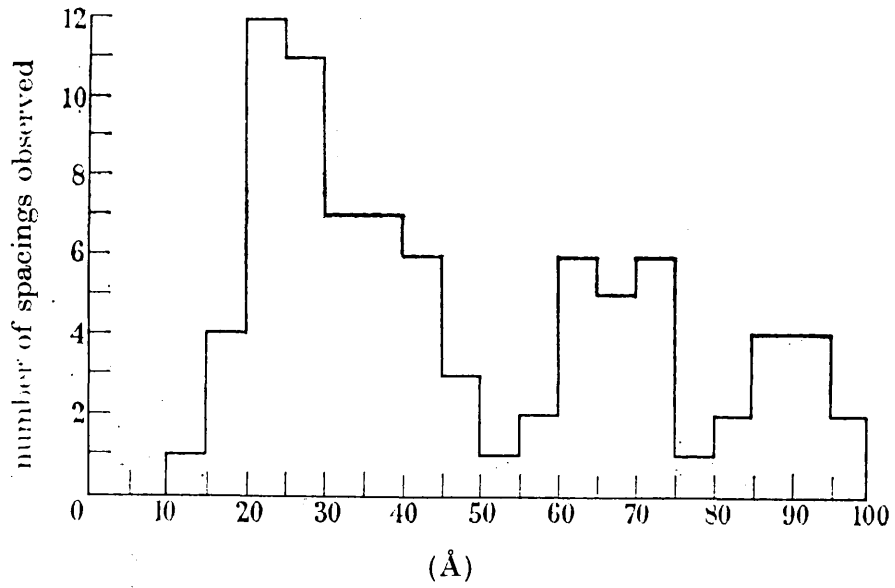
	1	2	3	4	5

	< 1.3	>			
	< 1.95		>		
	< 2.8			>	
	< 4.8				>
	5-2 = 3.5				
Ratios of moiré spacings	$\frac{24}{17.5} = 1.37$		$\frac{17\frac{1}{2}}{14} = 1.25$		$\frac{14}{10} = 1.4$
Ratios of distances between spots	$\frac{4.8}{3.5} = 1.37$		$\frac{3.5}{2.8} = 1.25$		$\frac{2.8}{1.95} = 1.43$
<u>Table 3.</u>					

The agreement is excellent and therefore these reflexions must be responsible for the moiré pattern. But they are parallel to the direction of the moiré pattern. However, these reflexions on the $(10\bar{1}0)$ ring have been used only as a means of measuring the angles between crystallites, and, therefore, the $(11\bar{2}0)$ ring should contain sets of reflexions corresponding in angular measurement to a, b, c, d and e. Moreover, the $(11\bar{2}0)$ planes are at 30° to the $(10\bar{1}0)$ and hence the $(\bar{2}110)$ are at 90° to the $(10\bar{1}0)$. This means that on the $(11\bar{2}0)$ ring in Plate 12 there must be a group of reflexions corresponding to a, b, c, d and e at 90° to the arm A. In this case, therefore, the planes producing the low angle reflexions are the $\{11\bar{2}0\}$, and the moiré pattern in Plate 12 is an image of the $\{11\bar{2}0\}$ planes.

Moiré Spacings

During the course of this work numerous moiré patterns were photographed and their spacing measured. As the spacing is related to the angle of twist ($S = d/\alpha$), a survey of the spacings should show if any preferred orientation exists between crystallites. A histogram of 84 spacings measured up to May 1959 is shown in Fig.(14). In no case was a spacing measured unless more than 15 lines were distinguishable on the micrograph. In this histogram, three distinct peaks are visible at $20\text{-}30\text{\AA}$, $60\text{-}75\text{\AA}$ and $85\text{-}95\text{\AA}$.



Histogram of values found for the moiré spacings measured from thirty-four micrographs.

Fig. 14.

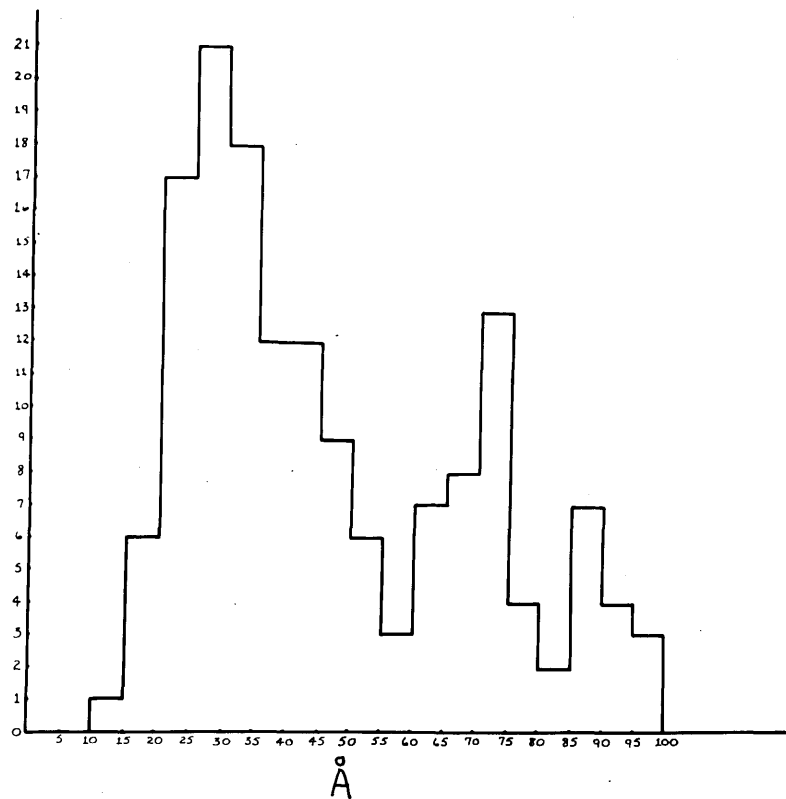


Fig. 15

Fig.(15) shows a second later histogram with almost double the number of spacings, 154. With increase in number, there has been no significant change, the three peaks only becoming more pronounced. It would appear, therefore, that certain preferred orientations exist between crystallites.

Grain Structure of Synthetic Graphite.

Crystallite Alignment.

According to Bacon's X-ray results, the average depth of a crystallite is six layers while its average width is $600\overset{\circ}{\text{A}}$. As the thin sections examined in this work were on average 9.5 crystallites in depth, between each crystallite there being an assumed random rotation, a variety of moiré patterns differing both in spacing and rotation should be observed in a large area of section. Plate 16 shows such an area, several different moiré patterns being evident. This micrograph shows a strong resemblance to the familiar grain structure of etched metal specimens as viewed under the light microscope. In the case of graphite, however, the individual grains are much smaller and are below the limit of resolution of the light-microscope, but with the higher resolving power of the electron microscope, the resemblance is apparent. Each moiré pattern in Plate 16 defines in extent and outline the area of a separate

PLATE 16.

Electron micrograph of a thin section showing the characteristic grain structure revealed by the moiré patterns. There is a sharp grain boundary along MN and a pore at A. (x250,000)



M

A

N

crystallite or grain, the sharpness of the boundaries between crystallites, such as MN, indicating that the edges of the layer nets in this section must be in perfect lateral alignment.

The sections shown in Plates 17 and 18 also show differing moiré patterns, but here the boundaries between them are more diffuse. Now, in a stack of crystallites it is unlikely that the dimensions of each crystallite are identical or that the crystallites are arranged in perfect lateral alignment. Fig.(16) shows a series of crystallites, of random thickness, with a random lateral displacement in the alignment of the layers.

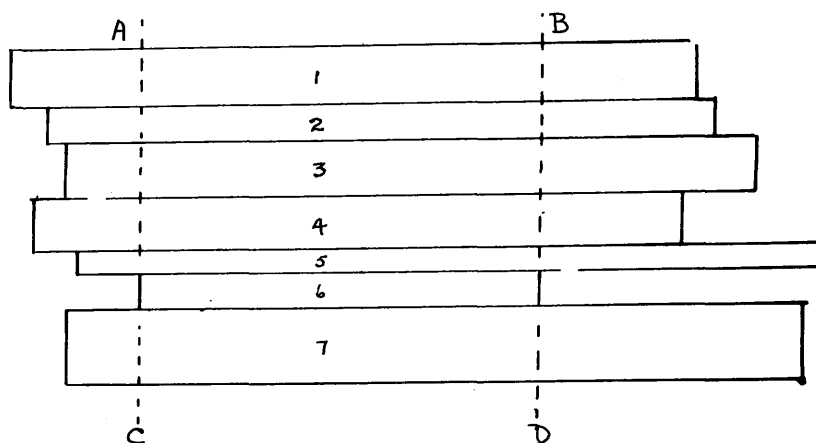


FIG. 16

Such an arrangement would naturally give rise to a very diffuse boundary between adjacent stacks. Moreover, if a resolvable moiré pattern is produced by an appropriate twist between stacks, e.g., 2 and 6, it will only cover the region AB or CD and hence will be representative neither of the dimensions of the component crystallites nor of the overall size of the grain. Measurement of such a pattern will therefore give only a minimum value for the grain size. Now, in several cases, e.g., Plate 16, the grains are well defined and the grain boundaries sharp indicating perfect lateral alignment. Lateral misalignment is therefore probably present to a greater or less extent in all graphite grains ranging from the extreme case where the boundary is very wide and diffuse to the other where it is so sharp that no misalignment can be detected in the electron microscope.

Grain Size.

During the course of this work, three different blocks of Calder 'A' quality graphite were examined. In each case, measurements of the grain size were made with a planimeter and the results are shown in Table 4.

PLATE 17.

Extensive area of thin section showing numerous complex moiré patterns. Grain boundaries are less well defined than in Plate 16 and pores are again evident at C, D and E. (184,000)



PLATE 18.

Further area of thin section showing a well defined grain structure. A rather diffuse pore is apparent along the grain boundary AB. (x260,000)



A

Sample	Number of Measurements	Minimum μ^2	Maximum μ^2	Mean μ^2	Overall Mean μ^2
G ₁	30	0.039	0.20	0.1	} 0.106
G ₂	47	0.035	0.68	0.132	
G ₃	61	0.016	0.47	0.088	

Table 4.

The measurements on G₂ and G₃ cover a much wider range than those on G₁. This is to be expected, however, as the G₁ measurements were made on the earliest sections and later, improvements in technique resulted in larger and therefore more representative areas of section becoming available. The overall mean of $0.106\mu^2$ with a standard deviation of $0.074\mu^2$ from 138 measurements is hence unlikely to be radically altered by further investigation on new samples.

Overlap.

From the breadth of the (000 ℓ) spectra in X-ray powder photographs, Bacon deduced that the lateral dimensions of the crystallites in synthetic graphite remained fairly constant to a depth of 400\AA , although within such a stack of layer net planes there were numerous twists or lattice rotations. As clearly defined moirés were only obtained from sections less than 200\AA in thickness, many sections show no trace of any alteration in the lateral dimensions of the crystallites with depth. Plate 19, however,

PLATE 19.

This micrograph as well as illustrating the packing of numerous crystallites of assorted shapes and sizes shows clear evidence of grain overlap. It also differs from previous micrographs in that the contrast varies widely from grain to grain giving it a mottled appearance.

(x170,000)



PLATE 20.

This micrograph, of the same area shown in Plate 19, was taken after the specimen had been removed then replaced in the microscope. Several overlapping grains are outlined and two pores are evident at A and B. The contrast of numerous grains has completely altered, some which were dark in Plate 19 now being comparatively light and vice-versa. (x170,000)



shows an area which does.

A study of the interaction of the moiré patterns in this plate and in the accompanying Plate 20, which is the same area taken slightly later, shows that several grains are overlapping each other. A few have been outlined in Plate 20. Although not common, this overlapping did occur in several sections. Now the measurements in Table 4 show that a grain can vary in size from $0.016\mu^2$ to $0.68\mu^2$, so that if we have two stacks of crystallites, each 400\AA in thickness, directly on top of each other, then the wide variation in the possible dimensions of a grain will make it inevitable that overlap will occur between groups. The section in Plate 18, therefore, must have been cut on either side of the boundary between two such stacks.

Extinction Effects.

A striking feature of Plates 19 and 20 is their mottled appearance due to the widely differing contrast in individual grains. Comparison of similar grains in the two plates reveals another remarkable feature: in some cases the contrast is reversed. Although Plate 20 was taken after 19 and after the specimen had been taken out and then replaced, the only change to occur would have been a slight alteration in the orientation of the specimen to the electron beam.

When an electron beam strikes a crystal oriented so that a set of its strongly diffracting planes satisfy the Bragg condition, a large proportion of the incident beam is removed from the central image forming beam. The image of the crystal thus appears abnormally dark in comparison with surrounding material. Any slight alteration in the orientation of the crystal to the beam immediately returns the contrast of the crystal to normal.

The dark grains in Plate 19, therefore, must be oriented at the Bragg angle to the electron beam. In Plate 20, a slight change in orientation has returned the dark grains of Plate 19 to normal contrast, but has oriented other grains at the Bragg angle. The mottled appearance of a section thus means that the layer net planes in different grains are tilted at a very small angle with respect to each other.

Grain Boundaries.

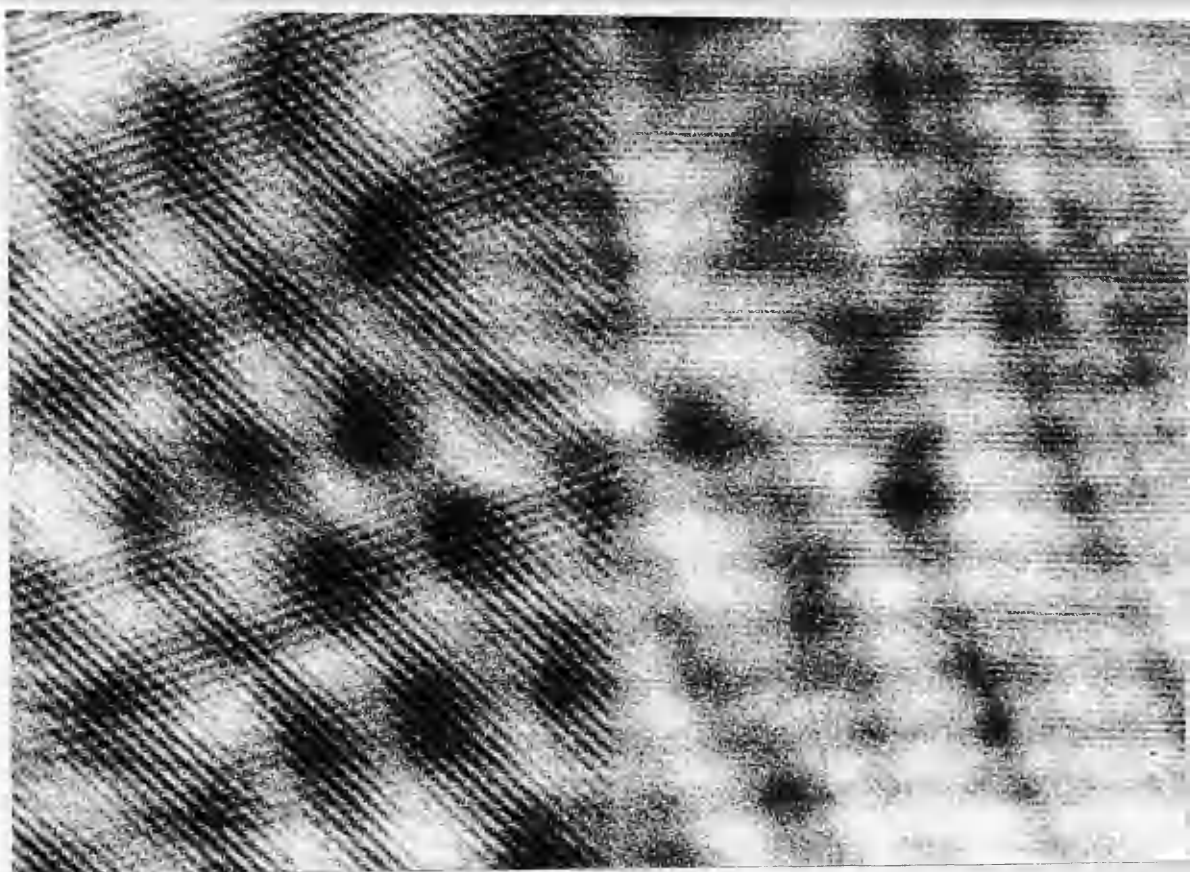
In the sections of synthetic graphite, two types of grain boundary have so far been observed. In the first type, illustrated in Plate 16, MN, and Plate 18, AB, the boundary is between two distinct grains with a pore separating the grains. This type of boundary leaves the free edges of the graphite sheets as possible reactive sites in the structure. Plate 21 shows an example of the second type, that between two different moiré patterns. In this

PLATE 21.

This micrograph is a good example of the type of boundary occurring between two moiré patterns of different spacing. (x320,000)

PLATE 22.

Here, the boundary illustrated is between two patterns of the same spacing, one being a spot pattern, one a line pattern. (x425,000)



type no pore is evident. As the moiré patterns differ both in orientation and spacing, the adjacent component lattices must be at an angle to each other. If, therefore, component crystallites of the moiré pattern in each grain are immediately adjacent, the boundary between them will be a series of edge dislocations. It is possible, however, that the component crystallites may not be adjacent, in which case it must be assumed that the separation between crystallites is too small to be resolved in the microscope.

Sub-Grain Boundary.

What could be defined as a type of sub-grain boundary is shown in Plate 22. Here, the left-hand side of the micrograph shows a spot pattern indicating that the lattice is exactly perpendicular to the electron beam, while the right-hand side shows only a line pattern. The right-hand side of this crystallite must therefore be tilted with respect to the electron beam and also with respect to the remaining area of the crystallite.

Pore Sizes.

As with grain boundaries, two distinct types of pore can be distinguished. The first type is well illustrated by A and B in Plate 20, the pore being caused by failure of several grains to close-pack due to their non-uniform shape. Neither of these pores extends right through the section,

in both cases grain overlap obscuring the edges of the pore. Measurements on this type have given values ranging from 615\AA to $2,200\text{\AA}$ for the maximum diameter.

The second type, illustrated by AB in Plate 18, occurs between only two grains. The width of this type can vary considerably - compare A in Plate 16, C, D and E in Plate 17. In Plate 17, these pores again do not extend through the section, the moiré patterns observed across the pores indicating the presence of, at least, two crystallites. As before, this is due to grain overlap. Measurements on this type give a range of from 50\AA to 450\AA for the maximum width of the pore.

Pore Distribution.

In comparison to the extent of the areas examined and the number of grains observed, the total number of pores was very small. It must be remembered, however, that any pore of less than 15\AA diameter will be theoretically invisible while, in practice, because of the rapid filling up of small holes by contamination in the microscope, the limit of observation is probably at least twice this value. The micropores of Loch et al. will therefore be undetectable in the electron microscope, except if filled with electron opaque material.

Observation of Dislocations.

In several moiré patterns, half-lines were observed indicating the presence of edge or screw dislocations in one of the component crystallites.

One Extra Half-Line.

The moiré pattern in the thin section in Plate 23 shows the presence of a dislocation in the area within the white rectangle. Seven lines are marked on the left-hand side of this enclosed area and six only are marked on the right-hand side. The extra half-line is number 4.

Plate 24 shows an example of a double line moiré pattern, the coarse spacing here merely being a modulation of the intensity. An enlargement of the left-hand side of Plate 24, shown in Plate 25, reveals that dislocations are present in the fine moiré pattern, but only in the areas between the dark bands. If Plate 24 is tilted and viewed along the direction of the fine spacing, it will be seen that, in some cases, the extra half-line introduced between the dark bands is not continuous throughout the lattice but terminates again within the area shown in the plate. Another example of a dislocation series is shown in Plate 26, this area having been oxidised at 350°C for 35 mns. In each example the distance between successive dislocations is approximately equal, in Plate 25 being 400\AA and in Plate 26, 340\AA .

PLATE 23.

In this area of thin section, an extra half-line is evident in the moiré pattern. Within the white rectangle, seven lines are marked on the left-hand side and only six on the right-hand side. The extra half-line is number 4. (x398,000)



PLATE 24.

In this double line pattern there is a series of dislocations present, these occurring only in the fine pattern, in the areas between the dark bands.

(x275,000)

PLATE 25.

Higher magnification view of left-hand half of Plate 21. The extra half-lines 8, 18 and 28 appear only in the top half of the micrograph. (x623,000)

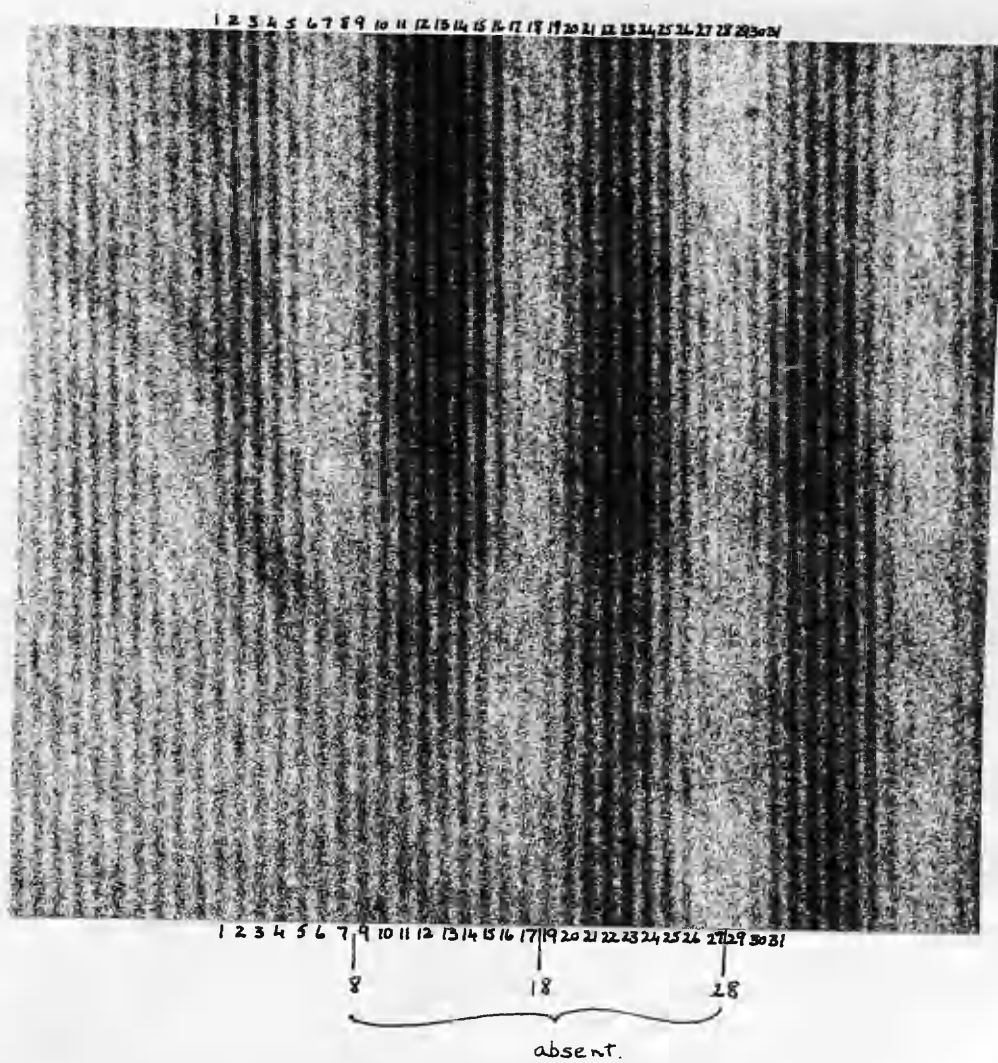
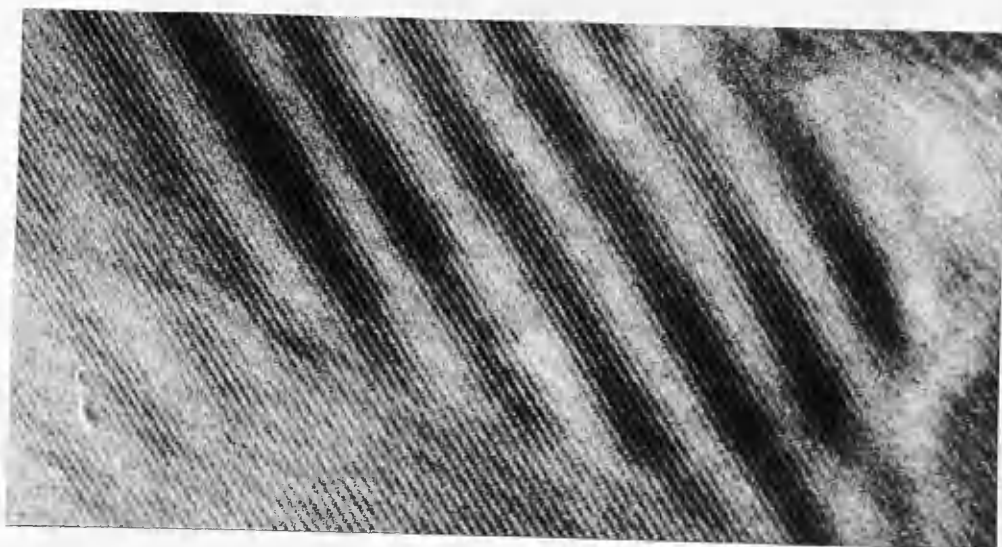
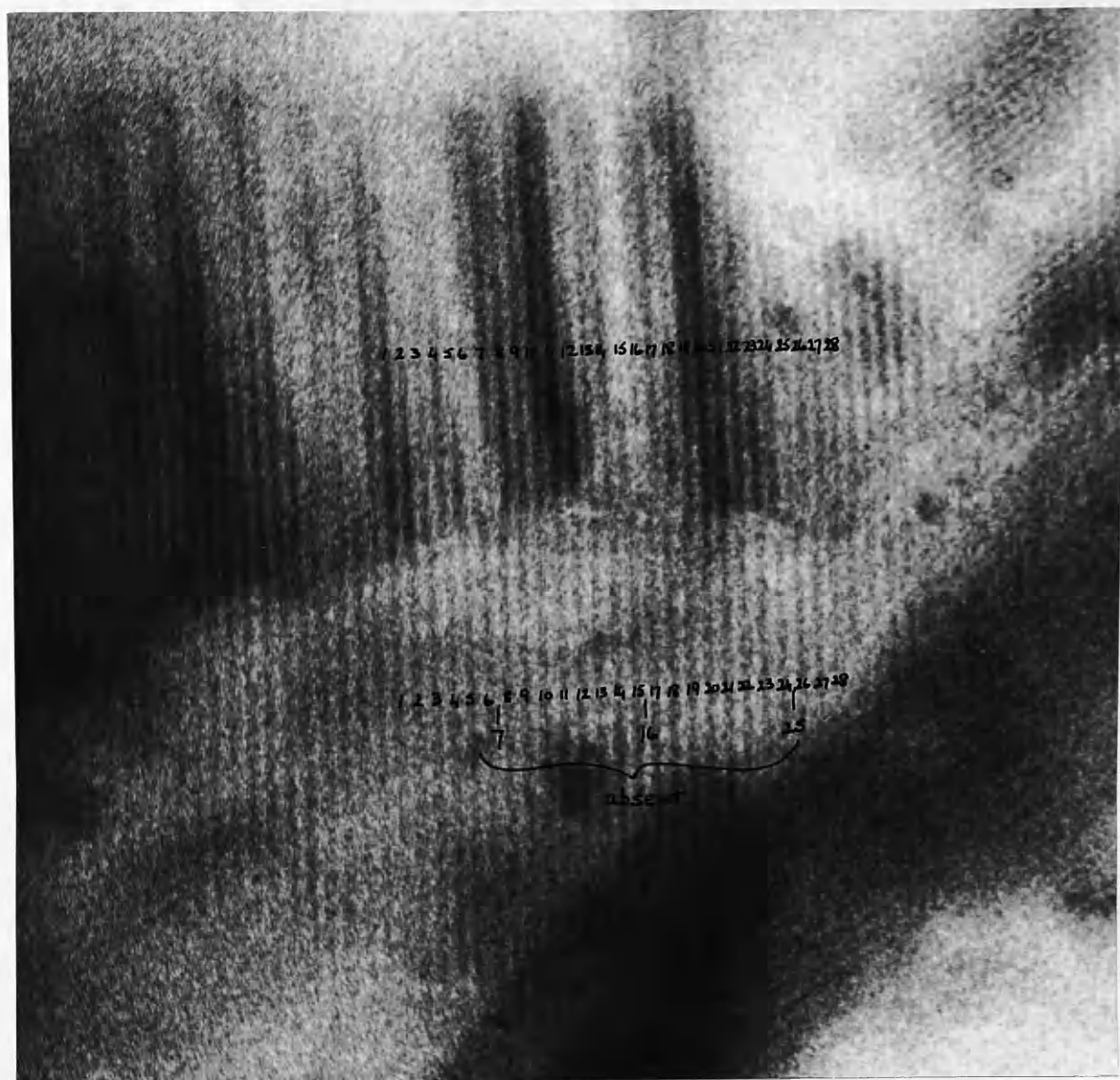


PLATE 26.

This thin section has been slightly oxidised.
A series of dislocations appears in the moiré
pattern, the extra half lines appearing only
in the top half of the plate. (x640,000)



Two Extra Half-Lines.

Only one example was found of a dislocation in a spot pattern, all others being in line or rectangular patterns. The pattern is shown in Plate 27, and here there are two extra half-lines evident in the direction indicated by the arrow A. As the spot pattern is not very clear, an enlargement is shown in Plate 28 and a trace of it has been drawn out in Fig.(17)a. In Figs.(17)b and (17)c lines have been drawn through the rows of dots at 60° to the direction of the two extra half-lines in Plate 28. In these directions only one extra half-line appears.

A slightly different case where two extra half-lines appear is shown in Plate 29. Within the rectangle there are 27 lines on the left-hand side and only 25 on the right. Here, however, the two extra half-lines do not appear together but singly, separated by two or three moiré spacings. Considerable strain appears to have been caused in the lattice by these dislocations, the moiré pattern being distorted along the line AB.

No moiré patterns were observed with three or four extra half-lines.

Dislocation Density.

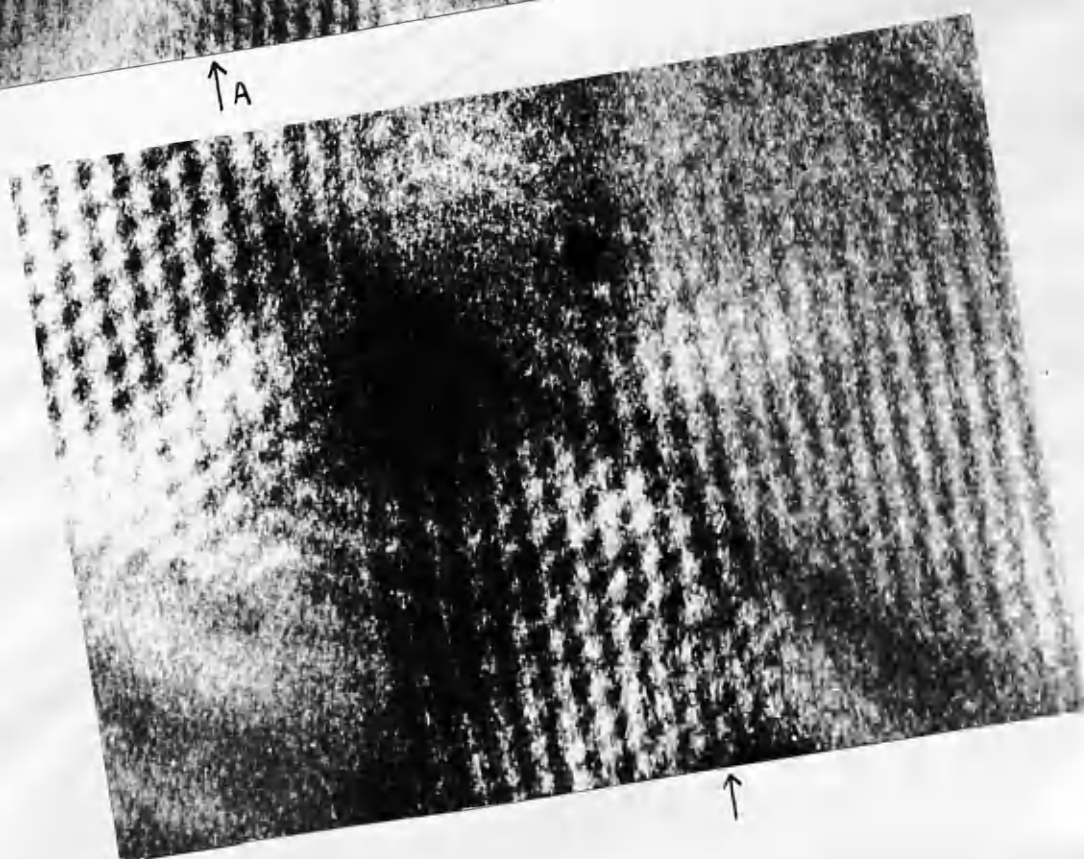
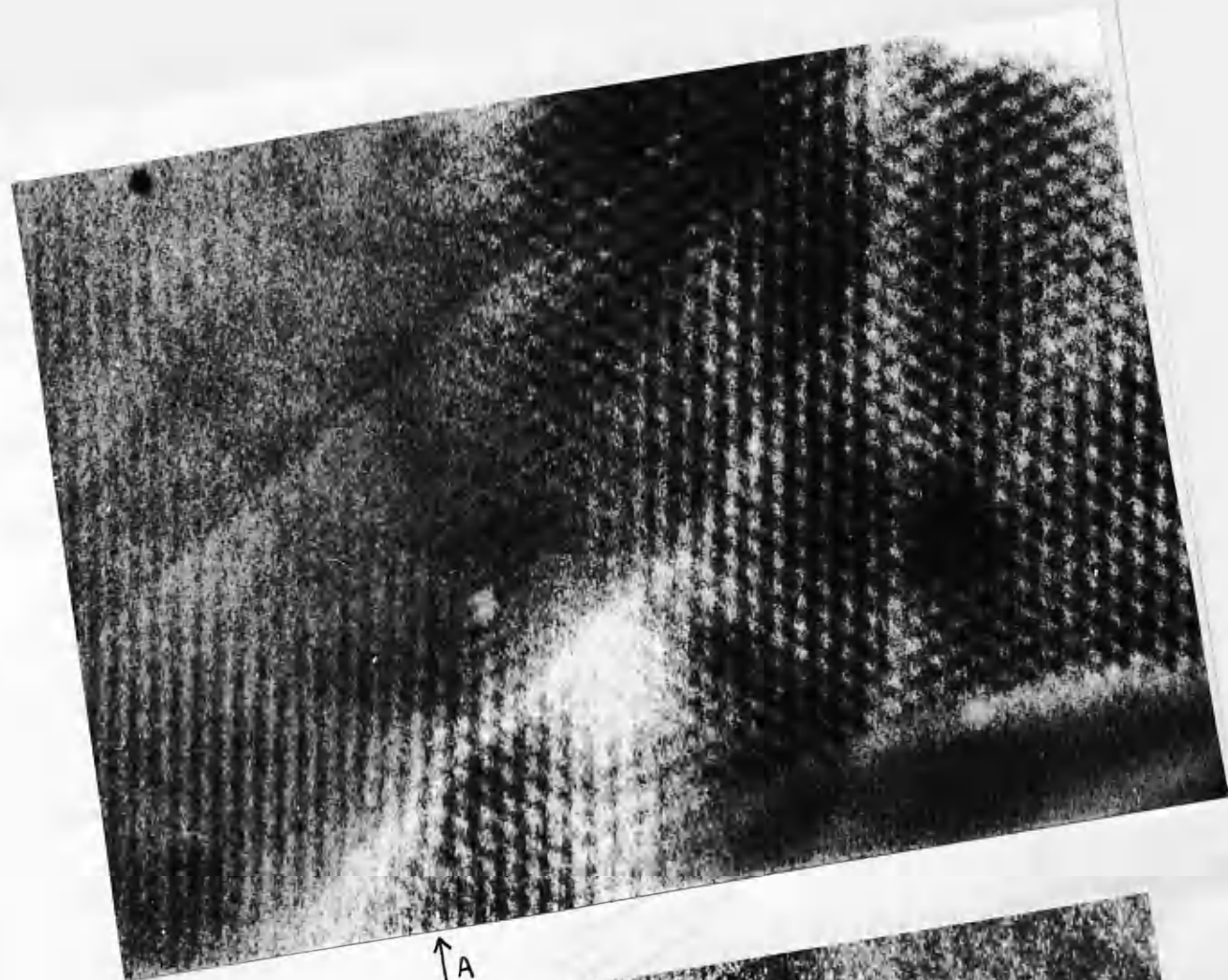
An estimate of the dislocation density in the three samples of graphite was obtained by determining the number

PLATE 27.

In this spot moiré pattern, there are two extra half-lines evident at the point marked by the arrow, A.

PLATE 28.

Enlargement of area in Plate 26 containing extra half-lines. (x640,000)



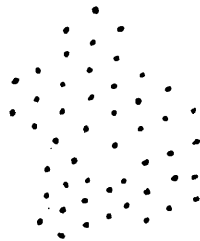


Fig 17a

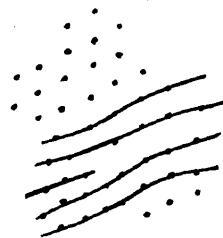


Fig. 17b.

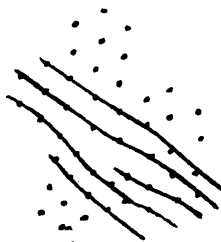


Fig. 17c.

PLATE 29.

Two extra half-lines appear in this line moiré pattern in the area within the rectangle. In this case, they are separated by a few moiré spacings. Considerable distortion has arisen in the surrounding lattice along the line AB. (x410,000)

A

27

V



B

of dislocations present in the grains used in grain size measurements. The results are given in Table 5.

Sample	Dislocation Density /cm ² .
G ₁	3.3 x 10 ⁷
G ₂	3.1 x 10 ⁷
G ₃	3.7 x 10 ⁷

Table 5.

Slip Lines.

In the top left-hand corner of Plate 9 the coarse pattern of the double-line moiré pattern is out of register across the line AB. One of the component lattices must also therefore have a similar discontinuity. The simplest way in which this can occur is by slip of one area of lattice past another. These discontinuities in otherwise regular patterns are thus evidence of slip planes in the graphite lattice perpendicular to the layer net planes. As they were fairly frequently observed slip appears to take place readily in this orientation.

After making improvements in technique, however, it proved possible to cut sections, extensive areas were suitable for a study of grain size. The electron diffraction evidence showed some small areas were of fairly perfect single crystals, or almost perfect parts of the crystals. The extent of the areas is small, and because of the grain size, the areas are small, and the areas are small.

DISCUSSION.

The question, as to the character of the grain effects, shows that the grain size is small, and the grain size is small, and the grain size is small.

Small grains

Small grains

A schematic diagram of the grain size is shown by a between the individual grains and a beam of electrons of plane in the first lattice and then again to other planes in the second lattice, but in the case of the first lattice, the beam is not in the same plane as the second lattice, but in the same plane as the first lattice.

Nature of Sections.

When this investigation began it was exceedingly doubtful if sections of synthetic graphite could be cut, and if so, if they would provide any useful information. With steady improvements in technique, however, it finally proved possible to cut sections, extensive areas of which were suitable for a study of grain size. The electron diffraction evidence showed that such areas were composed of basal planes lying parallel or almost parallel to the plane of the section. The extent of the areas indicates that the plane of the a-axis can remain the same, or almost the same, over a much larger area than previously supposed. The qualification is introduced because the extinction effects showed that adjacent grains in such an area could be tilted at a very small angle to each other.

Moiré Patterns.

a). Formation

A rotational moiré pattern is formed by interference between the undeviated beam and a beam diffracted by a set of planes in the first lattice and then again by a similar set of planes in the second lattice, but in the opposite sense. If the moiré pattern is interpreted as an image of these diffracting planes then, for complete analysis, the

spacing and Miller indices of the planes must be known. In the graphite sections there are two sets of strongly diffracting planes, the $\{10\bar{1}0\}$ and the $\{11\bar{2}0\}$. These planes are shown in Fig.(18). It did prove possible in one diffraction pattern to determine uniquely the diffracting

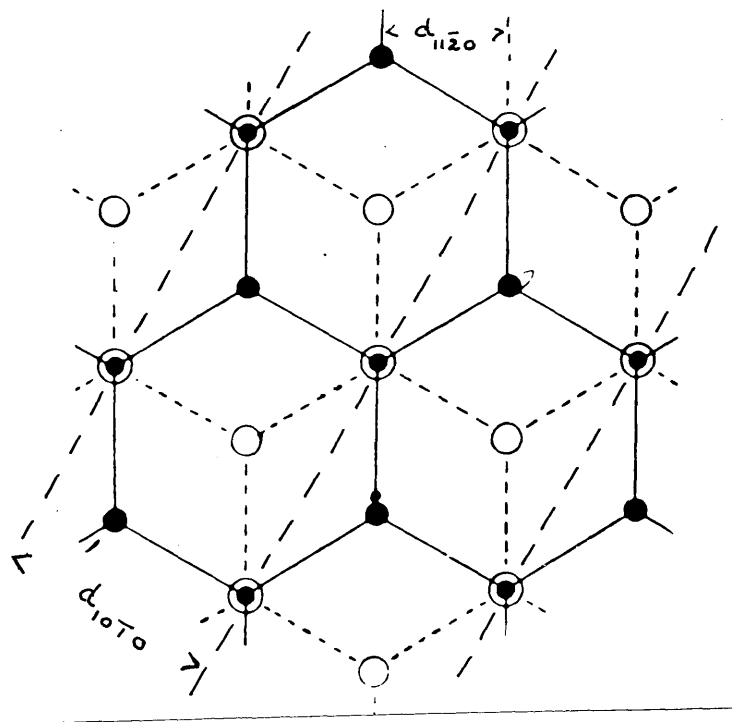


Fig.(18)

planes as $\{11\bar{2}0\}$ but this did not prove possible with every pattern, nor were diffraction patterns taken from every moiré pattern. Now Goodman (1957), examining crystals of boron nitride which has a structure similar to graphite, the layer nets being stacked directly on top of each other and not displaced alternately, has shown that line moiré patterns can be formed from the $\{10\bar{1}0\}$ as well as the $\{11\bar{2}0\}$. This should also, therefore, be possible in graphite and

consequently a line moiré pattern can be interpreted as arising from either set of planes. Although this problem cannot be resolved for a simple line moiré, in certain particular types of line moiré the diffracting planes can be uniquely determined.

Indexing from Rectangular Patterns.

While discussing the rectangular pattern, Plate 8, it was noted that, in all observed patterns, the ratio of spacings was 1.72 ± 0.06 . Now the ratio of $d_{10\bar{1}0}/d_{11\bar{2}0}$ is 1.73. As sets of planes of the required spacing occur at right-angles in the lattice, $(11\bar{2}0)$ and $(1\bar{1}00)$, it would appear that the moiré pattern is an image of these lattice planes. Hence, the lines in the moiré of larger spacing will be images of the $(1\bar{1}00)$ planes and those of smaller spacing, images of the $(11\bar{2}0)$ planes. In this way, it was possible to index the missing plane in Plate 23 as $(1\bar{1}00)$.

One of the conditions for direct resolution of lattice planes in the electron microscope is that the planes to be resolved must lie almost parallel to the electron beam. This condition also applies to the planes giving rise to doubly diffracted beams. If, now, a graphite lattice is tilted along the $(11\bar{2}0)$ direction, the $(11\bar{2}0)$ planes will still remain parallel to the beam, but the $(1\bar{1}00)$ at right-angles to them will not. Hence, the planes imaged at right-

angles to $(11\bar{2}0)$ will more likely be $(1\bar{1}01)$ or $(1\bar{1}02)$ with spacings 2.03\AA and 2.09\AA . The ratios of these spacings to the $(11\bar{2}0)$ spacing are still within the range observed on the moiré patterns.

Indexing from Double Line Moiré Patterns.

Fig.(19) shows three line gratings, P, Q and R, two, Q and R, making a very small angle with each other, the third, P, making a large angle with these two. The

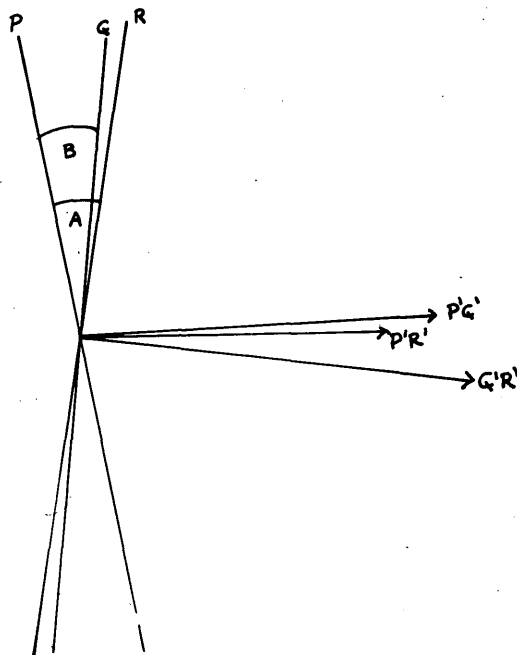


Fig. 19.

directions of the three resulting moiré patterns are indicated by the dotted lines. The two largest angles A and B produce the fringes P'R' and P'Q', while the small angle A-B gives the fringe Q'R'. As the direction of a moiré is perpendicular to the bisector of the angle between

the component gratings, it can easily be shown that the angle between the fringes $P'Q'$ and $P'R'$ is $\frac{A-B}{2}$. If this angle is very small, $P'Q'$ and $P'R'$ can be treated as two parallel line gratings of different spacing - thus giving rise to the moiré $Q'R'$. Now, Bassett et al. have shown that the effect of a small lattice rotation in the case of the parallel moiré is simply to alter the direction of the moiré. Moreover, they deduced that if the two lattices are rotated through a small angle, Θ , the moiré pattern rotates through an angle ω given by

$$\omega = \frac{\Theta \cdot a_1}{a_2 - a_1} \quad (1)$$

where a_1 and a_2 are the lattice spacings. In a double line moiré, the angle Θ is $\frac{A-B}{2}$ and ω is the angle between the coarse and fine patterns, it being assumed that the fine spacings are too close to be resolved. Also, the spacing of the coarse pattern, $a_{Q'R'}$ is related to the spacings of the fine patterns, $a_{P'Q'}$ and $a_{P'R'}$ by the formula

$$a_{Q'R'} = \frac{a_{P'Q'} \cdot a_{P'R'}}{a_{P'Q'} - a_{P'R'}}$$

As $a_1 = a_{P'Q'}$ and $a_2 = a_{P'R'}$, (1) becomes

$$\omega = \frac{\frac{A-B}{2} \cdot a_{Q'R'}}{a_{P'R'}}$$

Provided $\frac{A-B}{2}$ is very small, $a_{P'R'}$ can be taken to be the spacing of the fine moiré. Thus, $\frac{A-B}{2}$ can be calculated.

Now the two fine moirés, spacing $\alpha_{P'Q'}$ and $\alpha_{R'R'}$, arose from rotation between gratings. If the fundamental spacing of the gratings, d , is assumed to be the same in each case,

$$\alpha_{Q'R'} = \frac{d/B \cdot d/A}{d/B - d/A}$$

$$\text{i.e. } \alpha_{Q'R'} = d/A-B$$

Hence, it is possible to calculate d .

Due to the difficulty in measuring the very small angles between the coarse and fine moirés and to the error introduced by taking the fine spacing to be a measure of one component, the results are very approximate. However, as there is a large difference between the $\{10\bar{1}0\}$ and $\{11\bar{2}0\}$ spacings, these calculations provided a useful method of uniquely determining the diffracting planes.

The results of calculations on the double line moirés illustrated in this thesis are shown below.

Plate No.	Spacing $\frac{d}{A}$
7	1.16
	1.52
9	2.13
24	1.18
30	1.15.

Plate 9 is a rectangular pattern and hence the interpretation of the formation of such a pattern, discussed above,

is confirmed. The moiré pattern in Plate 24 contains a series of extra half-lines, the above measurement showing that they are associated with the $\{11\bar{2}0\}$ planes in the lattice.

Although only one spacing calculated corresponded to a $(10\bar{1}0)$ plane and that in a rectangular pattern, spectra were often observed on diffraction patterns near the bisector of the 60° angle between two series of double diffraction spots. These could presumably arise from $(10\bar{1}0)$ if the other reflections were from $\{11\bar{2}0\}$ or vice-versa. Hence, double diffraction does occur from the $(10\bar{1}0)$ planes and therefore the possibility that a resolvable moiré will be produced cannot be excluded.

b). Interpretation.

Lattice Image

Line Pattern.

The majority of the moiré patterns observed in this investigation were of the line variety, either single or double. From the few cases in which it proved possible to index the planes producing the doubly-diffracted beams, it was concluded that a line moiré pattern could arise from either $(10\bar{1}0)$ or $\{11\bar{2}0\}$ planes. A line moiré can therefore be regarded as an image of these planes. Now, in graphite, the $\{11\bar{2}0\}$ planes consist of three sets inclined at 60° to

each other, these all being perpendicular to the layer nets, and, therefore, in the microscope, parallel to the electron beam, assuming that the layer nets are exactly perpendicular to the beam. If a series of layer nets are tilted along the $(11\bar{2}0)$ direction, then the $(11\bar{2}0)$ will remain parallel to the beam but the $(\bar{2}110)$ and $(1\bar{2}10)$ will not. Therefore, only a single series of lines will be imaged in the moiré pattern. In a similar way, tilt along the $(10\bar{1}0)$ direction will produce only an image of the $(10\bar{1}0)$ planes.

Spot Patterns.

Ideal Case.

When the layer nets in a series of crystallites are exactly perpendicular to the beam, both the $\{11\bar{2}0\}$ and $\{10\bar{1}0\}$ will be suitably oriented for double diffraction. The resulting moiré pattern will be a superposition of both sets of fringes produced by the doubly diffracted beams. Now, considering first the $\{11\bar{2}0\}$, the three sets will all give interesting fringes and hence, a hexagonally symmetrical spot pattern will result. Similarly, the $\{10\bar{1}0\}$ will produce a hexagonal system of spots; but for the same angle of rotation, the periodicity of these spot systems will differ. As these intersecting fringe systems can be looked upon as images of the planes producing them, the

nature of the moiré pattern can be deduced by considering the interaction of these planes in the direct lattice.

From the unit cell projection in Fig.(20), it can be seen that the $\{11\bar{2}0\}$ intersect at every peak, both single and

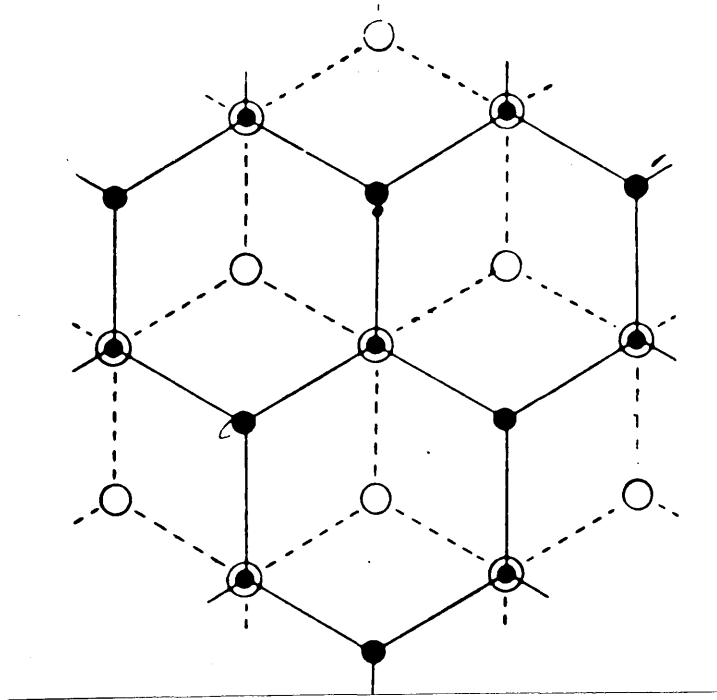


Fig. 20

double, in the projection while the $\{10\bar{1}0\}$ do so only at double peaks. Superposition of the two sets of fringes from such planes should therefore produce a pattern of spots of varying intensity, the strong corresponding to the double peaks of the projection and the weak to the single peaks, or, very simply, a magnified image of the lattice projection.

In order to confirm that this intensity variation, based purely on theory, was practically possible, a large scale reciprocal lattice was constructed of only the first

order doubly diffracted $\{10\bar{1}0\}$ and $\{11\bar{2}0\}$ reflexions which would arise from two rotated lattices. By means of a pantograph punch, a mask was made for an optical diffractometer. The pattern produced by this mask, in which the doubly diffracted $\{10\bar{1}0\}$ and $\{11\bar{2}0\}$ reflexions were given the same intensity, this being one ninth of the central beam, did exhibit intensity variations and corresponded exactly to a magnified image of the lattice projection. It is shown in Fig.(21).

The related interpretation given to moiré patterns is that they represent the Patterson distribution of the lattice projection. In the case of graphite, the Patterson projection of the lattice shows two sets of prominent peaks, one being much higher than the other, and can be qualitatively represented also by Fig.(21). According to this interpretation, therefore, a spot moiré pattern should show spots of varying intensity.

The relative strengths of the $\{10\bar{1}0\}$ and $\{11\bar{2}0\}$ diffracting planes given by the A.S.T.M. index indicate that the $\{11\bar{2}0\}$ is the more strongly diffracting. To allow for this, a mask was made in which the $\{11\bar{2}0\}$ doubly diffracted beams were given four times the intensity of the $\{10\bar{1}0\}$. The resulting pattern is shown in Fig.(22). An intensity variation is still obvious but it is not so marked

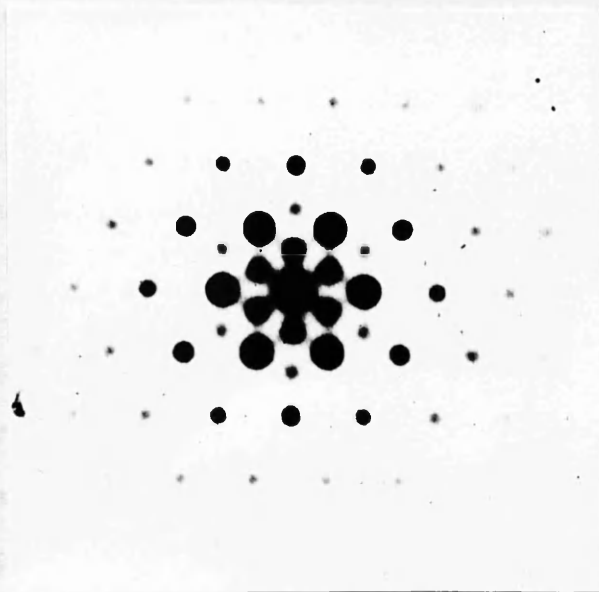


Fig. 21.

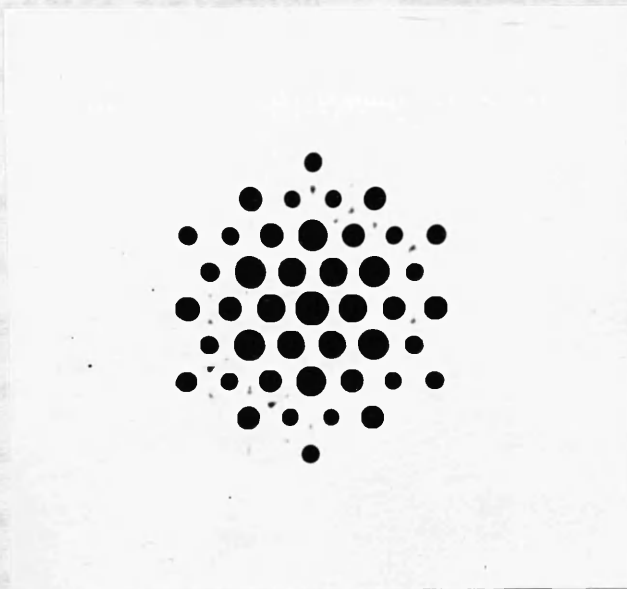


Fig. 22.

as previously. Now, this is an extreme case as no electron diffraction patterns observed showed an intensity difference in the $(10\bar{1}0)$ and $(11\bar{2}0)$ rings approaching the value used in this mask. It can be concluded, therefore, that spot moiré patterns should show intensity variations.

Observed Spot Patterns.

Although numerous spot patterns of widely varying periodicity were observed during this investigation, on not one was there any variation in the intensity of the spots. Now, in the experiments with the diffractometer it was noted that the closely spaced weaker spots in the moiré pattern often coalesced to form a diffuse background, the resulting spot pattern corresponding to only the double peaks of the lattice projection. Moreover, examination of any moiré pattern in this thesis will show that the width of the fringe and thus the diameter of a spot varies directly with the spacing of the moiré. Hence, if a spot pattern is formed from only the double peaks in direct and Patterson projections, then, as the weaker spots corresponding to the single peaks must occur between these spots, it is possible that these weaker spectra will be indistinguishable from the general background.

This explanation of the uniform intensity of spot patterns means that all such patterns are images of the intersecting $\{10\bar{1}0\}$ planes. However, in a few cases

where there was a double line moiré in at least one of the $\{10\bar{1}0\}$ directions, the d spacing of the fringe forming planes could be calculated. In 80% of such patterns the calculated d spacing showed that the planes giving rise to the spot pattern were $\{11\bar{2}0\}$. An example is shown in Plate 30, the spot pattern in the areas L being due to intersection of $\{11\bar{2}0\}$ planes ($d_{\text{calc.}} = 1.18$). A further spot pattern has been produced at M and the corresponding sets of planes in the two spot patterns are at 32° to each other, suggesting that they are formed from the same lattices, this M pattern corresponding in direction and spacing to the $\{10\bar{1}0\}$ type. Confirmation is obtained from Plate 31 where a slight tilt of Plate 30 has produced a rectangular pattern, analysis of which shows that the spots in M are from $\{10\bar{1}0\}$ and those at right angles to L from $\{11\bar{2}0\}$. Plate 30 therefore illustrates that in synthetic graphite, it is possible to produce, from the same two crystallites, two separate spot patterns corresponding to the $\{10\bar{1}0\}$ and $\{11\bar{2}0\}$ planes.

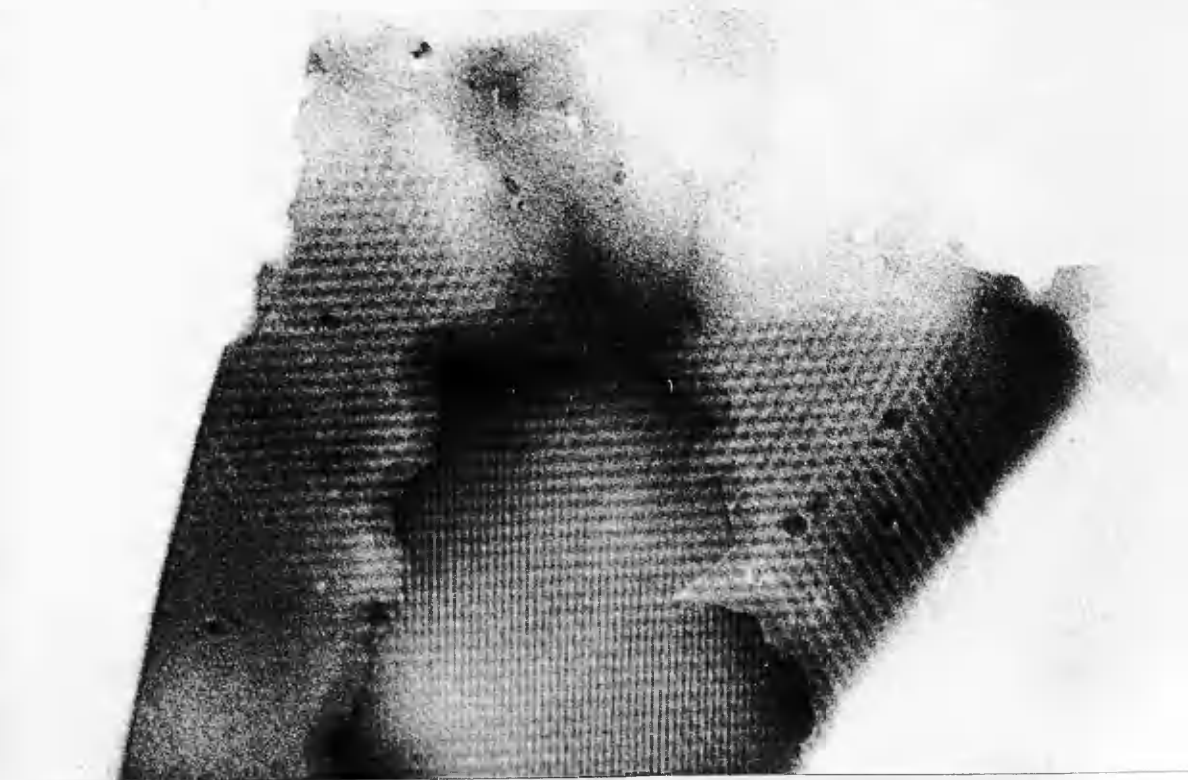
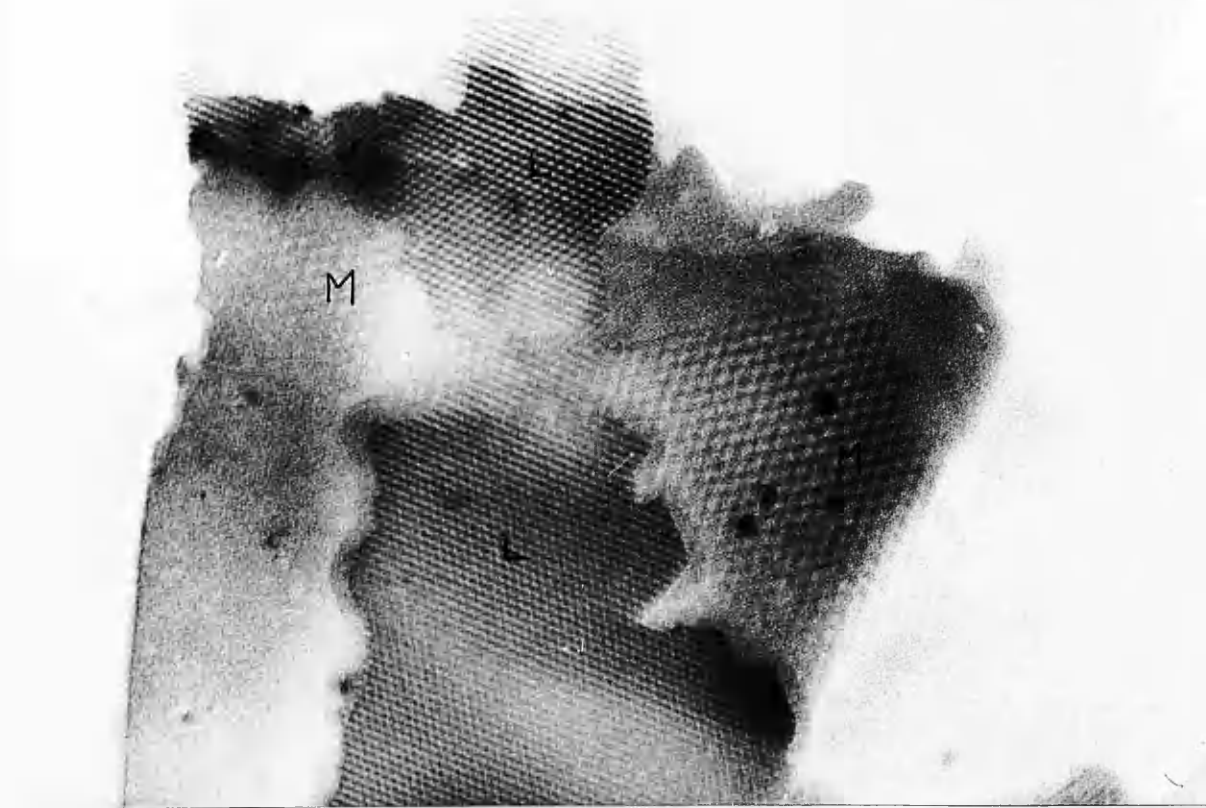
A possible explanation of this rather peculiar effect can be deduced from consideration of the nature of the patterns in Plate 30. The patterns L and M differ markedly in contrast and within all the areas L and M, extinction effects are obvious. Moreover, over the whole section is a

PLATE 30.

Two different types of spot pattern arising from the same component crystallites are illustrated in this micrograph. The spot pattern in the areas L arises from the $\{11\bar{2}0\}$ planes, and in M, from the $\{10\bar{1}0\}$ planes. (x286,000)

PLATE 31.

The area shown in Plate 30 has been tilted and a rectangular moiré has been produced. (x286,000)



very fine moiré of spacing $15\overset{\circ}{\text{\AA}}$ and in no one area is this resolved in three equivalent directions; indeed, in most areas it is a single line pattern. Far from being perfectly planar, therefore, the hexagonal layer nets of the composite crystallites must be tilted and buckled W.R.T. each other. Non-ideal conditions thus exist and non-ideal moirés result, namely a $\{11\bar{2}0\}$ spot pattern.

As all spot moirés cannot be considered simply as an image of the strongest peaks in the direct and lattice projections, further limitations are imposed on indexing moiré patterns, and related double line and rectangular moirés have to be relied on for indexing. These observations emphasise the care required when indexing any moiré pattern and also show that neither of the generalised interpretations quoted by many workers for moiré patterns is correct, a spot pattern being neither an image of the lattice projection nor a Patterson projection, but being only related to both.

Moiré Spacings.

Although the histogram of moiré spacings shows three peaks, this is not necessarily indicative of a preferred orientation for two reasons. Firstly, as a graphite section contains 9-10 crystallites and as a moiré can be formed from any two, e.g., 3 and 8, the histogram may contain examples

of moirés from twists between non-adjacent crystallites. The second objection is that these spacings arise from more than one type of plane both $\{10\bar{1}0\}$ and $\{11\bar{2}0\}$ producing moirés. That a non-Gaussian distribution is still obtained would seem to indicate that a preferred orientation does exist, its value, however, being unascertainable.

Crystallite Size.

a). Depth.

The average depth for a crystallite of 5 layers obtained in this investigation is in good agreement with the X-ray value of six layers measured by Bacon (1957). The major source of error in the electron microscope is inadequate screening of the area selected for diffraction, and this, plus the possibility of unobserved overlap of grains when a section has been cut through the boundary between groups of crystallites, will give high values of \bar{n} and hence low values for the depth. A further source of error is incorrect focussing of the selected area which in extreme cases can lead, as has been shown by Agar (1959), to a diffraction pattern being observed from an area completely outwith the selecting aperture. In view of these possible sources of error Bacon's value must be taken as being the more accurate.

In a graphite section 150\AA thick, with an average crystallite depth of six layers, there will be on average approximately 7 twists or rotations between crystallites. These twists will give rise to many moiré patterns, but whether these will be observed in the microscope depends on the resolution of the instrument and the spacing of the diffracting planes. For routine resolution in the microscope, the spacing of the moiré pattern must lie between 15\AA and 150\AA , and, therefore, for the $\{11\bar{2}0\}$ planes, the twist between crystallites must lie between $\frac{1}{2}^\circ$ and $4\frac{1}{2}^\circ$ and for the $\{10\bar{1}0\}$ between $50'$ and $8^\circ 8'$.

In order to verify that seven twists in a stack of layers could give rise to a resolvable moiré pattern, sixty series of seven random numbers lying between 0 and 60 have been taken from tables of random numbers and the average number of times any two numbers in a series differed by less than 4 has been worked out. Numbers were taken only between 0 and 60 because of the hexagonal symmetry of the graphite lattice, and a difference of 4 was used as only the $\{11\bar{2}0\}$ planes were being considered. A value of 2.6 was found and hence, on average, a stack of graphite layers will give rise to two or three resolvable moiré patterns. The sixty values were analysed as shown below.

No. of times twist between $\frac{1}{2}^\circ$ and $4\frac{1}{2}^\circ$ occurs	0	1	2	3	4
%	5	16.33	31.66	26.66	8.3.

Single, double and triple patterns are indeed frequently observed as predicted by the table (a double line moiré must be considered as three moirés), and study of the large areas of sections in Plates 15, 16 and 18 will show that the majority observed are double or triple as expected from the table. It is also interesting to note that even with seven twists in a stack, it is possible to have no resolvable moiré pattern, although failure to observe a moiré pattern could also be due to the orientation of the specimen to the beam.

For the $\{10\bar{1}0\}$ planes with a difference of 7, the average value worked out at 5.4. As no patterns of this complexity were observed, it would appear that very few such planes give moiré patterns or that a preferred orientation exists between crystallites, thus limiting the number of different twists. Now, double diffraction spots have been observed from $\{10\bar{1}0\}$ planes and hence would indicate the preferred orientation alternative, but, as the majority of moirés fit into the analysis in the above table based on random orientation, no definite conclusions can be made from these observations.

b). Extent.

The most unexpected result in this investigation was the value of $0.11 \pm 0.076\mu^2$ obtained for the grain size.

This gives a value of $3,700\text{\AA}$ for the layer diameter compared to Bacon's value of 600\AA . As 137 measurements were made on three different samples, this large increase cannot be explained as being due to an especially crystalline sample. Moreover, even Bacon's most crystalline sample only gave a maximum layer diameter of 2000\AA . Hence, these results would suggest that the values obtained by X-ray line broadening studies are rather low.

In all cases, grain size measurements were made over a uniform area of moiré pattern and as even a rotation of $\frac{1}{2}^\circ$ will produce a perceptible change in a moiré, it is unlikely that sub-units corresponding to Bacon's 600\AA layer diameter exist in these grains. The possible objection that the values given by these measurements are due to the nature of the preparative technique, only those sections containing large grains remaining perfect, can be met by considering the standard deviation of $0.076\mu^2$ which shows a wide variation in grain size, the actual grains ranging from 1400\AA to $9,100\text{\AA}$ in diameter. It should also be emphasised that, due to lateral misalignment, the grain sizes obtained will, in many cases, be minimum values.

Although, therefore, these measurements show a marked deviation from the X-ray values, no attempt can be made to relate this type of X-ray measurement to these values until the grain size of the material used in this work has been

determined by X-ray techniques.

Pore Size and Distribution.

The sections of synthetic graphite examined in the microscope represent areas in a block of material which were, before graphitization, the interior of primary coke particles. Consequently, these areas yield no information on the large open macropores associated with the packing of the primary particles and moreover, as the open pore volume is derived chiefly from these open macropores, the pores observed here are probably representative of the closed pore volume. Evidence in support of this is that in several cases the pore did not even penetrate the 150⁰ thick section.

Macropores.

The large open macropores are caused by the packing of the coke grains and the results of this investigation indicate that the closed macropores, of much smaller dimensions, are due to poor packing of the component crystallites within what was formerly a coke grain. This direct evidence that pores occur only between crystallites confirms a similar suggestion put forward by Loch et al. based on X-ray data. Moreover, the scarcity of pores in these sections supports Dresel and Robert's conclusion that closed pores are sparsely distributed through the material.

Micropores.

No micropores of the kind defined by Loch et al. (1957) were observed, but the observation of diffuse boundaries caused by lateral misalignment of layer nets indicates, at such a boundary, the almost certain existence of very small pores. Hence, Loch et al.'s association of these pores with inter-crystallite boundaries is probably correct. The observations of Dresel and Roberts (1953) and Walker and Rusinko (1958) that the closed pores are made more accessible by oxidation can also be explained. If oxidation is assumed to attack the lattice edges, then the pores along grain boundaries will be widened. Consequently, pores may be exposed between grains which before oxidation were completely closed due to overlap. If micropores are present along grain boundaries, then it is possible that these may widen and thus, that channels may develop permitting a reactant to reach a previously inaccessible area of material.

Dislocations.

Edge or Screw.

According to Bassett et al. (1958) the observation of an extra half-line in a moiré pattern does not uniquely determine the type of dislocation but merely gives the Burgers vector whether it be edge or screw. Before even the Burgers vector can be determined, however, the indices

of the imaged planes must be ascertained. The few cases where this has been possible are tabulated below.

Plate	No. of Half-Lines	Index
23	1	$10\bar{1}0$
25	1	$11\bar{2}0$
27	2	$11\bar{2}0$.

Now, in a layer lattice such as graphite, screw dislocations are most likely to occur by displacement of the layers along the c -axial direction. The Burgers vector will hence be $(000c)$ and not $(hki0)$. The observed dislocations, therefore, with Burgers vectors $(10\bar{1}0)$ and $(11\bar{2}0)$ are most likely edge dislocations.

Structure.

Single Dislocations

The simplest edge dislocation which can exist in the graphite structure is one with Burgers vector $(10\bar{1}0)$. A possible structure for a single layer net containing such a dislocation is shown in Fig.(22).

The number of extra half-lines associated with the six most likely sets of moiré fringes are shown below.

$10\bar{1}0$	$1\bar{1}00$	$11\bar{1}0$	$11\bar{2}0$	$1\bar{2}10$	$\bar{2}110$
1	1	0	1	1	2.

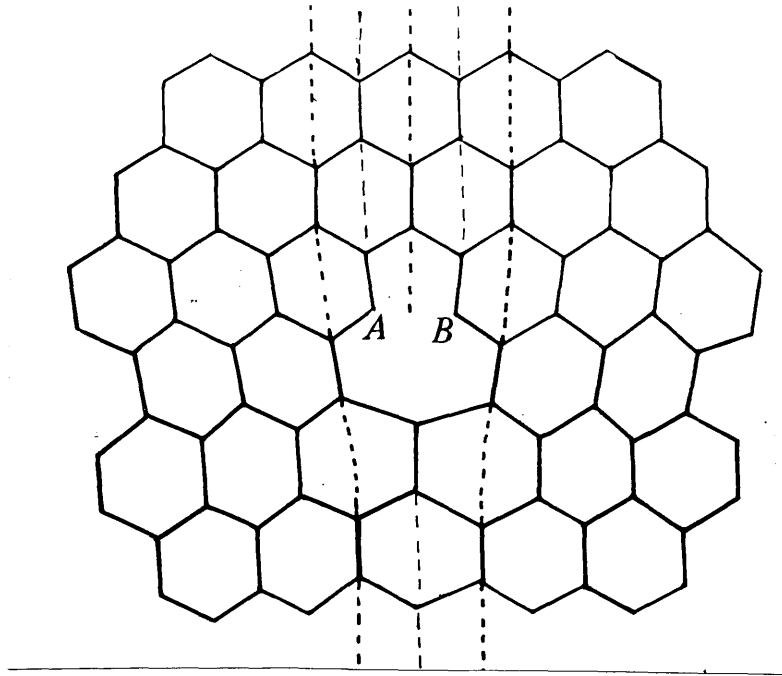


Fig. 22

The structure postulated in Fig.(22) is therefore also representative of moiré fringes with both one and two extra $(11\bar{2}0)$ half-lines. Now, it has already been shown that one extra half-line is also present in each of the two sets of fringes at 60° to those containing the two extra half-lines in Plate 26. As the moiré fringes are known to be produced by $\{11\bar{2}0\}$ planes in this case, these single extra half-lines must correspond to $(11\bar{2}0)$ and $(1\bar{2}10)$ as in the above table. The dislocation imaged in Plate 26 must therefore have the structure shown in Fig.(22), while those imaged in Plates 23 and 25 may have this structure.

In the other example illustrated where only two

extra half-lines were observed in a moiré pattern, the fringes could not be indexed and hence, the Burgers vector is not known. However, as compared to the other observed dislocations, this had produced severe distortion in the lattice, it is unlikely that the two extra half-lines, which were separated by several moiré spacings, were due to dislocations of the type shown in Fig.(22).

Periodic Dislocations.

In only two cases, illustrated in Plates 25 and 26, in this entire investigation were periodic dislocations observed. A technique commonly used in metallurgy to reveal grain boundaries is etching, this producing a series of pits along the boundaries due to preferential attack at the dislocations present in them. These dislocations as first suggested by Burgers (1939) and Bragg (1940) are edge dislocations and are spaced out regularly along the boundary, the spacing being primarily dependent on the angle of rotation of the two adjacent lattices. If, therefore, two sets of $\{11\bar{2}0\}$ planes are rotated through a very small angle θ ($\sim 10'$), a series of edge dislocations will be produced. Such a series of dislocations can be imaged in a moiré pattern if a second perfect lattice is superimposed at a suitable angle on the two oriented lattices. Moreover, if the angle θ is very small there will be no marked change

in the direction of the moiré pattern on crossing the boundary between the two oriented lattices, and hence a series of extra half-lines will be observed in an apparently continuous moiré pattern. This is indeed what is observed in Plates 25 and 26, and therefore would appear to indicate the presence of a grain boundary.

A second moiré pattern is present in Plate 25 in the form of a series of broad, wide fringes. This must therefore be caused by a lattice rotated through a very small angle W.R.T. either of the two component lattices of the fine moiré. Such a lattice would be present if an area of the lattice containing the dislocations did not misorient on crossing the boundary. The situation now envisaged is shown in Fig.(23), A and B being the two slightly mis-

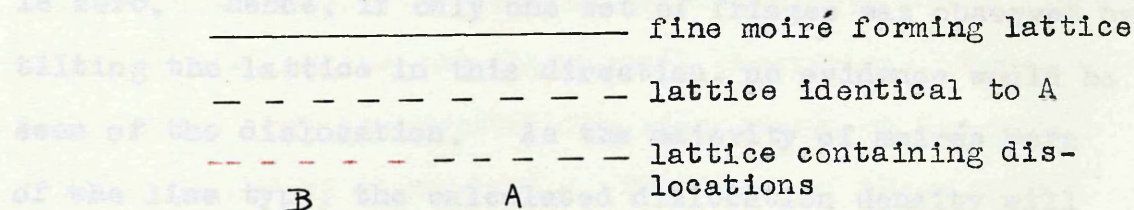


Fig.(23)

oriented lattices giving rise to the series of dislocations. The broad moiré spacing would therefore be due to the mis-orientation angle θ . Now a similar series of moiré

patterns would be formed if lattice A were not present at all, B merely being a portion of the underlying lattice which had become misoriented. This is probably the true explanation of Plate 26 where there is an edge of a superposed lattice area along the dislocation line. In Plate 25, the fact that the broad moiré is only observed in the dislocation region points to a similar conclusion. Whether this lattice misorientation was actually present in the original material or was produced on heating or on cutting cannot be decided.

Limitations of Technique.

Dislocation Density.

The number of extra half-lines associated with a dislocation of Burgers vector $(10\bar{1}0)$ in the $(01\bar{1}0)$ direction is zero. Hence, if only one set of fringes was observed by tilting the lattice in this direction, no evidence would be seen of the dislocation. As the majority of moirés were of the line type, the calculated dislocation density will be low.

Dislocation Type.

Due to the orientation of the crystallites, only edge dislocations are made visible in the moiré patterns. Assuming that a dislocation of Burgers vector $2(10\bar{1}0)$ would show

twice as many half-lines as one of $(10\bar{1}0)$, from the observation in a line moiré of two extra $(11\bar{2}0)$ half-lines it would be impossible to differentiate between the single and double dislocations. Hence, a dislocation can only be completely and accurately defined when all the possible sets of fringes are resolved, i.e., from a spot moiré pattern.

Moiré patterns can, therefore, only provide an estimate of the dislocation density and, because of the difficulty in indexing a pattern, only in occasional cases any information on the Burgers vector of the dislocation.

Reactivity.

The reactivity in solid graphite must be greatly influenced by the rate of diffusion of reactants into the solid. As this diffusion can only take place through pores and as this investigation has shown that these pores occur between grains and along grain boundaries, it would be expected that the crystallite edges would be the areas first attacked by a reactant. The edges of these crystallites contain atoms less firmly bound than those within the layer nets and several workers have shown them to be consequently more reactive. This work, however, has shown that similarly bound atoms can occur within the layer nets at dislocation sites, thus providing a reactive site within the layer nets.

The suggested structure of the lattice defect provides two types of reactive site, A and B with two orbitals each available for interaction, and the remainder with only one. If, however, as is very probable, a bond is formed across AB to give a five and a seven membered ring, only one type will be present and the reactivity, according to Long and Sykes, therefore limited. As the exact structure of the dislocation is not known with certainty, this is therefore merely conjectural.

The number of these reactive sites, $3.3 \times 10^7/\text{cm}^2$, is greater than the number of screw dislocations observed in crystalline n-hexatriacontane by Dawson and Vand (1951), but less than the number observed, $10^{11}/\text{cm}^2$, in metal films by Basset et al. (1958) using a similar technique.

assumed that the lattice is composed of spheres of equal size and mass. The spheres are arranged in a regular array, and the distance between the centers of two adjacent spheres is the lattice constant. The spheres are assumed to be in contact with each other, and the force between two spheres is assumed to be a function of the distance between them. The force is assumed to be zero when the spheres are in contact, and to increase as the distance between them increases. The force is assumed to be a function of the distance between the spheres, and the force is assumed to be a function of the distance between the spheres.

GENERAL CONCLUSIONS.

The first important result of the present study is the discovery that the force between two spheres is a function of the distance between them. This result is in agreement with the results of other studies, and it is in agreement with the results of the present study. The second important result of the present study is the discovery that the force between two spheres is a function of the distance between them. This result is in agreement with the results of other studies, and it is in agreement with the results of the present study.

The second important result of the present study is the discovery that the force between two spheres is a function of the distance between them. This result is in agreement with the results of other studies, and it is in agreement with the results of the present study. The third important result of the present study is the discovery that the force between two spheres is a function of the distance between them. This result is in agreement with the results of other studies, and it is in agreement with the results of the present study.

Two major advances in the study of synthetic graphite and associated carbons have been achieved by this investigation. Firstly, a widely applicable technique has been developed and proved. Using this technique to obtain areas from any part of a block of material, it is possible to show directly the size and arrangement of the crystallites within the area and the width and type of grain boundaries and pores. It should therefore now be possible to study the reactions of the material with various gases and under varying conditions either by taking samples from a block which has been subjected to reactive conditions, or by carrying out the reactions on the thin sections themselves. With this latter technique, the course of a reaction could be followed on a given area of section, and the reactive sites in the lattice directly observed.

The second important advance produced by this work lies in the application to the study of the structure of synthetic graphite. The results on grain size as well as implying, as they do, a major revision of the hitherto-accepted values given by X-ray methods, are of importance in kinetic studies as they indicate a greatly diminished total grain boundary length and would thus denote a reactivity lower than that previously calculated for reactor

graphite from X-ray results. For the first time in synthetic graphite, a reactive site has been observed and defined within the layer net planes and the estimate of this number/cm². obtained is again of importance in kinetic studies.

- Agar, A.W., Frank, F.C. & Keller, A. Phil.Mag., 4, 32 (1959).
- Amberg, C.H., Spencer, W.B. & Beebe, R.A. Can.J.Chem., 33, 305 (1955).
- Amelinckx, S. Acta Cryst., 8, 530 (1955).
- Amelinckx, S. Acta Cryst., 9, 16 (1956).
- Amelinckx, S. Acta Cryst., 9, 217 (1956).
- Anderson, N.G. & Dawson, I.M. Proc.Roy.Soc.A., 218, 255 (1953).
- von Ardenne, M. Z.wissensch.Mikroskop., 56, 8 (1939).
- Bacon, G.E. Acta Cryst., 3, 137 (1950).
- Bacon, G.E. Acta Cryst., 4, 558 (1951).
- Bacon, G.E. Acta Cryst., 5, 392 (1952).
- Bacon, G.E. Conference on Industrial Carbon and Graphite, London, 1957.
- Bacon, G.E. Crystallographic Studies on Graphite.
U.K.A.E.A. Report.
A.E.R.E. M/R, 2702 (1958).
- Bassett, G.A. & Menter, J.W. Phil.Mag., 2, 1482 (1957).
- Bassett, G.A., Menter, J.W. & Pashley, D.W. Proc.Roy.Soc., A246, 345 (1958).
- Bernal, J.D. Proc.Roy.Soc., A106, 749 (1924).
- Biscoe, J. & Warren, B.E. J.Appl.Phys., 13, 364 (1942).
- Borysko, E. J.Biophysic. and Biochem.Cytol., 2,
- Bradley, D.E. Brit.J.Appl.Phys., 5, 65 (1954).
- Bradley, D.E. Brit.J.Appl.Phys., 10, 198 (1959).
- Bragg, W.L. Proc.Roy.Soc., A89, 248 (1913).
- Bragg, W.L. Proc.Phys.Soc., 52, 54 (1940).
- Burgers, J.M. Proc.Koninkl.Wed.Akad.Wetenschap, 42, 293 (1939).

- Burton, W.K., Cabrera, N. & Frank, F.C. *Nature*, 163, 398 (1949); *Phil.Trans.Roy.Soc.*, A243, 299 (1949).
- Cabrera, N. & Vermilyea, D.A. *Proc.Int.Conf. on Crystal Growth*, New York (1958).
- Cowley, J.M. & Moodie, A.F. *Acta Cryst.*, 12, 423 (1959).
- Dawson, I.M. & Vand, V. *Proc.Roy.Soc.*, A206, 555 (1951).
- Dawson, I.M. *Proc.Roy.Soc.*, A214, 72 (1952).
- Dawson, I.M. & Watson, D.H. *Proc.Roy.Soc.*, A239, 349 (1957).
- Dawson, I.M. & Watson, D.H. *J.Mol.Biol.*, 1, 30 (1959).
- Dowell, W.C.T., Farrant, J.L. & Rees, A.L.G. *Proc. of 1st Reg.Conf. in Asia and Oceania* (Tokyo 1956).
- Dresel, E.M. & Roberts, L.E.J. *Nature*, London, 171, 170 (1953).
- Dupré La Tour, F. *Compt.Rend.*, 202, 1935 (1936).
- Emmett, P.H. & Cines, M. *J.Phys.Chem.*, 51, 1329 (1947).
- Fernandez-Moran, H. *Exp.Cell Research*, 5, 255 (1953).
- Forty, A.J. *Philosophical Mag.*, Ser.7, Vol.XLIII, p.72 (1952).
- Forty, A.J. *Philosophical Mag.*, Ser.7, Vol.XLIII, p.377 (1952).
- Francis, F., Collins, F.J.E. & Piper, S.H. *Proc.Roy.Soc.*, A158, 691 (1937).
- Frank, F.C. *Disc.Far.Soc.*, 5, 48, 186 (1949).
- Frank, F.C. *Phil.Mag.*, 42, 1014 (1951).
- Franklin, R.E. *Acta Cryst.*, 4, 253 (1951).
- Fullam, E.F. & Gessler, A.E. *Rev.Scient.Instruments*, 17, 23 (1946).
- Glauert, A.M., Rogers, G.E. & Glauert, R.H. *Nature*, 178, 803 (1956).
- Green, T.A. & Weigle, J. *Helv.phys.Acta*, 21, 217 (1948).

- Griffin, L.J. Phil.Mag., 41, 196 (1950).
- Hashimoto, H. & Uyeda, R. Acta Cryst., 10, 143 (1957).
- Hassel, O. & Mark, H. Z.Physik., 25, 317 (1924).
- Hennig, G.R., Dienes, G.J. & Kosiba, W. Second U.N. Conference
on Peaceful Uses of Atomic Energy.
Geneva, June 1958.
- Hillier, J. Nat.Bur.Stand.Circ. No.527, Electron Physics,
(1954).
- Hillier, J. & Gettner, M.E. J.Appl.Physics, 21, 889 (1950).
- Hillier, J. & Gettner, M.E. Science, 112, 520 (1950).
- Horn, F.H. Nature, Lond., 170, 581 (1952).
- Konig, H. & Helwig, G. Z.Phys., 129, 491 (1951).
- Labaw, L.W. & Wyckoff, R.W.G. Proc.Nat.Acad.Sci. Wash.,
43, 1032 (1957).
Koninkl.Ned.Akad. Amsterdam, B59,
449 (1956).
- Latta, H. & Hartmann, J.F. Proc.Soc.Exp.Biol.Med., 74,
436 (1950).
- Lipson, H. & Stokes, A.R. Proc.Roy.Soc., A181, 101 (1942).
- Loch, L.D. & Austin, A.E. Proc. 1st & 2nd Carbon Conf.
Buffalo (1956).
- Loch, L.D., Austin, A.E., Harrison, R.J. & Duckworth, W.H.
U.S.Atomic Energy Authority Report.
- Long, F.J. & Sykes, K.W. Proc.Roy.Soc., A193, 377 (1948).
- Mahl, H. Z.Techn.Phys., 19, 17 (1940).
- Markham, R., Smith, K.M. & Wyckoff, R.W.G. Nature, 159,
574 (1947).
- Menter, J.W. Proc.Roy.Soc., A236, 119 (1956).
- Mitsuishi, T., Nagasaki, H. & Oveda, R. Proc.Imp.Acad.Japan,
27, 86 (1951).

- Müller, A. Proc.Roy.Soc., A114, 522 (1929).
- Newman, S.B., Borysko, E. & Swerdlow, M. Science, 110, 66 (1949).
- O'Brien, H.G. & McKinley, G.M. Science, 98, 55 (1943).
- Pashley, D.W., Menter, J.W. & Bassett, G.A. Nature, Lond., 179, 752 (1957).
- Pease, D.C. & Baker, R.F. Proc.Soc.Exp.Biol. and Med., 67, 470 (1948).
- Piper, S.H., Malkin, T. & Austin, H.E. J.Chem.Soc., 2310 (1926).
- Porter, K.R. & Blum, J. Anat.Rec., 117, 685 (1953).
- Richards, A.G., Anderson, T.F. & Hance, R.T. Proc.Soc.Exp. Biol. and Med., 51, 148 (1942).
- Rooksby, H.P. Elect.Times, 102, 19 (1942).
- Schaefer, V.J. & Harker, D. J.Appl.Phys., 13, 427 (1942).
- Schoon, Th. Z.Phys.Chem., B39, 385 (1938).
- Seki, Y. J.Phys.Soc.Japan, 8, 149 (1953).
- Sjostrand, F.S. Experientia, 9, 114 (1953).
- Smith, W.R. & Polley, M.H. J.Phys.Chem., 60, 689 (1956).
- Smith, W.R., Thornhill, F.S. & Bray, R.I. Ind.Eng.Chem., 33, 1303 (1941).
- Suito, E. & Uyeda, N. Proc. of Japan Academy, 33, 7 (1957).
- Thibaud, J. & Dupré La Tour, F. C.R.Acad.Sci., Paris, 191, 200 (1930).
- Trzebiatowski, W. Roczniki Chem., 17, 73 (1937).
- Tsuzuku, T. Proc. of 3rd Conference on Carbon. Buffalo, New York, (1958).
- Verma, A.R. Phil.Mag., 42, 1005 (1951).

Verma, A.R. Proc.Phys.Soc., B65, 525 (1952).

Verma, A.R. Proc.Roy.Soc., A228, 34 (1955).

Verma, A.R. & Reynolds, P.M. Proc.Phys.Soc., BLXVI,
414 (1953).

Volmer, M. & Schultze, W. Z.phys.Chem., A156, 1 (1931).

Walker, P.L. & Rusinko, F. Proc. of 3rd Conference on
Carbon.. Buffalo, New York (1958).

Walker, P.L., Rusinko, F., Rakszawski, J.F. & Liggett, L.M.
Proc. of 3rd Conference on Carbon.
Buffalo, New York (1958).

Williams, R.C. & Wyckoff, R.W.G. J.Appl.Phys., 17, 23
(1946).

An electron microscope study of synthetic graphite

BY I. M. DAWSON AND E. A. C. FOLLETT

An electron microscope study of synthetic graphite

By I. M. DAWSON AND E. A. C. FOLLETT

An electron microscope study of synthetic graphite

BY I. M. DAWSON AND E. A. C. FOLLETT

Department of Chemistry, The University, Glasgow, W. 2

(Communicated by J. M. Robertson, F.R.S.—Received 15 June 1959—

Revised 9 July 1959—Read 3 December 1959)

[Plates 24 to 29]

The ultra-microtome has been used to obtain thin sections of synthetic graphite blocks. The thickness of the sections was measured by shadowcasting and measuring the shadow length at appropriate edges. An average value of 150 \AA was obtained. Transmission electron micrographs of thin sections showed moiré patterns and the interrelation of these moiré patterns revealed a characteristic grain structure in graphite akin to that seen in metals but with component microcrystals of smaller dimensions. The area of the individual microcrystals forming the grain structure was measured and was found to be $0.11 \pm 0.074 \mu^2$. The boundary between neighbouring microcrystals was narrow and of around 50 \AA in width. Pores were visible at the junction of three or more contiguous microcrystals and were of diameter 400 to 800 \AA .

The selected-area electron diffraction technique was used to determine the orientation of individual microcrystals in the graphite sections. It was found that the hexagonal layer net planes were lying parallel or at a very small angle to the plane of the section. The electron diffraction patterns were also used to correlate the layer stacking faults in individual microcrystals both by counts of individual reflexions on the $(11\bar{2}0)$ diffraction ring and by counts of the extra reflexions due to the long spacings between successive displaced layers. The average value of 13 \AA found for the distance between successive stacking faults is equivalent to the distance between four hexagonal layer net planes.

The moiré patterns in the electron micrographs could be related to the long spacings in the electron diffraction patterns. It was possible to calculate the angle of twist between successive stacking faults from the long spacing or from the moiré pattern.

Dislocations were seen in many of the thin sections and were observed as extra terminating half-lines in the moiré patterns; these dislocations were present in the hexagonal layer net planes themselves and indicated that there was in this region a considerable deformation of the benzenoid structure of the hexagonal layer nets. The measured frequency for their occurrence was $3.3 \times 10^7/\text{cm}^2$. Slip planes were also detected in some specimens.

1. INTRODUCTION

(a) *The structure of graphite*

Since the determination of the structure of graphite by Bernal (1924) more detailed studies of natural and artificial graphites prepared by a variety of methods and from a variety of starting materials have shown that, although the classical structure described by Bernal is still the prototype for all graphite structures, variations exist. These variations manifest themselves in modified X-ray diffraction patterns. Lipson & Stokes (1942) described the rhombohedral form with *ABC* layer stacking instead of the *AB* layer stacking of the classical form, and in a study of natural and synthetic graphites Franklin (1950, 1951) and Bacon (1951, 1958) have shown that, in addition to the modification of layer stacking which gives rise to the rhombohedral form, local changes in the stacking and arrangement of the hexagonal layer nets in graphites produce considerable variations in lattice parameters.

The available evidence suggests that both natural graphite and synthetic graphite have the accepted hexagonal structure but that they contain a proportion of much less highly ordered material in which the layer stacking pattern may be modified and the lattice parameters relaxed. Further, the results would suggest that the chemical reactivity of the solid is associated with the imperfect regions in the lattice rather than with the normal hexagonal structure.

The use of the classical methods of X-ray diffraction to study those regions of imperfection is made difficult by the statistical nature of all diffraction data. In the interpretation of the diffraction diagrams the spectra due to the modified forms are often obscured by the relatively much stronger spectra given by the preponderant amount of the hexagonal form which is present in all cases. On the other hand, the electron microscope offers a direct method of studying crystal structure and crystal imperfection and in the present investigation the two techniques of electron microscopy and electron diffraction were combined.

There have been relatively few electron microscope studies of graphite. Mitsuishi, Nagasaki & Uyeda (1951) observed moiré patterns on thin sheets of graphite. In a general discussion of electron interference and phase effects Dowell, Farrant & Rees (1956) mention that graphite will give interference patterns and in a very brief abstract Grenall (1958) confirms this observation. The first attempt to give a detailed treatment of the mechanism of fringe formation was made by Dowell *et al.* (1956, 1957), and these authors suggest that the moiré pattern obtained from two overlapping crystals, one of which is rotated at a small angle α to the other, represents the Patterson function of the crystal structure for the projection under observation, magnified by a factor d/α , where d is the lattice spacing. This conclusion they sustained by means of an optical analogue. Recently Hennig, Dienes & Kosiba (1958) reported on an electron microscope study of radiation effects on the oxidation and other properties of graphite and in this investigation they confined themselves to replica methods. Probably this was due to the size and shape of synthetic graphite blocks and the serious limitations on specimen thickness imposed by electron microscopy. As a result, however, no evidence on the molecular structure of the graphite was obtained and the resolution achieved in the surface replicas was of necessity rather poor. Much of the preliminary work in our present investigation was directed towards the preparation of thin specimens suitable for transmission microscopy so that information at the molecular level would be available to us.

(b) *The observation of lattice defects by means of moiré fringes*

Hashimoto & Uyeda (1957) were first to point out that atomic dislocations too fine to be observed by present-day electron microscopes can be detected through the moiré pattern, and showed that in rotational moiré patterns dislocations appear as extra half-lines on the pattern. Pashley, Menter & Bassett (1957) showed that a similar effect occurred in the case of parallel moiré patterns and these authors (Bassett, Menter & Pashley 1958) have pointed out that it is only when a dislocation in the one lattice is superimposed on a dislocation in the other that the

dislocation is invisible in the moiré pattern. Therefore investigation of the moiré patterns in graphite seems to offer a means of studying the distribution of dislocations within the graphite structure.

2. EXPERIMENTAL

(a) *Specimen preparation*

The material used in this investigation was Calder 'A' quality graphite kindly supplied by Dr D. M. Donaldson, U.K.A.E.A., Dounreay. This graphite is synthetically prepared and is consequently microcrystalline in structure with no extensive alinement of these crystallites in any particular direction. For transmission microscopy flakes of graphite less than 800 Å in thickness had to be obtained from this material and the three following techniques were evolved for preparing suitable specimens.

(i) *Direct preparation of fine surface material*

The first method used for the preparation of thin flakes was simply to scrape a fine powder from the surface of a graphite block with a razor blade and grind this powder under benzene. Evaporation of one drop of such a suspension on a Formvar covered mount gave a suitable specimen. Although flakes of the required thickness were observed on these specimens and several moiré patterns photographed, most of the material was much too thick and caused extensive break-up of the Formvar film when bombarded by the electron beam.

Our second method involved rubbing a large block of graphite on a clean glass slide, when continued rubbing removed fine material from the surface of the block to the slide. This slide was then covered with a collodion or Formvar film and both film and graphite floated on to a water surface. Areas of this film were easily mounted on specimen grids. Examination of these specimens showed that, although the amount of gross material had been greatly reduced compared to those prepared by the previous technique, the single flakes observed were either partially or completely covered in debris produced by the rubbing. A typical specimen is shown in figure 6, plate 27.

These two methods, although providing some material of the required standard, were considered to be unsatisfactory for a rigorous quantitative examination of graphite.

(ii) *Thin-section cutting*

To overcome these faults a method was developed of cutting very thin sections of graphite by means of an ultra-microtome. The Porter & Blum (1954) microtome used was primarily designed for cutting very thin sections of biological material. Before such tissue can be cut successfully it has to be embedded in polybutyl-methacrylate (Newman, Borysko & Swerdlow 1949) or in the epoxy resin Araldite as described by Glauert & Glauert (1958). No preliminary drying is necessary with graphite and blocks 1 mm square were therefore embedded directly in a mixture of 5 % methyl and 95 % *n*-butyl methacrylate, 1 % benzoyl peroxide being used as catalyst. Heating overnight at 60 °C gave sufficient hardness for cutting.

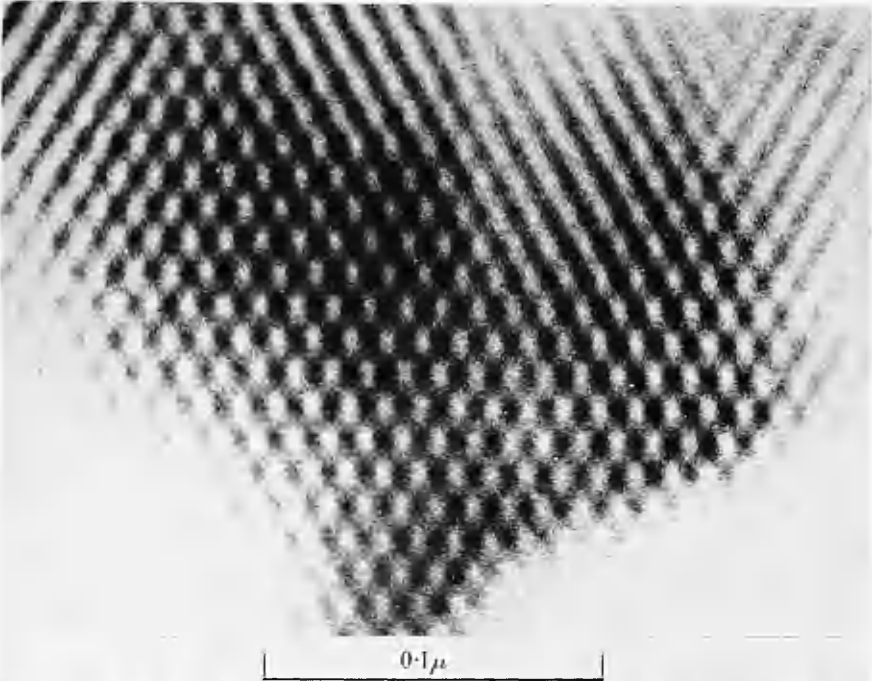


FIGURE 1. Electron micrograph of a thin section of synthetic graphite prepared by the method described in §2(a), 3. The sharp grain boundary MN is perpendicular to the line of viewing in this section. The clear area A appears to be a pore at the junction of three microcrystals. The area B which shows greater electron scattering than A has no sharply defined moiré patterns.

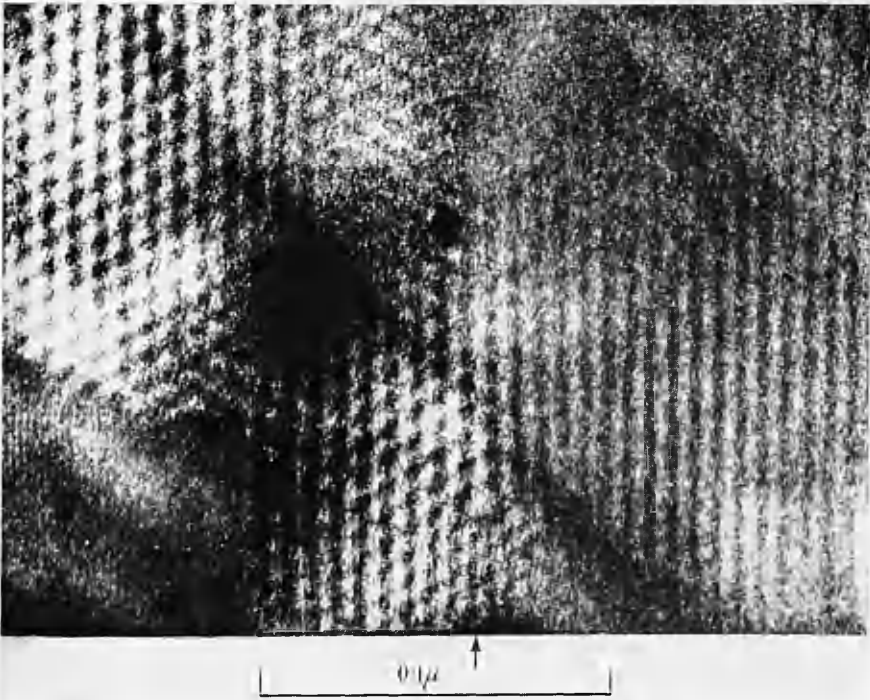
(Facing p. 392)



FIGURE 2. Electron micrograph of a thin section of synthetic graphite showing the presence of a dislocation in the area within the white rectangle. Seven lines are marked on the left-hand side of this enclosed area and six only are marked on the right-hand side. The extra terminating half-line is line number 4.



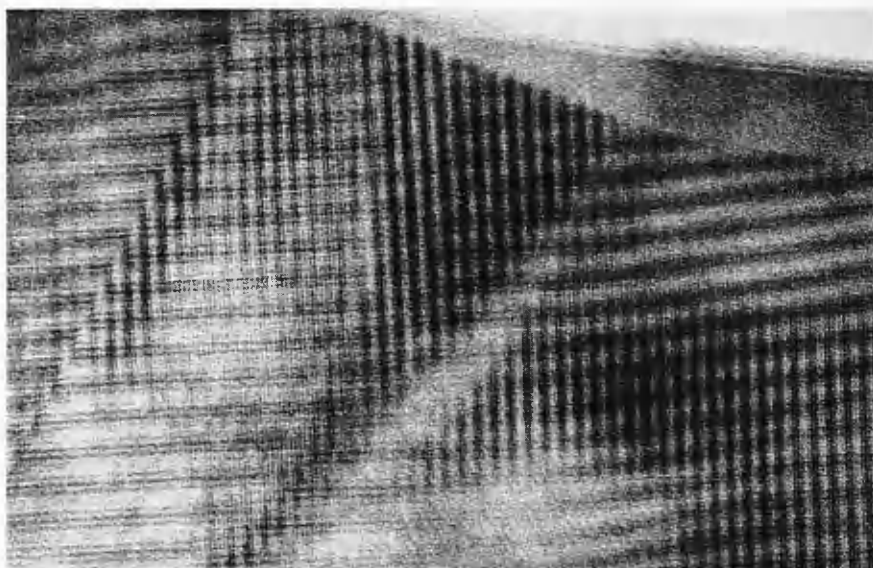
3



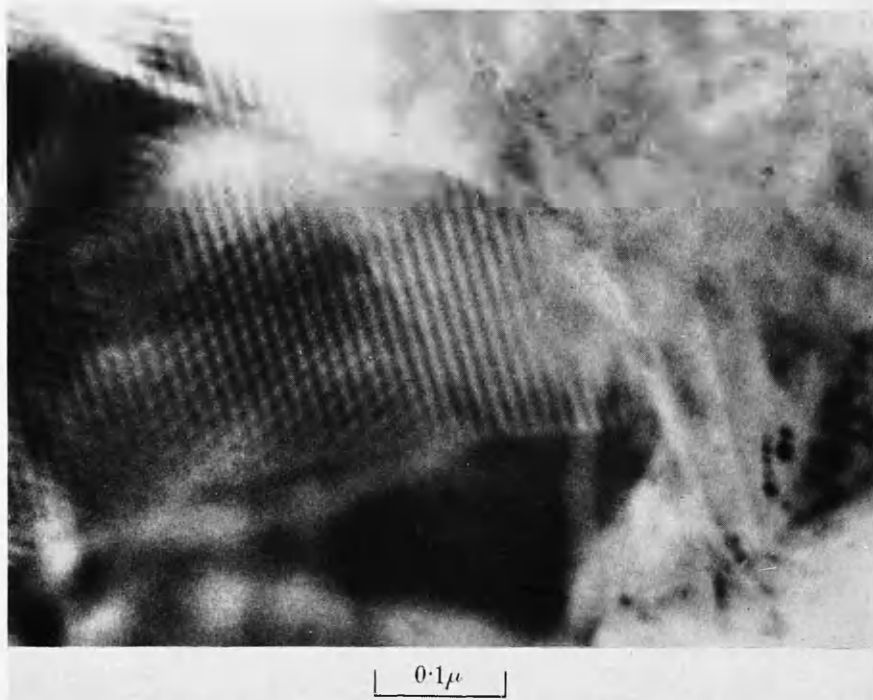
4

FIGURE 3. Electron micrograph of a small area of a thin section showing a characteristic hexagonal pattern.

FIGURE 4. Electron micrograph of a small area of a thin section showing a dislocation with two extra terminating half-lines at the point marked on the bottom right-hand side of the micrograph.



5

 0.1μ 

6

 0.1μ

FIGURE 5. Electron micrograph of a thin section showing a rectangular moiré pattern.

FIGURE 6. Electron micrograph of a fragment of graphite prepared by rubbing. Good moiré patterns can be obtained from this material but amorphous debris, such as is seen in the bottom right-hand corner of this micrograph, tends to confuse the picture.

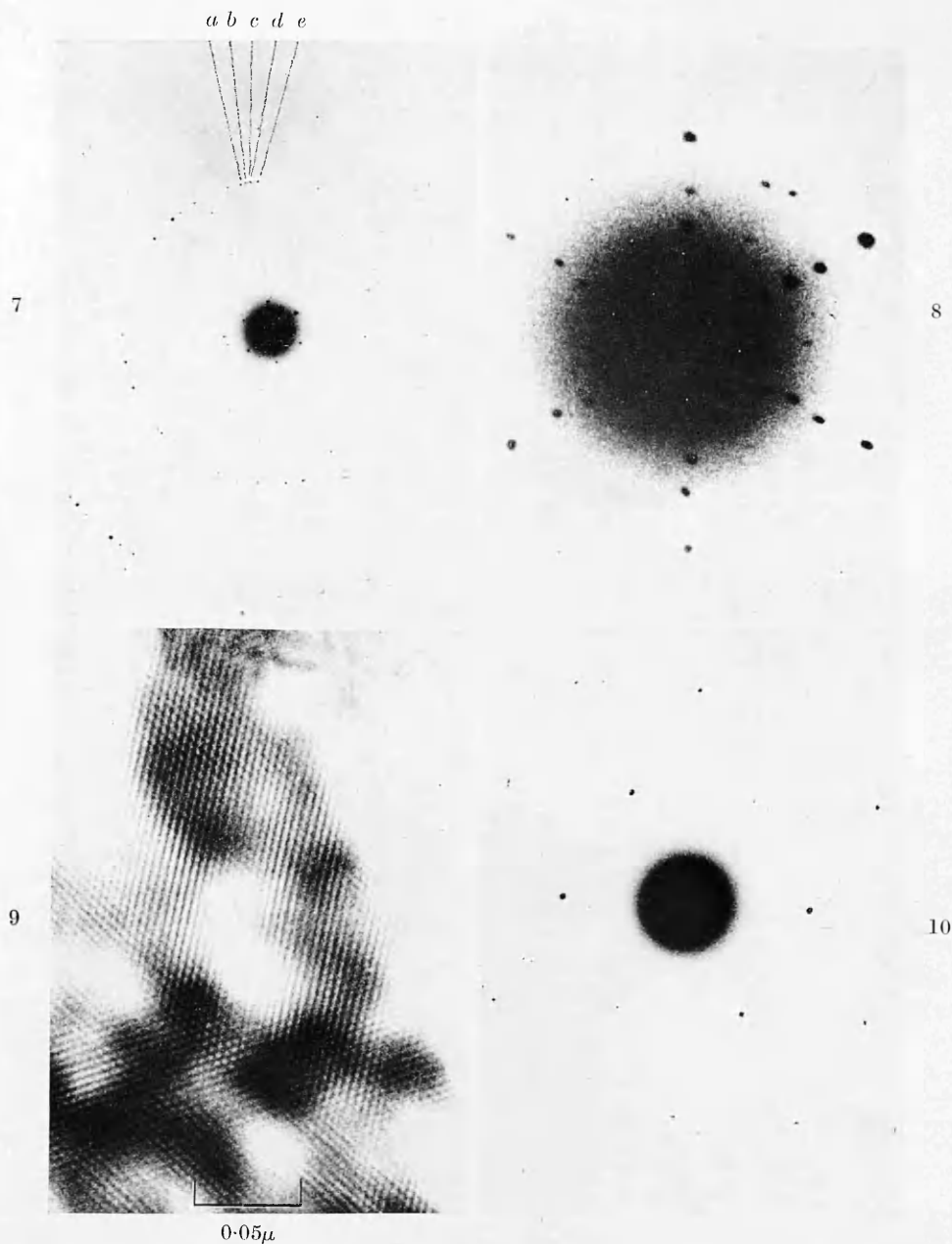
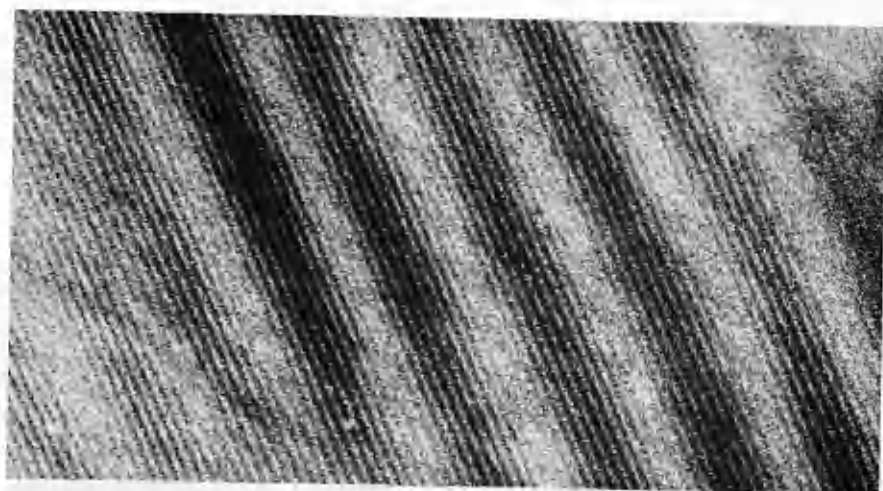


FIGURE 7. Selected-area diffraction pattern of the area shown in figure 9.

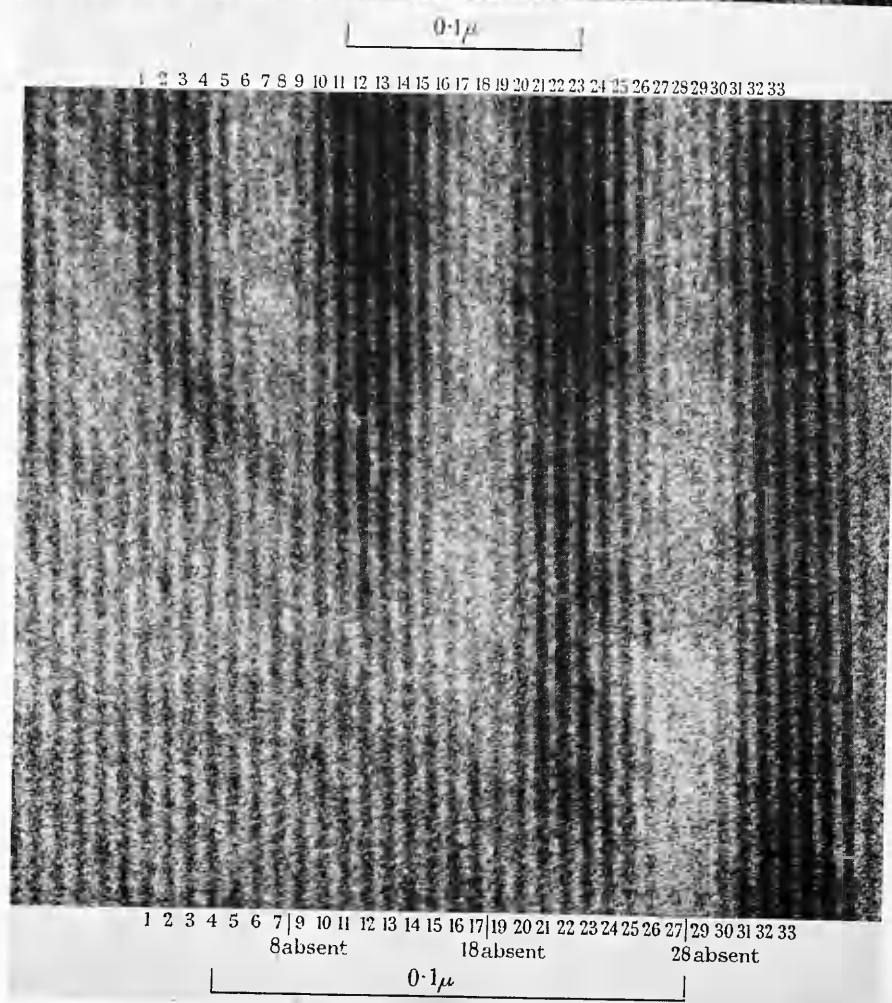
FIGURE 8. Enlargement of the central region of the electron diffraction pattern shown in figure 7.

FIGURE 9. Electron micrograph of the area selected for electron diffraction which gave the patterns illustrated in figures 7 and 8. The total area has been somewhat reduced in this illustration so that the observed spacing of 39 \AA can be clearly seen.

FIGURE 10. Single crystal electron diffraction pattern showing the $(h, k, \overline{h+k}, 0)$ reciprocal lattice net.



11



12

FIGURE 11. Electron micrograph of an area of a thin section showing several dislocations.

FIGURE 12. Higher magnification view of the area shown in the top left-hand corner of figure 11. The extra terminating half-lines, 8, 18 and 28 appear only in the top half of the micrograph.

Similar blocks were embedded in Araldite, the temperature in this case being maintained at 48 °C for several days.

The embedded graphite block 1 mm square was then trimmed to about one-tenth of this size and sections cut with glass knives prepared according to the method of Latta & Hartmann (1950). These sections were floated on to a 20 % acetone–water solution (Hillier & Gettner 1950) and then picked up on a Formvar covered specimen mount. A typical good section is shown on figure 1, plate 24.

The thickness of the areas of graphite exhibiting moiré patterns was determined by shadowcasting specimens with nickel-palladium (Williams & Wyckoff 1946).

(b) Electron microscopy

Preliminary survey work was carried out on a Philips E.M. 100B electron microscope. Since the maximum possible resolution was required in all micrographs most specimens were examined in a Siemens Elmiskop I, the accelerating voltage being 80 kV and plate magnification being either 40 000 or 80 000.

(c) Electron diffraction

Single condenser illumination was used for microscopy. This leads to greater overall contamination of the specimen than is the case with the double condenser system of illumination but enables selected area diffraction to be carried out at the same time as high resolution microscopy. Calibration of the diffraction patterns thus obtained was achieved by measurement of the three diffraction maxima at 1.56, 2.71 and 3.82 Å in a thallium chloride powder pattern recorded under identical conditions.

3. RESULTS

Micrographs from specimens prepared by scraping, rubbing and by thin section cutting all show moiré patterns. A comparison of representative photographs shows that there is a considerable overlap in the fringe patterns from the specimens prepared by rubbing and by scraping (figure 6, plate 27) and there is no sharply defined boundary between the various regions. It was generally found, moreover, that only a few areas were thin enough for photography and a considerable amount of amorphous debris covered graphite and film support alike. In contrast, specimens prepared by thin-sectioning methods were completely free from surface debris and gave an apparently much more informative picture of the structure within the graphite blocks. Thin sections of the quality illustrated by figures 1, 2, 11 and 12 cannot as yet be obtained as a matter of routine because thin sections tend to disintegrate as soon as they are cut and difficulty is usually encountered in transferring the sections from the collecting bath to the electron microscope specimen holders. This disintegration may be due either to unsatisfactory embedding before cutting or to the differing cleavage of graphite itself in different lattice directions.

Several blocks were prepared from each of the samples of Calder 'A' graphite and the thin sections obtained in each case showed the characteristic moiré patterns. The quantitative results described in this paper were obtained from blocks prepared from one sample, designated sample G_1 .

(a) The grain structure of crystalline graphite

The most striking feature of the micrographs of thin sections at moderate magnification is the pronounced grain structure shown by the material. Figure 1, plate 24, shows a typical area in which twelve individual grains can be recognized. This micrograph shows a strong resemblance to the familiar grain structure of etched metal specimens as viewed under the light-microscope and we can assume that we are, in fact, observing a similar structure. In the case of graphite the individual grains are much smaller and are below the limit of resolution of the light-microscope but with the higher resolving power of the electron microscope the resemblance is apparent. This superficial resemblance is maintained at a fundamental level. Each grain in the graphite specimen consists of a single microcrystal whose extent and outline are made visible by the moiré pattern.

Measurements on sections of sample G_1 gave a value of $0.11 \pm 0.074 \mu^2$ for the area of individual microcrystals. This figure is the mean of 138 measurements. It indicates a considerably higher value (around 3300 Å) for the layer diameter than that obtained for similar materials by Bacon (1958), who used calculations based on line broadening in X-ray diffraction studies to determine the layer diameter L and reported values in the range 270 to 790 Å for all but one of the samples he examined. This exceptional sample he considered to be highly crystalline and for it he found a layer diameter of 1100 to 2000 Å. We have no reason to suppose that the graphite sample G_1 is exceptionally crystalline and the value of $0.11 \pm 0.074 \mu^2$ obtained for the layer area suggests that values obtained by X-ray line broadening studies may in fact be rather low. Only when a more complete investigation of the results of the two methods is made on identical samples will it be possible to correlate the values and explain the source of error.

Several micrographs have been obtained showing clear areas between contiguous microcrystals similar to that seen at A in figure 1. This clear structureless area may well be a pore in the graphite structure since pores are known to be present from studies of diffusion rate and of density. The diameter measured was in the region 400 to 800 Å. These pores appear at the point of contact of three or more microcrystals. The grain boundaries are otherwise quite narrow, e.g. the boundary MN in figure 1, where the section has been cut with this boundary perpendicular to the line of sectioning, is of about 50 Å width.

The thickness of the sections was determined by measurement of the shadow lengths cast by evaporation of nickel-palladium alloy on to the specimen at an angle of 15° . Measurements were only made on areas exhibiting moiré patterns or on very thin areas as only the thinnest areas give the high-resolution moiré patterns which make the detection of lattice defects possible. Twenty measurements were made on five specimens of the graphite sample G_1 . The magnification in each case was 8500. It is exceedingly unlikely that any methacrylate embedding material was present in these areas since, although the methacrylate monomer will penetrate the pores in synthetic graphite, it is improbable that it will penetrate between actual graphite sheets. The average value of 150 ± 25 Å therefore represents, assuming an interplanar spacing of 3.4 Å, a stack of 44 parallel graphite layers.

(b) *Electron diffraction and layer orientation*

The 'selected area' diffraction method makes it possible to obtain direct micrographs and electron diffraction patterns of individual small areas in the specimens. We could, by this means, examine the orientation of individual crystal planes in the thin sections and relate the known crystal structure of graphite to the observed moiré pattern. Table 1 summarizes detailed measurements made on five different areas and figures 7 and 8, plate 28, show the diffraction pattern given by the area shown in figure 9. Figure 8 is an enlargement of the central region of the pattern in figure 7. This was necessary to show the low-angle diffraction pattern, a long spacing pattern which can be related to the moiré pattern of the micrographs.

TABLE 1

specimen	wide-angle reflexions		no. of crystals contributing/ 60° arc, <i>n</i>	low-angle reflexions		
	(11 $\bar{2}$ 0)	(10 $\bar{1}$ 0)		total observed/ 60° sector, <i>N</i>	long spacing	moiré spacing
<i>G</i> ₁ S59/366	2.10	1.22	16	26	10.4 (1) 13.2 (2) 20 (3) 34 (4)	34 49 (2-1)
<i>G</i> ₁ S59/404	2.05	1.20	9	14	7.9 (1) 8.3 (2) 20 (3)	44 136 (2-1)
<i>G</i> ₁ S59/407	2.05	1.20	10	17	18.5 (1) 20 (2)	19 240 (2-1)
<i>G</i> ₁ S59/417	2.08	1.21	11	21	10 (1) 14 (2) 17.5 (3) 24 (4)	39 (4-3) 70 (3-2)
<i>G</i> ₁ S59/456	2.10	1.22	12	26	9.9 (1) 11 (2) 23.5 (3) 29 (4)	26 97 (2-1)

The wide-angle spacings recorded were 2.07 ± 0.04 Å, 1.23 ± 0.01 Å and 1.15 ± 0.03 Å. These correspond to the (11 $\bar{2}$ 0), (10 $\bar{1}$ 0) and (20 $\bar{2}$ 1) planes in graphite. The measurements were made over 20 plates and for each a thallium chloride standard pattern (§2(c)) was recorded in the same exposure series. In two cases only did we find evidence of very weak 3.44 Å spacings corresponding to the (0001) plane and in these specimens the micrographs of the area selected for diffraction showed considerable buckling of the section. It was possible that in these specimens an area of the section was parallel to the electron beam rather than normal to it as is usually the case. The 1.15 Å reflexions corresponding to the (20 $\bar{2}$ 1) plane were, where present, extremely weak and showed a preferred orientation which differed from that shown by the 2.07 and 1.23 Å spacings corresponding to the (11 $\bar{2}$ 0) and (10 $\bar{1}$ 0) planes. Extensive visual survey of the electron diffraction patterns given by several sections failed to show spectra due to (0001) on the

microscope fluorescent screen in spite of the fact that (0001) is of very high intensity in randomly oriented graphite. Thus all the available evidence suggests that in the thin sections of graphite which we have obtained the hexagonal layer net planes, the (0001) planes, are parallel or at a small angle to the plane of the section.

In a few cases, instead of a powder diffraction pattern as in figure 7, a single crystal pattern was obtained as in figure 10. Here again, however, the orientation was such that the hexagonal layer net planes were all parallel to the plane of the section and the photograph in figure 10 is in fact a direct photograph of $(h, k, \overline{h+k}, 0)$ reciprocal lattice net. Figures 7 and 8 both show other reflexions which cannot be directly related to the classical graphite lattice. For example, figure 7 shows many spectra within the $(11\bar{2}0)$ ring. Detailed study of this $(11\bar{2}0)$ diffraction ring shows that it is composed of numerous individual reflexions each of which arises from a single crystalline fragment of the area selected for diffraction. A count of individual spots for this ring gives a value of 66 and since there is hexagonal symmetry this suggests at least 11 contributing crystal fragments. Further examination makes it possible to relate the individual reflexions on the $(11\bar{2}0)$ ring and the low-angle diffraction pattern which is shown at higher magnification in figure 8. In this low-angle diffraction pattern we have a hexagonal array of spots of spacings 10, 14, 17.5 and 24 Å. There is no simple relationship between these values and the 10, 14 and 17.5 Å spacings are not successive higher orders of the largest spacing 24 Å. From figure 7 we see that each line of reflexions points in the general direction of a compact group of reflexions on the $(11\bar{2}0)$ diffraction ring (the group a, b, c, d and e in figure 7), and measurement of the successive lattice rotations between a and b , a and c , a and d , and a and e gives the values $1^\circ 51'$, $2^\circ 46'$, $3^\circ 59'$ and $6^\circ 49'$. Using these values to calculate the moiré magnification from this rotation gives the values 38, 25, 17.5, 10.4 Å and the combinations 14.2, 17.4, 25, 33, 58 and 77 Å of which we observe 10, 14, 17.5 and 24 Å. In table 1 we have listed the average number n of reflexions counted in a 60° arc of the $(11\bar{2}0)$ diffraction ring and the number of extra reflexions N counted in the 60° sector which this arc subtends. If the extra reflexions do, in fact, arise by a combination of any two of the individual microcrystalline areas responsible for the reflexions seen in the $(11\bar{2}0)$ plane, these two quantities n and N should be related by the simple formula for such combinations

$$N = {}^nC_2.$$

The values ranging from 14 to 26 found for N give values of n in the range 6 to 8, agreeing reasonably well with the experimentally observed values of from 9 to 16.

This quantity n represents the number of rotational stacking faults in each of the areas selected. Errors in it may arise from two causes. First, too brief an exposure to the electron beam would give low values because of failure to record all possible reflexions. Secondly, inadequate screening would give high values because of the intrusion of extra reflexions from neighbouring microcrystals. It is exceedingly improbable, however, that these errors could affect the value by more than 50%.

The measurements of section thickness (§3(a)) above give a value of 150 Å for the average thickness so that the average value for the distance between stacking

faults is 13 Å or one stacking fault in every four layers. This value agrees well with the value of one fault in every six layers obtained by Bacon (1958) in a study of X-ray line broadening.

Inspection of the various patterns suggests that layer rotation is random and that no particular interlayer angle is especially favoured. In the case of the moiré patterns, where a great many more observations have been made (figure 13, §3, below) some tendency to grouping is apparent.

It is noteworthy that no moiré fringe pattern could be obtained from the area which gave the good single crystal diffraction pattern shown in figure 10 and we can conclude that moiré patterns occur in graphite only when stacking faults give rise to twist between individual hexagonal layer nets. However, it seems reasonable to suppose that, in figure 1, area *B*, showing no moiré pattern and appearing in a thin section which otherwise contains good patterns, is an area in which stacking faults are absent or in which if stacking faults are present the angle of rotation is greater than 7°.

(c) *The observation of moiré patterns in graphite*

The electron diffraction evidence discussed in §3(b) shows that all the sections examined have the graphite hexagonal layer nets lying in, or at a small angle to, the plane of the section. This observed orientation is not due to any preferred orientation in the synthetic material but arises from the anisotropic properties of graphite microcrystals. It is much easier to cut through the weak interlayer bonds than to cut the C—C bonds in the hexagonal layer nets. As a result, good sections are obtained only from those regions where the hexagonal layer nets are nearly parallel to the direction of cutting.

The moiré patterns shown in the electron micrographs arise from rotational stacking faults in the hexagonal layer nets in such a way that the moiré pattern is formed by the simple magnification effect where $m = d/\alpha$. The long spacings and moiré spacings measured for identical areas and listed in table 1 show several examples of correspondence between the two, e.g. the moiré spacing of 34 Å measured in specimen *G*₁S 59/366 corresponds to the long spacing of 34 Å shown in the electron diffraction pattern. Most of the remaining moiré spacings can be related to the observed long spacings by the difference formula $m = d_1 d_2 / d_1 - d_2$, e.g. the 240 Å moiré spacing observed in *G*₁S 59/407 is a difference spacing which arises from the 20 and 18.5 Å long spacings. These difference relationships are indicated in table 1. For each selected area the number of extra reflexions due to layer rotation is much greater than the number of moiré patterns, since the moiré patterns are only observed for small angles of rotation. The limit of resolution of the electron microscope used for this work is around 10 Å. This value corresponds to an angle α of 7° so that all the moiré patterns due to rotations greater than 7° will be below the limit of resolution. The actual values measured range from 14 up to 250 Å, and figure 13 shows a histogram of measurements of spacings from thirty-four micrographs taken on fifteen specimens. From the histogram it would appear that there is some concentration at angular values of 2.5° and 1°. In X-ray diffraction studies Lukesh (1950) found evidence of a preferred orientation at an angle of 2.5°.

Three types of moiré pattern have been observed in thin sections of graphite. These are the line pattern (figure 2, plate 25), the hexagonal pattern (figure 3, plate 26) and the rectangular pattern (figure 5, plate 27). The line pattern is obtained when the hexagonal layer planes in the section are tilted at a small angle to the specimen plane or when the specimen plane itself is not strictly normal to the electron beam. The hexagonal pattern occurs when the hexagonal layer planes are normal to the electron beam and, in this case, the moiré image can be considered as a two-dimensional Patterson projection of the graphite structure in terms of the treatment given by Dowell *et al.* (1956, 1957) or as a direct magnified image of the

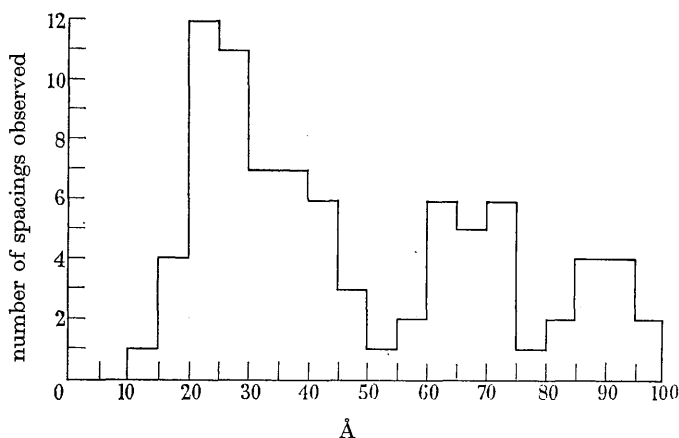


FIGURE 13. Histogram of values found for the moiré spacings measured from thirty-four micrographs.

structure, since in this instance the Patterson projection and the direct projection are indistinguishable. The image in this case arises from interference effects from the $(10\bar{1}0)$ planes in graphite. The rectangular pattern, which is the least common, arises from interference between the $(10\bar{1}0)$ planes in one direction and the $(11\bar{2}0)$ in the other. These planes, as the electron diffraction patterns show, are the two strongest reflexion planes in graphite in this particular orientation.

(d) *The observation of dislocations in graphite*

Figure 2 shows a typical dislocation in the graphite lattice. In the area within the white rectangle there are seven lines present on the left-hand side and six on the right. The extra half-line (number 4) is clearly visible in this micrograph. Bassett *et al.* (1958) have pointed out that, contrary to their previous conclusion (Menter 1956), an observation of this kind does not distinguish between an edge dislocation and a screw dislocation, but gives rather the Burgers vector of the dislocation in question whether it be edge or screw. However, one would expect a screw dislocation, if present in the structure, to have its Burgers vectors parallel to the hexagonal layer net planes in the graphite lattice since this is the commonly observed orientation in layer structures and indeed Hennig, Dienes & Kosiba (1958) have shown such a screw dislocation in a single crystal of graphite. It is

probable then that this dislocation and the others observed in thin sections are indeed edge dislocations.

Figure 4, plate 26, shows an example in which two extra terminating half-lines appear in the moiré pattern and in this instance the dislocation has a Burgers vector of two lattice translations. In figures 11, 12, plate 29, a more complex distribution is illustrated. Extra terminating half-lines are visible in the regions between the seven darker bands in figure 11. The individual dislocations can be more easily seen by first studying figure 12 which is an enlargement of the left-hand corner of figure 11, and has three dislocations visible on it. If one then tilts figure 11 so as to give a foreshortened picture and views down the direction of the lines the dislocations in each of the seven less dense bands can be seen.

The estimated distribution density is 3.3×10^7 dislocations/cm². This value was determined for the area used to measure crystallite area. In many examples, e.g. figure 2, the area at the top right-hand corner, and figure 5, slip lines are clearly visible in the micrographs.

We have, as yet, no direct evidence of dislocations in the direction perpendicular to the hexagonal layer nets in the graphite lattice because it has not yet been possible to view the lattice in this direction. However, it seems safe to assume that edge dislocations are present in which extra incomplete hexagonal layer nets are interposed between normal completed layer nets in the microcrystal lattice.

This type of edge dislocation causes no very serious strain in the crystal lattice since the layer-to-layer distance of 3.44 Å shows that the bonding in this direction is extremely weak.

It is a matter of some considerable interest that dislocations should have been detected within the hexagonal layer nets themselves. These are unlikely to be the screw dislocations responsible for growth and are, as suggested earlier, most probably edge dislocations, in which case there must be a considerable modification of the normal hexagonal layer net structure at the end of the terminating half-line in the crystal lattice. The simplest possibility is shown in figure 14, in which an extra terminating half-line has been introduced parallel to *a* in the hexagonal layer net. This represents the smallest defect which can exist in the lattice. If the area is larger than shown in figure 14 then the strain and bond distortion is correspondingly reduced. If, as in figure 4, plate 26, two extra terminating half-lines are introduced then the strained area becomes more complex and, for this case, the simplest arrangement is shown in figure 15.

Although the results obtained indicate that this deformation of the hexagonal layer net is present around the dislocation they do not enable us to specify the exact structure of the deformed region. However, the mere observation is valuable because it is the first indication that there is a reactive centre in graphite microcrystals, the reactivity of which can be greater than the reactivity of the microcrystal edges. The defects described by Ubbelohde (1957) should have their Burgers vector perpendicular to the vector observed in this investigation. As mentioned in §4(*a*) below, we are at present endeavouring to obtain sections which would show these defects, if present.

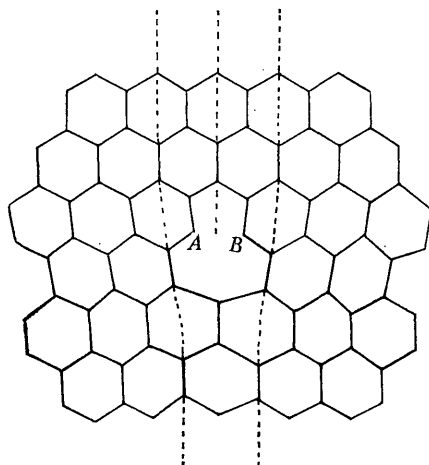


FIGURE 14. Diagram showing an edge dislocation of Burgers vector $[20\bar{2}0]$ in the hexagonal layer net plane in graphite.

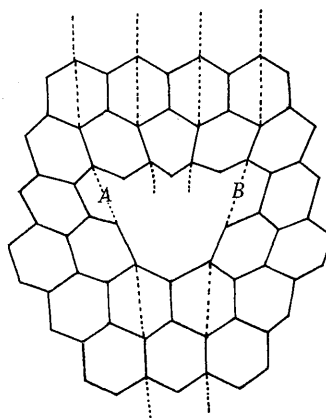


FIGURE 15. Diagram showing an edge dislocation of Burgers vector $[40\bar{4}0]$ in the hexagonal layer net plane in graphite.

4. CONCLUSIONS

(a) *Further application of thin-section cutting to the study of graphite*

At present a diamond knife is being used instead of glass knives to cut thin sections and it is hoped that with the much harder cutting edge which this affords it will be possible to cut along any lattice direction in carefully embedded material. This would yield information on the distribution of dislocations in all the lattice directions and thus enable us to determine the number of edge dislocations due to the interpolation of extra hexagonal layer net planes as suggested in §3(d) above.

(b) *The micro-structure of crystalline graphite*

The value of $0.11 \pm 0.074 \mu^2$ obtained for the area of individual microcrystals gives a larger value (3300 Å) for the layer diameter L than that calculated from measurements of X-ray line broadening by Bacon (1958). The difference is fourfold

for all but one exceptionally crystalline specimen which Bacon examined. Since we have no reason to suspect that our specimen G_1 is exceptional we must conclude that this fourfold discrepancy is due to the failure of the indirect method to yield results of as high accuracy as does this direct approach.

In contrast to the discrepancy between the above results, the determination by both methods of average distance between stacking faults gives values in good agreement, namely, six layers and four layers. One would expect this agreement. Since the distance between the stacking faults is small compared with the layer diameter L the X-ray line broadening method should give results of much greater accuracy here where line broadening effects are greatest.

The direct micrographs of thin sections show for the first time the extent of crystallinity in synthetic graphite. The boundary region between microcrystals is quite narrow and except where pores are present is limited to 50 Å or less. There is thus direct evidence of a sharp boundary between microcrystals rather than a gradual transition.

We are as yet unable to cut good sections perpendicular to the hexagonal layer nets in graphite microcrystals and cannot therefore determine crystallite thickness by direct methods. Layer stacking faults can of course be measured indirectly but it would be interesting to determine whether in this direction in the lattice there is again a sharp boundary or whether here the change is gradual with successive stacking faults giving a transition from one region to the next.

(c) *The reactivity of solid graphite*

In view of the microcrystalline structure of synthetic graphite and the sharply defined grain boundaries one would expect the greatest reactivity to occur at pores and at the boundary areas, the rate of diffusion of reactants into the solid being the main rate-determining factor in macroscopic blocks of the material. The observed edge dislocations are centres of high reactivity in the material and as such would be expected to provide reaction centres at which chain reactions could be initiated. The number observed, namely 3.3×10^7 dislocations/cm², takes no account of the dislocations due to the interpolation of extra hexagonal layer net planes in the lattice, but since these would have a different reactivity the figure of 3.3×10^7 /cm² has probably greater applicability to kinetic studies. This value 3.3×10^7 /cm² is greater than the value 3.6×10^6 /cm² observed for the number of screw dislocations in crystalline *n*-hexatriacontane, $nC_{36}H_{74}$, by Dawson & Vand (1951) and is smaller than the value of 10^{11} /cm² observed by Bassett *et al.* (1958) in metal films.

The suggested structure of the lattice defects themselves (figures 14 and 15, §3(d)) is at present merely conjectural, since we do not have accurate knowledge of the size of the defect. If it is larger than the size shown then the strain and distortion in the bonds surrounding the region where it occurs will be greatly reduced. In the example illustrated in figure 14 it may well be that the defect could best be represented by a formal bond between *A* and *B* to give effectively a five- and a seven-membered ring in the graphite lattice. In the example illustrated in figure 15 there might equally well be two five-membered rings *A* and *B*. These schematic structures are suggested, at the present time, not because we feel that

they do in fact represent the structure of the defects concerned but because they illustrate two of the possibilities. It is hoped that further work will give more detailed information about the exact structure.

We thank Professor J. Monteath Robertson, F.R.S., for his interest and encouragement and Dr D. M. Donaldson, U.K.A.E.A., Dounreay for valuable discussion in the course of this work.

We are indebted to the United Kingdom Atomic Energy Authority for a grant supporting the investigation and to the Department of Scientific and Industrial Research for a Research Grant to E.A.C.F. We also thank Sir Leonard Owen, Managing Director of the Industrial Group of the U.K.A.E.A., for permission to publish this paper.

REFERENCES

- Bacon, G. E. 1951 *Acta Cryst.* **4**, 558.
 Bacon, G. E. 1952 *Acta Cryst.* **5**, 392.
 Bacon, G. E. 1958 *Crystallographic studies on graphite*. United Kingdom Atomic Energy Authority Report. A.E.R.E. M/R 2702.
 Bassett, G. A., Menter, J. W. & Pashley, D. W. 1958 *Proc. Roy. Soc. A*, **246**, 345.
 Bernal, J. D. 1924 *Proc. Roy. Soc. A*, **106**, 749.
 Dawson, I. M. & Vand, V. 1951 *Proc. Roy. Soc. A*, **206**, 555.
 Dowell, W. C. T., Farrant, J. L. & Rees, A. L. G. 1956 *Proc. Int. Conf. Electron Microscopy, London, 1954*, p. 279. Royal Microscopical Society.
 Dowell, W. C. T., Farrant, J. L. & Rees, A. L. G. 1957 *Proc. Regional Conf. Electron Microscopy, Tokyo, 1956*, p. 320. Electrotechnical Laboratory, Nagata-cho Chiyoda-ku, Tokyo.
 Franklin, R. E. 1950 *J. Chim. phys.* **47**, 573.
 Franklin, R. E. 1951 *Acta Cryst.* **4**, 253.
 Glauert, A. M. & Glauert, R. H. 1958 *J. Biophys. Biochem. Cytol.* **4**, 191.
 Grenall, A. 1958 *J. Appl. Phys.* **29**, 11.
 Hashimoto, H. & Uyeda, R. 1957 *Acta Cryst.* **10**, 143.
 Hennig, G. R., Dienes, G. J. & Kosiba, W. 1958 *Radiation Effects on the Oxidation Rate and on other Chemical Properties of Graphite*. Second United Nations Conference on the Peaceful Uses of Atomic Energy. Report A/CONF. 15/P/1778. U.S. Government Printing Office.
 Hillier, J. & Gettner, M. E. 1950 *J. Appl. Phys.* **21**, 889.
 Latta, H. & Hartmann, J. F. 1950 *Proc. Soc. Exp. Biol. Med.* **74**, 436.
 Lipson, H. & Stokes, A. R. 1942 *Proc. Roy. Soc. A*, **181**, 101.
 Lukesh, J. S. 1950 *Phys. Rev.* **80**, 2.
 Menter, J. W. 1956 *Proc. Roy. Soc. A*, **236**, 119.
 Mitsuishi, T., Nagasaki, H. & Uyeda, R. 1951 *Proc. Imp. Acad. Japan*, **27**, 86.
 Newman, S. B., Borysko, E. & Swerdlow, M. 1949 *Science*, **110**, 66.
 Pashley, D. W., Menter, J. W. & Bassett, G. A. 1957 *Nature, Lond.* **179**, 752.
 Porter, K. R. & Blum, J. 1954 *J. Histochem. Cytochem.* **2**, 346.
 Ubbelohde, A. R. 1957 *Nature, Lond.* **180**, 380.
 Williams, R. C. & Wyckoff, R. W. G. 1946 *J. Appl. Phys.* **17**, 23.